LIÈGE université
Gembloux
Agro-Bio Tech

Novel and potent antiviral strategies against porcine coronaviruses infection

ZHANG Yunhang

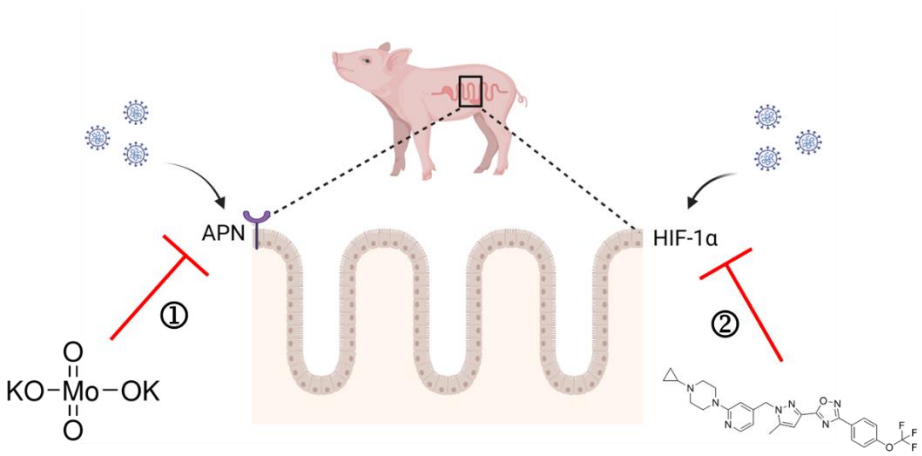

Promoter: Luc WILLEMS
Co-promoter: Guangliang LIU
2024

COMMUNAUTÉ FRANÇAISE DE BELGIQUE

UNIVERSITÉ DE LIÈGE – GEMBLOUX AGRO-BIO TECH

Novel and potent antiviral strategies against porcine coronaviruses infection

ZHANG Yunhang

Dissertation originale présentée (ou essai présenté) en vue de l'obtention du grade de doctorat en sciences agronomiques et ingénierie biologique

Promoteur: Luc WILLEMS
Co-promoteur: Guangliang LIU
Année civile: 2024

Abstract

Coronavirus infection has threatened human and animal health for a long time. Despite multiple efforts, porcine coronavirus has caused large financial losses in the global swine industry. Thus, identifying novel and potent strategies to combat porcine coronaviruses and elucidating the underlying mechanisms are urgently needed. We aim to develop two strategies to control coronaviruses infection. The first strategy focuses on discovering a method to control viral cell receptors, thereby closing the door to viral entry and combating viral infections. The second strategy is to elucidate the mechanism of inflammatory responses induced by porcine coronavirus, identifying critical host factors involved, and thereby developing methods to effectively control the viral infection.

1. Potassium molybdate blocks APN-dependent coronavirus entry by degrading receptor via PIK3C3-mediated autophagy

Aminopeptidase N (APN) is one of the most important receptors of coronavirus. Modulating APN expression can represent a novel approach for controlling APN-dependent coronaviruses and their variants infection. Here, we found that a chemical compound potassium molybdate (PM) negatively regulates APN expression by inducing PIK3C3-mediated autophagy against APN-dependent coronavirus internalization, including transmissible gastroenteritis virus (TGEV) and porcine respiratory coronavirus (PRCV). Furthermore, PM can promote PIK3C3-BECN1-ATG14 complex assembly to induce autophagic degradation of APN by upregulating PIK3C3 Ser249 phosphorylation. Lastly, pig experiments also confirmed that PM can trigger PIK3C3-mediated autophagic degradation of APN to restrict TGEV pathogenicity *in vivo* without toxicity. Our findings underscore the promising potential of PM as an effective agent against APN-dependent coronavirus and potentially emerging viral diseases entry.

2. Inhibition of HIF-1α restricts TGEV replication and mitigates virus-induced inflammation.

In the second part of research explores the mechanism of inflammatory responses induced by porcine coronaviruses. We developed intestinal organoids to investigate immune responses to virus infection, which can better represent the physiological environment compared with well-established cell lines. In addition, the results demonstrated that inflammatory responses induced by TGEV infection were regulated by the RIG-I/NF-κB/HIF-1α/glycolysis axis in apical-out porcine organoids and in pigs. Our findings contribute to understanding the mechanism of intestinal inflammation upon viral infection and highlight apical-out organoids as a physiological model to mimic virus-induced inflammation.

Apart from its role in inflammation, HIF-1α was shown to facilitate TGEV infection by targeting viral replication, which was achieved by restraining type I and type III interferon (IFN) production. *In vivo* experiments in piglets demonstrated that the HIF-1α inhibitor BAY87-2243 (BAY87) significantly reduced HIF-1α expression and inhibited TGEV replication and pathogenesis by activating IFN expression. In summary, we unveiled that HIF-1α can be a novel antiviral target and BAY87 can be a candidate drug against TGEV replication *in vitro*, *ex vivo*, and *in vivo.*

In conclusion, this thesis provides two novel and potent antiviral strategies against porcine coronaviruses infection. First of all, we unveil that PM can control cell receptor APN expression to block APN-dependent coronavirus entry by PIK3C3-mediated autophagy. In addition, inhibition of HIF-1α restricts TGEV replication and mitigates virus-induced inflammation. These studies provide new directions for the prevention and control of porcine coronaviruses.

Keywords: Porcine coronaviruses; PM; APN; inflammation; HIF-1α; IFN responses;

Résumé

L'infection par le coronavirus menace la santé humaine et animale depuis longtemps. Malgré de multiples efforts, le coronavirus porcin a causé de grandes pertes financières dans l'industrie porcine mondiale. Il est donc urgent d'identifier des stratégies nouvelles et puissantes pour combattre le coronavirus porcin et élucider les mécanismes sous-jacents. Nous visons à développer deux stratégies pour contrôler l'infection par le coronavirus. La première stratégie se concentre sur la découverte d'une méthode pour contrôler les récepteurs cellulaires viraux, fermant ainsi la porte à l'entrée virale et combattant les infections virales. La deuxième stratégie consiste à élucider le mécanisme des réponses inflammatoires induites par le coronavirus porcin, identifier les facteurs clés de l'hôte et ainsi contrôler l'infection virale.

1. Le molybdate de potassium bloque l'entrée du coronavirus dépendant de l' aminopeptidase N en dégradant le récepteur via l'autophagie médiée par PIK3C3

L'aminopeptidase N (APN) est l'un des récepteurs les plus importants du coronavirus. La modulation de l'expression de l'APN peut représenter une nouvelle approche pour contrôler l'infection par les coronavirus dépendants de l'APN et leurs variantes. Ici, nous avons découvert qu'un composé chimique, Le molybdate de potassium (PM), régule négativement l'expression de l'APN en induisant l'autophagie médiée par PIK3C3 contre l'internalisation de coronavirus dépendant de l'APN, y compris le virus de la gastro-entérite transmissible (TGEV) et le coronavirus respiratoire porcin (PRCV). De plus, PM peut promouvoir l'assemblage du complexe PIK3C3-BECN1-ATG14 pour induire la dégradation autophagique de l'APN en augmentant la phosphorylation de PIK3C3 Ser249. Enfin, des expériences sur des porcs ont également confirmé que PM peut déclencher la dégradation autophagique de l'APN médiée par PIK3C3 pour restreindre la pathogénicité du TGEV in vivo sans toxicité. Nos découvertes soulignent le potentiel prometteur de PM en tant qu'agent efficace contre l'entrée du coronavirus dépendant de l'APN et potentiellement contre les maladies virales émergentes.

2. L'inhibition de HIF-1α restreint la réplication du TGEV et atténue l'inflammation induite par le virus.

La deuxième partie de la recherche explore le mécanisme des réponses inflammatoires induites par le coronavirus porcin. Nous avons développé des organoïdes intestinaux pour étudier les réponses immunitaires à l'infection virale, qui peuvent mieux représenter l'environnement physiologique par rapport aux lignées cellulaires bien établies. De plus, les résultats ont démontré que les réponses inflammatoires induites par l'infection par le TGEV étaient régulées par l'axe RIG-I/NF-κB/HIF-1α/glycolyse dans les organoïdes porcins apicaux et chez les porcs. Nos découvertes contribuent à la compréhension du mécanisme de l'inflammation intestinale lors d'une infection virale et mettent en lumière les organoïdes apicaux comme modèle physiologique pour imiter l'inflammation induite par le virus.

En plus de son rôle dans l'inflammation, il a été démontré que HIF-1α facilite l'infection par le TGEV en ciblant la réplication virale, ce qui a été réalisé en restreignant la production d'interférons de type I et de type III (IFN). Des expériences in vivo chez les porcelets ont démontré que l'inhibiteur de HIF-1α, BAY87-2243

(BAY87), réduisait significativement l'expression de HIF-1α et inhibait la réplication et la pathogénicité du TGEV en activant la production d'IFN. En résumé, nous avons révélé que HIF-1α peut être une nouvelle cible antivirale et que BAY87 peut être un médicament candidat contre la réplication du TGEV *in vitro*, *ex vivo* et *in vivo*.

En conclusion, cette thèse propose deux stratégies antivirales nouvelles et puissantes contre l'infection par les coronavirus porcins. Tout d'abord, nous révélons que PM peut contrôler l'expression du récepteur cellulaire APN pour bloquer l'entrée du coronavirus dépendant de l'APN par l'autophagie médiée par PIK3C3. De plus, l'inhibition de HIF-1α restreint la réplication du TGEV et atténue l'inflammation induite par le virus. Ces études fournissent de nouvelles directions pour la prévention et le contrôle du coronavirus porcin.

Mots clés: Coronavirus porcin ; PM ; APN ; inflammation ; HIF-1α ; réponses IFN.

Acknowledgments

First and foremost, I would like to express my gratitude to my two supervisors for jointly guiding my doctoral project. **Prof. LIU,** thank you for allowing me to join your lab and begin my Ph.D. studies. During this time, I am grateful for your careful guidance and support with my doctoral research. When I encountered difficulties, it was your encouragement and support that gave me the courage to keep moving forward. **Prof. WILLEMS**, thank you for allowing me to be your student and for all the help you've provided. During this year in your lab, I have learned many professional skills and expanded my research perspective. I am also grateful for your revisions and suggestions on my thesis.

I extend my sincere appreciation to the members of my thesis committee, **Prof. SOYEURT, Prof. SCHROYEN, Prof. NAUWYNCK and Prof. HAMAÏDIA**. Your expertise and perspectives have greatly improved the quality of my work.

I also would like to thank my colleagues from Lanzhou Veterinary Research Institute. **Dr. Yuguang FU, Dr. Baoyu LI, Dr. Jianing CHEN, Dr. Bin YANG,** Thank you for your help and support both in my research and in my life. **Dr. Yang LI, Dr. Na ZHANG, Dr. Yue ZHANG, Dr. Ning YANG, Dr. Shanshan YANG, Dr. Caiying WANG, Dr. Shuxian LI, Xin HUANG, Wenjie LI, Chen TAN, Jing ZHAO, Jing YANG, Yifei CAI, Xue RUI, Yuanyuan LIU and other colleagues in the AIG group.** Thank you for your tremendous help and valuable insights in my research work. I have greatly benefited from every collaboration and discussion with you. Moreover, my sincere thanks to my colleagues from TERRA. **Jacques Jean-Rock, Dr. Joris Thomas, Jouant Thomas and Mei.** I am truly grateful for the support and assistance you've provided, both in my work and in my personal life in Gembloux.

Finally, I would like to express my heartfelt gratitude to my family. To **my beloved parents**—thank you for your unwavering support, which has given me the courage to pursue my goals and explore new horizons. To my wife, **Xiaotong Zhu**—thank you for your steadfast encouragement and support. To my brother, **Dr. Yunchong Zhang**, and my sister-in-law, **Xiaoyue Song**—thank you for being an inspiring example that motivates me to keep progressing. And to my sister, **Xiaoyu Zhang**—thank you for all the ways you have supported me in life.

Remark: ChatGPT (OpenAI, 2022, GPT-3.5) was utilized to refine and enhance the clarity of the text in this work. It is important to clarify that while ChatGPT assisted in the writing process by reformulating and correcting various sections, the content itself was not generated by ChatGPT.

Table of contents

List of figures

List of tables

List of acronyms

ACE2	angiotensin-converting enzyme 2
ALDA	aldolase a
AP-1	activator protein 1
APN	aminopeptidase n
ARDS	acute respiratory distress syndrome
AST	aminotransferase
ATG14	autophagy related gene 14;
ATP	adenosine triphosphate
BAY11	bay11-7082
BAY87	bay 87-2243
BECN1	beclin-1
BHK-21	baby hamster syrian kidney-21 cells
CEACAM1a	carcinoembryonic antigen-related cell adhesion molecule 1a
CREA	creatinine
CK	creatine kinase
CMA	chaperone-mediated autophagy
CME	clathrin-mediated endocytosis
Co-ip	co-immunoprecipitation
CoVs	coronaviruses
DAPI	4′,6-diamidino-2-phenylindole
DMEM	dulbecco's modified eagle's medium
DPP4	dipeptidyl peptidase-4
E protein	envelope protein
EGFR	epidermal growth factor receptor
ENO1	enolase 1
EPO	erythropoietin
ER	endoplasmic reticulum
FP	fusion peptide
GAPDH	glyceraldehyde-3-phosphate dehydrogenase
GFP	green fluorescent protein
GLUT1	glucose transporter 1
H&E	hematoxylin and eosin
HEK-293T	human embryonic kidney 293t cells
HIF-1α	hypoxia-inducible factor-1α
HMGB1	high mobility group box-1
HREs	hypoxia response elements
HS	heparin sulfate
HSV-1	herpes simplex virus type 1
IFA	immunofluorescence assay
IFNs	interferons
IL-1β	interleukin 1β
IL-6	interleukin 6

IL-8	interleukin 8
IRF	interferon regulatory factor
ISGs	interferon-stimulated genes
LDHA	lactate dehydrogenase a
LTR	long terminal repeat
M protein	membrane protein
MAPK	mitogen-activated protein kinase
mGluR2	metabotropic glutamate receptor subtype 2
MDA5	melanoma differentiation-associated factor 5
MOI	multiplicity of infection
mTOR	mammalian target of rapamycin
Muc2	mucin 2
MyD88	myeloid differentiation primary response protein 88
N protein	nucleocapsid protein
NEK7	nima-related kinase 7
NF-κB	nuclear factor kappa-light-chain-enhancer of activated b cells
NLRs	nuclear oligomeric domain (nod)-like receptors
NSP	non-structural protein
OASL	oligoadenylate synthetase-like
ORF	open reading frame
PAMPs	pathogen-associated molecular patterns
PDCoV	porcine delta coronavirus
PED	porcine epidemic diarrhea
PEDV	porcine epidemic diarrhea virus
PFKL	phosphofructokinase liver type
PGK1	phosphoglycerate kinase 1
PHDs	prolyl hydroxylases
PHEV	porcine hemagglutinating encephalomyelitis virus
PIK3C3	phosphatidylinositol 3-kinase catalytic subunit type 3
PKM2	pyruvate kinase m2
PM	potassium molybdate
PRCV	porcine respiratory coronavirus
PRRs	pattern recognition receptors
PtdIns3K	class iii phosphatidylinositol 3-kinase
RBD	receptor-binding domain
RdRP	rna-dependent rna polymerase
RFP	red fluorescent protein
RIG-I	retinoic acid-inducible gene i
RLRs	retinoic acid-inducible gene i (rig-i)-like receptors
RSV	respiratory syncytial virus
RT-qPCR	real-time quantitative pcr
S protein	spike protein
SA	sialic acid
SADS-CoV	swine acute diarrhea syndrome coronavirus
SARS-CoV-2	severe acute respiratory syndrome coronavirus 2
siRNA	small interfering rna

ST cells	swine testis cells
TCID50	50 % tissue culture infective dose
TfR1	transferrin receptor 1
TGE	transmissible gastroenteritis
TGEV	transmissible gastroenteritis virus
TLRs	toll-like receptors
TNF-α	tumor necrosis factor-α
TRIF	tir-domain-containing adaptor-inducing interferon-β
ULK1	unc-51-like autophagy activating kinase 1
UTR	untranslated region
VHL	von hippel-lindau
VSV	vesicular stomatitis virus

Chapter 1

Introduction

Coronaviruses (CoVs) are the positive-sense RNA viruses, belonging to the *Coronaviridae* family within the order *Nidovirales*. they have four genera: *alphacoronavirus, betacoronavirus, gammacoronavirus and deltacoronavirus.* CoVs are responsible for a variety of respiratory, digestive, and nervous system infections in both mammals and birds[1-2]. Due to their propensity for recombination and the naturally high mutation rates, coronaviruses have posed a significant threat to both human and animal health[3]. This thesis mainly focuses on porcine coronaviruses, which pose a significant challenge to the global pig industry. Firstly, this thesis developed antiviral approach by targeting virus entry. Secondly, the mechanisms by which porcine coronaviruses induce inflammation were elucidated, leading to the discovery of novel antiviral targets. This work provides valuable insights and potential strategies for the preventing of porcine coronaviruses infection.

1.1 Overview of porcine coronaviruses

Six CoVs are known to infect pigs. Among them, four are categorized under the genus *Alphacoronavirus*. These include transmissible gastroenteritis coronavirus (TEGV), porcine respiratory coronavirus (PRCV), porcine epidemic diarrhea virus (PEDV), and swine acute diarrhea syndrome coronavirus (SADS-CoV). Additionally, one CoV falls under the genus *Betacoronavirus*, known as porcine hemagglutinating encephalomyelitis virus (PHEV). Lastly, the sixth CoV is classified under the genus *Deltacoronavirus*, identified as porcine deltacoronavirus (PDCoV) [4-6].

1.1.1. Epidemiology and pathogenic characteristics

Transmissible gastroenteritis (TGE) was initially reported in the United States in 1946, marking the beginning of a global spread. Subsequent outbreaks in Europe, Asia, Africa, and South America ensued, causing substantial economic losses in the swine industry worldwide[7-8]. TGEV infects pigs, particularly affecting piglets under 1 week of age. The primary clinical signs of TGEV infection include severe diarrhea, vomiting, dehydration, and enteritis etc. The disease progresses rapidly and can be fatal within days of infection[9].

The discovery of PRCV was based on a survey performed in 1984 in Belgium[10]. PRCV has been observed in several European countries, Asia and United States[4]. This virus causes respiratory infections and emerged as a variant of TGEV through a natural deletion in the S gene[11]. PRCV typically manifests as mild to moderate respiratory symptoms, such as coughing and nasal discharge, in pigs of all ages. Unlike TGEV, PRCV generally does not cause gastrointestinal disease. It spreads through direct contact with infected pigs or their respiratory secretions[12].

Porcine epidemic diarrhea (PED) was initially identified in the United Kingdom in 1971 as a severe enteric disease characterized by sporadic outbreaks[13]. PED inflict substantial economic losses on breeding farms due to the elevated mortality rates among piglets. In Asia, PEDV was initially identified in 1982 and has since become endemic[13]. Since 2010, PEDV has been responsible for substantial economic losses to pork producers in many Asian countries[14]. This virus predominantly targets the epithelial cells of the small intestine, inducing acute watery diarrhea, vomiting, dehydration, and anorexia, particularly affecting nursing piglets[15].

SADS-CoV, a new member of the genus *Alphacoronavirus*, was initially detected as the causative agent of a severe swine disease outbreak in southern China in 2017[6, 16]. This virus results in significant mortality rates, particularly among young pigs. The outbreak resulted in the deaths of approximately 24,500 piglets and inflicted significant economic losses. Similar to TGEV and PEDV, SADS-CoV mainly attacks intestine of pigs [17-18].

PHEV was first reported in Canada in 1957 and firstly isolated in 1962[19-20]. It has been reported in various countries, including the United States, Canada, Mexico, Japan, Korea, and China[21]. PHEV primarily targets the central nervous system of pigs, causing encephalomyelitis characterized by neurological symptoms such as tremors, ataxia, and hind limb paralysis[21]. Histopathological examination typically reveals perivascular cuffing, gliosis, and neuronal degeneration in the brain and spinal cord[22].

PDCoV was first identified in Hong Kong in 2012[23]. Since then, it has been detected in several countries, including the United States, Canada, South Korea, and Thailand[24-25]. PDCoV primarily affects the gastrointestinal tract of pigs, leading to clinical signs such as diarrhea, vomiting, dehydration, and reduced feed intake. In severe cases, PDCoV infections can result in high mortality rates, particularly among piglets[26].

1.1.2. Virus structure and genome

Porcine coronaviruses possess a distinct spherical morphology, characterized by a core particle housing elongated RNA polymers and phosphorylated nucleocapsid (N) proteins, enveloped by an outer membrane[27]. This membrane is embellished with membrane (M) proteins, envelope (E) proteins, and spike (S) proteins, collectively referred to as structural proteins[28]. The M protein, functioning as a transmembrane glycoprotein, plays a pivotal role in maintaining the virus structural integrity and facilitates assembly in conjunction with the E protein, a membrane-associated polypeptide[1, 29-30]. Meanwhile, the S protein, prominently showcased on the viral envelope, orchestrates crucial steps in virus entry and infection, including host cell recognition, binding, and subsequent membrane fusion[31-33] **(Figure 1)**.

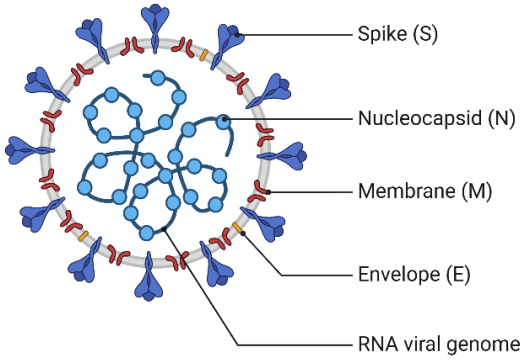

Figure 1. The schematic diagram illustrates the structure of the coronaviruses.

The lipid bilayer, embedded with the S, M, and E proteins, encases the core structure consisting

of the viral RNA genome. This genome is bound to the N protein, forming an extended helical ribonucleoprotein (RNP) complex. The diagram was created in BioRender.com.

The genomes of TGEV and PRCV are approximately 28 kb in length and organized as follows: they start with a 5' untranslated region (UTR), followed by the open reading frame 1a/1b (ORF1a/1b), which encodes non-structural proteins (NSP)1–10 and NSP11–16. Subsequently, the genes encoding the S, E, M, N proteins are sequentially arranged, with a 3' UTR following them. Additionally, three accessory genes—named 3a, 3b, and 7—are interspersed within the structural genes in the 3' region of the genome[28, 34]. PRCV S protein gene has a specific deletion mutation compared to TGEV S protein **(Figure 2)**.

The PEDV genome is about 28 kb and comprises two overlapping ORFs encoding two polyproteins (pp1a and pp1ab) and five other proteins, S, ORF3, E, M and N; several mutations or deletion in the S1 and N protein regions have been identified and showed a trend of high prevalence in recent years[31, 35] **(Figure 2)**.

The genome of SADS-CoV spans approximately 27 kb and encompasses nine ORFs, including ORF1a, ORF1b, and genes encoding the S, E, M, and N proteins. Additionally, it harbors three accessory genes: NS3a, NS7a, and NS7b[6]. Notably, SADS-CoV exhibits a high degree of similarity, with 95% identity, to a coronavirus discovered in bats known as HKU2-CoV[6, 36] **(Figure 2)**.

PHEV is a large enveloped virus with a non-segmented, positive-sense RNA genome of approximately 30 kb, comprising 11 ORFs. ORFs 1a and 1b encode replicase polyproteins pp1a and pp1ab, which are cleaved into 16 NSPs (NSP1–16)[21]. The remaining ORFs encode four canonical structural proteins –S, E, M, and N proteins – along with accessory proteins NS2, NS4.9, NS12.7, and N2. Furthermore, like other hemagglutinating coronaviruses, PHEV also contains an envelope-associated glycoprotein, hemagglutinin-esterase (HE), encoded by ORF3[37] **(Figure 2)**.

The genome organization of PDCoV includes a structured arrangement starting with a 5' UTR, followed by ORF1a/1b, S, E, M, nonstructural protein 6 (NS6), N, nonstructural protein 7 (NS7), and finally, a 3' UTR[38] **(Figure 2)**.

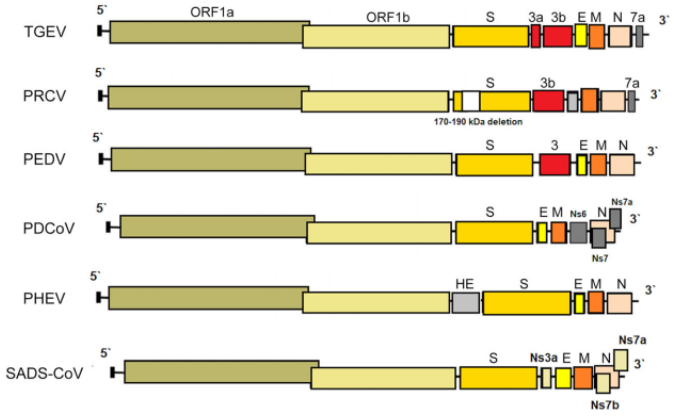

Figure 2.The genome structures of porcine coronaviruses.

S-Spike structural gene, E-envelope, M-membrane, N-nucleoprotein, HE-hemagglutinin-

esterase, Ns3a, Ns6, Ns7, Ns7a, Ns7b-accessory genes[4].

1.1.3. Virus Infectious cycle

1.1.3.1 Attachment and entry

The initial stage of porcine coronaviruses infection entails recognition and binding to host cell surface receptors, triggering invasion. Following this, mechanisms like endocytosis facilitate the release of the viral genome into the host cell, promoting replication and proliferation[1]. The S protein of coronavirus is crucial for the virus binding to host cell receptors and membrane fusion. The S protein is a type I transmembrane fusion protein with a large molecular weight. During viral particle packaging, it is cleaved by proteases into two subunits, S1 and S2. In specific, S1 contains the receptor-binding domain (RBD), responsible for virus-host cell recognition and binding, while S2 contains the fusion peptide (FP), crucial for membrane fusion during virus-host cell interaction[39-40]. The coronavirus S protein directly influences virulence, and the types of receptors it recognizes and their distribution within the host organism are key factors in determining porcine coronaviruses host specificity and tissue tropism[41].

It has been reported that coronaviruses can be internalized into host cells by four kinds of cell receptors, including angiotensin-converting enzyme 2 (ACE2), aminopeptidase N (APN), dipeptidyl peptidase 4 (DPP4), and carcinoembryonic antigen-related cell adhesion molecule 1 (CEACAM1)[42-44]. It is reported porcine coronavirus mainly depends on APN. In specific, studies found that APN is the functional receptor of TGEV and PRCV by binding with its S protein[44-45]. APN knockout pigs are resistant to TGEV[46]. In addition, epidermal growth factor receptor (EGFR) and sialic acid are reported to be the co-factors of TGEV entry[47-48]. In contrast, although PEDV also has a high affinity for APN, it is not the functional receptor for PEDV infection. APN-null neonatal piglets are protected from TGEV but not PEDV[49]. In addition, PEDV S protein has sialic acid binding activity to facilitate cell entry[50]. Some studies reported that transferrin receptor 1 (TfR1) can interacts with PEDV S1 protein to promote viral entry[51]; ALIX and TSG101 also play indispensable roles in the cellular entry and replication of PEDV[52]. But the functional receptor for PEDV infection in hosts remains undetermined and requires further research. Moreover, it is reported that PDCoV S protein can bind with APN to enter cells[53]. Studies have analyzed the crystal structure of the PDCoV S protein RBD in complex with human and porcine APN cell receptors. These studies revealed that PDCoV binds to conserved amino acid sites on the receptors of both species. Furthermore, it was found that the RBD of PDCoV has highly similar binding regions on both human and porcine APN, which may underlie its ability to infect both pigs and humans[54]. For SADS-CoV, although Chen et. reported ALIX and TSG101 are essential for cellular entry of SADS-CoV, the functional receptor is still unclear and need to be further explored. Lastly, some studies identified the receptor molecules that PHEV relies on to invade neural cells, including the carbohydrate co-receptors neuraminic acid (SA) and heparin sulfate (HS), as well as the protein functional receptor DPP4. Furthermore, it was demonstrated that the key amino acid sites in the binding interface of the PHEV S protein RBD with DPP4 are A288, R289, and the glycosylation site N223[42, 55-56].

1.1.3.2 Replication and release

coronaviruses can enter host cells through endocytosis and membrane fusion, releasing their genomic RNA into the cytoplasm. The positive-sense RNA is translated to produce precursor proteins for negative-sense RNA polymerase, which subsequently undergoes proteolytic processing to produce RNA-dependent RNA polymerase (RdRP)[1, 57-58]. The RdRP synthesizes full-length negative-sense RNA templates, which serve as a template for the production of subgenomic mRNAs. Translation of these subgenomic mRNAs produces viral structural proteins[59]. Viral membrane proteins are assembled in the endoplasmic reticulum (ER) and transported out in vesicles (small sacs). Within the ER-Golgi intermediate compartment (ERGIC), the positive-sense RNA by capsid proteins is recognized by membrane proteins, forming vesicles that enclose the RNA. Subsequently, the virus is released through exocytosis (fusion of Golgi-derived vesicles with the plasma membrane), allowing the virus to infect other cells[4, 60] **(Figure 3)**.

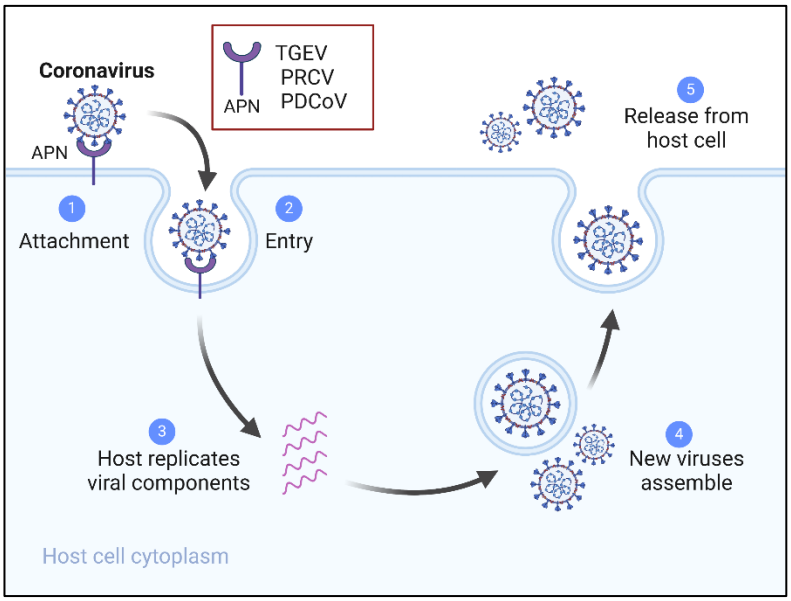

Figure 3. Infectious cycle of porcine coronaviruses

Coronavirus spike protein will interact with the cell receptor to enter the cell by endocytosis. Once inside, the viral RNA genome is released and replicated, leading to the production of viral proteins and new viral genomes. These components are then assembled into new virus particles, which are released from the host cell to infect other cells. TGEV, PRCV and PDCoV depend on cell receptor APN to entry. The diagram was created in BioRender.com.

1.1.4. Immune responses

1.1.4.1. Pattern recognition receptors

The innate immune response constitutes the body's primary defense mechanism against viral invasion and forms the prerequisite and foundation for the adaptive immune response, playing a pivotal role in antiviral defense. During viral infection of

host cells, conserved elements such as genomic nucleic acids, replication intermediates, and encoded proteins are produced, collectively referred to as pathogen-associated molecular patterns (PAMPs)[61]. Host cells possess three principal classes of pattern recognition receptors (PRRs) that identify viral PAMPs: Toll-like receptors (TLRs), RIG-I-like receptors (RLRs), and nucleotide oligomerization domain-like receptors (NLRs)[62]. Activation of these receptors subsequently triggers downstream adaptor molecules, initiating a series of signal transduction cascades that activate transcription factors such as interferon regulating factor 3 (IRF3) and nuclear factor-kappa B (NF-κB). This activation leads to the host innate immune response, inducing the production of interferons (IFNs) and proinflammatory cytokines, thereby facilitating the elimination of the pathogens[63].

1.1.4.2. IFNs responses

IFNs are multifunctional cytokines that were initially discovered due to their antiviral activity. There are three main types identified to date: type I IFNs type II IFNs, and type III IFNs[64]. Type I IFN signaling occurs through the dimeric IFN-α/β receptor, composed of IFNAR1 and IFNAR2. IFNAR2 is responsible for ligand binding, while IFNAR1 induces intracellular signaling cascades. Upon phosphorylation, IFNAR1 phosphorylates the signal transducer STAT2, which subsequently leads to the phosphorylation of STAT1. This forms either STAT1 homodimers or STAT1/STAT2 heterodimers, which then translocate to the nucleus to induce the expression of interferon-stimulated genes (ISGs)[65]. Type II IFN (IFN-γ) signaling is mediated by the heterodimeric IFNGR complex, comprising IFNGR1 and IFNGR2, which are highly expressed on myeloid and lymphoid cells and broadly present on most cell types, including intestinal epithelial cells. IFNGR1 is essential for ligand binding, while IFNGR2 mainly participates in signal transduction. IFN-γ signaling involves multiple pathways, including the classical JAK-STAT pathway, the CRKL-RAP1 pathway, and the PI3K pathway[66]. Type III IFN receptors consist of the heterodimeric complex IFNLR1 and IL10RB, primarily expressed on the surface of epithelial cells. Therefore, they play a crucial role in antiviral defense in epithelial cells. This receptor complex signals through a pathway similar to the JAK-STAT pathway used by the type I IFN receptor complex and induces many of the same ISGs[67] **(Figure 4).** It is reported that IFNs play a vital role in the defense against virus infection[68]. For example, IFN-β and IFN-λ1/3 have a strong antiviral effect on coronavirus infections, especially among pigs[69-70]. In addition, IFNs can bind to their own receptors to induce the expression of the ISG-oligoadenylate synthetase-like (OASL) which can significantly inhibit PEDV and TGEV infection[71] .

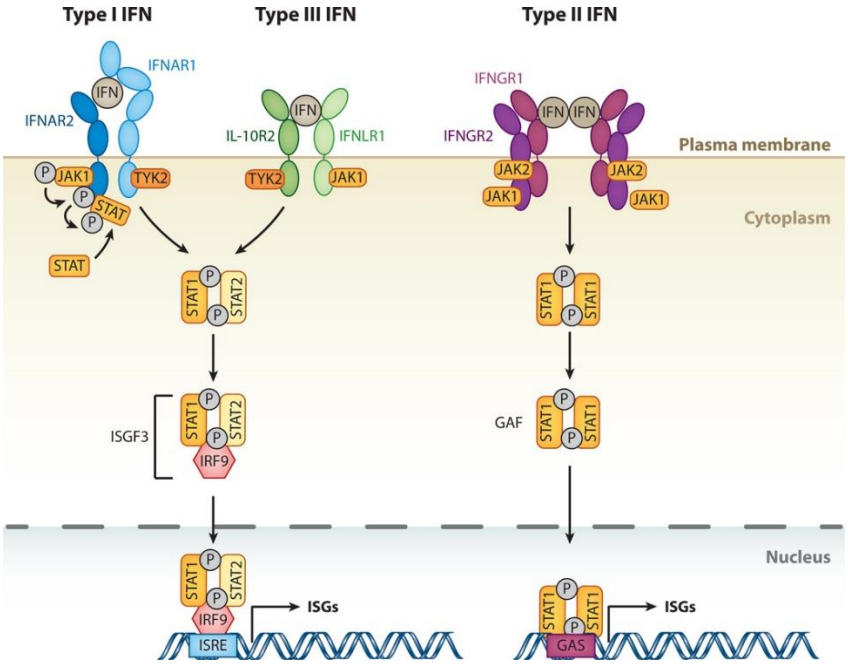

Figure 4. IFN signaling cascade.

The three different classes of IFNs signal through distinct receptor complexes on the cell surface: type I IFNs interact with IFN-α receptor 1 (IFNAR1) and IFN-α receptor 2 (IFNAR2) heterodimers; type III IFNs bind to interleukin-10 receptor 2 (IL-10R2) and IFN-λ receptor 1 (IFNLR1) heterodimers; and type II IFNs engage dimers of heterodimers consisting of IFN-γ receptors 1 (IFNGR1) and 2 (IFNGR2). The binding of both type I and type III IFNs to their respective IFNAR1/2 or IL-10R2/IFNLR1 complexes, which triggers the phosphorylation of JAK1 and TYK2, which then phosphorylate the receptors. This recruits and phosphorylates STAT1 and STAT2, forming a heterodimer that combines with IRF9 to create ISGs. Type II IFN binding to the IFNGR1/2 complex phosphorylates JAK1 and JAK2, leading to STAT1 phosphorylation. Phosphorylated STAT1 binds GAS to induce ISGs[72].

1.1.4.3. Inflammatory responses

The inflammatory response is an innate immune reaction that the body employs to combat invading pathogenic microorganisms and respond to injury. It serves as a crucial mechanism for recognizing and transmitting "danger" signals. Excessive inflammation can lead to damage to tissues and organs[73]. When coronavirus invades, PRRs recognize PAMPs released by coronavirus. This recognition activates downstream signaling pathways, including: NF-κB pathway and mitogen-activated protein kinase (MAPK) pathway[74] **(Figure 5)**.

After viral infection, the host can induce an inflammatory response through multiple pathways, among which the NF-κB signaling pathway is most frequently activated[75]. This pathway plays a crucial role in the process of virus-induced inflammation. The NF-κB signaling pathway can regulate the expression of various cytokines at the

transcriptional level, thereby influencing numerous cellular and physiological activities of the organism[76]. When cells are stimulated by inflammatory factors, bacterial or viral products, signals are transmitted into the cell via TLRs or various cellular stressors. This triggers a series of adaptor proteins that activate IKKs (primarily IKKα and IKKβ) and the regulatory factor NEMO, forming a complex. The activated IKKs complex stimulates the phosphorylation and ubiquitination of IκBs, leading to their degradation and the release of the p65/p50 complex[77]. The p65/p50 complex is further phosphorylated and translocated into the nucleus, where it binds to target sites, thereby activating downstream gene transcription. The phosphorylation of NF-κB is essential for mediating the transcription of target genes[77]. It is reported that TGEV contributes to inflammation via NF-κB activation[78-79]. These reports underscore the critical role of NF-κB on porcine coronaviruses-induced inflammation.

Moreover, MAPK acts on downstream transcription factors, playing a significant role in mediating the inflammatory response and cytokine production[80]. Activator protein 1 (AP-1) is a crucial transcription factor targeted downstream of JNK and p38. It is a dimeric complex formed by members of the c-Jun, c-Fos, Maf, and ATF families. When upstream signals are activated, JNK1/2 and p38 translocate into the nucleus, where they specifically phosphorylate serine and threonine residues on AP-1 subunits. The activated AP-1 then initiates the transcription of inflammatory cytokines[81]. Studies have shown that various viruses can activate different MAPK signaling pathways upon infecting host cells, which induces the production of pro-inflammatory cytokines[82-84].

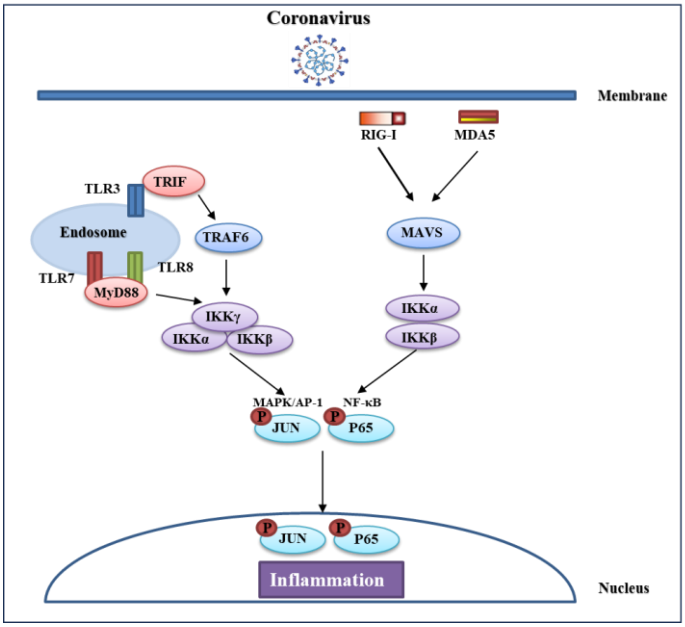

Figure 5. Inflammatory pathways related to coronavirus

PRRs related to coronavirus, including TLR3, TLR7, TLR8, retinoic acid-inducible gene 1 (RIG-I) and melanoma differentiation-associated gene 5 (MDA5) are appointed to sense

PAMPs. Through a series of signaling cascades, it can activate many pathways associated with inflammation, involving MAPK and NF-κB to induce inflammatory responses.

1.2 Autophagy

1.2.1. Concept and classification of autophagy

The process of autophagy, where cells "eat themselves," is a cellular mechanism for self-degradation and recycling of intracellular components. It can be classified into three types based on physiological functions and transport mechanisms: macroautophagy, microautophagy and chaperone-mediated autophagy (CMA)[85]. Macroautophagy, commonly referred to as autophagy, involves the formation of double-membrane autophagosomes that capture cytoplasmic proteins or damaged organelles and deliver them to lysosomes for degradation. Microautophagy involves the lysosomal membrane directly engulfing cytoplasmic components[86]. In CMA, the chaperone Hsc70 recognizes substrate proteins with a specific amino acid sequence (KFERQ) and transports them into lysosomes via the receptor LAMP2A for degradation[87]. These processes are interconnected and collectively maintain cellular function by degrading and recycling cellular components. The interaction between autophagy and the ubiquitin-proteasome system is essential for cellular homeostasis, requiring coordinated action to regulate cellular metabolism and function[88] **(Figure 6)**.

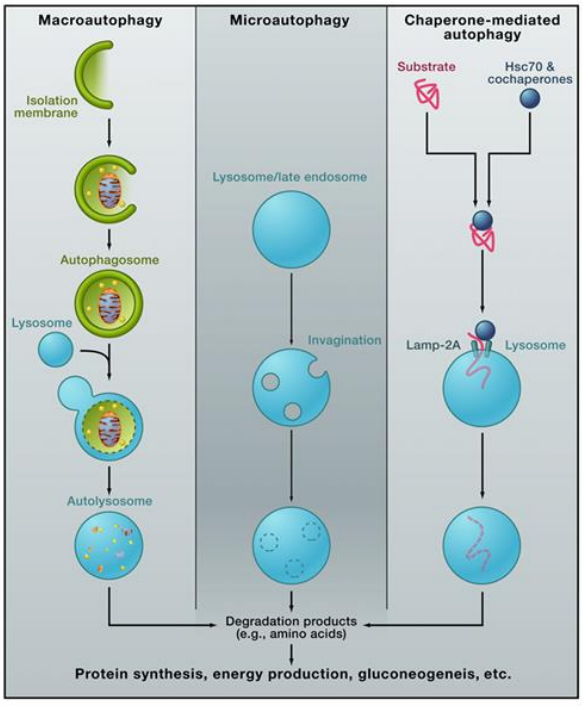

Figure 6. Three types of autophagy.

Autophagy, the process of cellular self-degradation, comprises three main mechanisms:

macroautophagy, microautophagy, and chaperone-mediated autophagy. In macroautophagy, a portion of cytoplasm and organelles is enclosed by an isolation membrane to form an autophagosome, which fuses with a lysosome for material degradation. Microautophagy directly engulfs small cytoplasmic pieces by invagination of the lysosomal membrane. Chaperone-mediated autophagy recognizes specific protein sequences, guiding their translocation into lysosomes for degradation. These pathways collectively maintain cellular health and respond to stress[89].

1.2.2. The mechanism of autophagy

The process of autophagy comprises several steps: induction, vesicle nucleation, selective substrate recognition, autophagosome formation, autophagosome-lysosome fusion, substrate degradation, and nutrient recycling[90].

The initial step involves the regulation and nucleation of vesicles. The serine/threonine kinase mammalian target of rapamycin (mTOR) is a key regulator of autophagy. mTOR inhibits autophagy, and treatment with rapamycin enhances autophagy[91]. Downstream of mTOR lies a group of autophagy-related proteins[92]. The yeast ATG1 kinase, downstream of the rapamycin target site, regulates autophagosome formation. ATG6 is another autophagy regulatory factor. Yeast studies have shown that ATG6 is essential for the formation of isolation membranes and recruits other ATGs[93]. The mammalian homolog of ATG6 is Beclin 1 which forms a complex with phosphatidylinositol 3-kinase (PI3K or hVps34), promoting autophagy. This process requires the interaction between Beclin 1 and hVps34, which is regulated by other components of the multiprotein complex[94]. UVRAG and Ambra1 bind to Beclin 1, enhancing the interaction between Beclin 1 and hVps34, thereby stimulating autophagy[95-96].

In the second step, vesicle elongation and completion occur. The elongation of isolation membranes depends on the recruitment of other ATG proteins, including two ubiquitin-like conjugation systems: ATG12 and LC3. ATG12 forms a covalent bond with ATG5, and the ATG12-ATG5 conjugate associates with ATG16L to form a ~800 kDa complex[97]. ATG16L targets the ATG12-ATG5 conjugate to the isolation membrane, facilitating the binding of LC3 to phosphatidylethanolamine (PE). This process converts cytosolic LC3-I into the membrane-bound form PE-LC3-II, which serves as a classical marker of autophagy[98].

In the third step, autophagosomes and lysosomes merge to create autolysosomes. STX17 binds with SNAP29 and VAMP8 to assemble a SNARE complex, which is then transferred to the autophagosomal membrane, facilitating the fusion of lysosomes with autophagosomes to generate autolysosomes[99].

Finally, in the fourth step, vesicle rupture and content degradation occur, which are recycled[100] **(Figure 7)**.

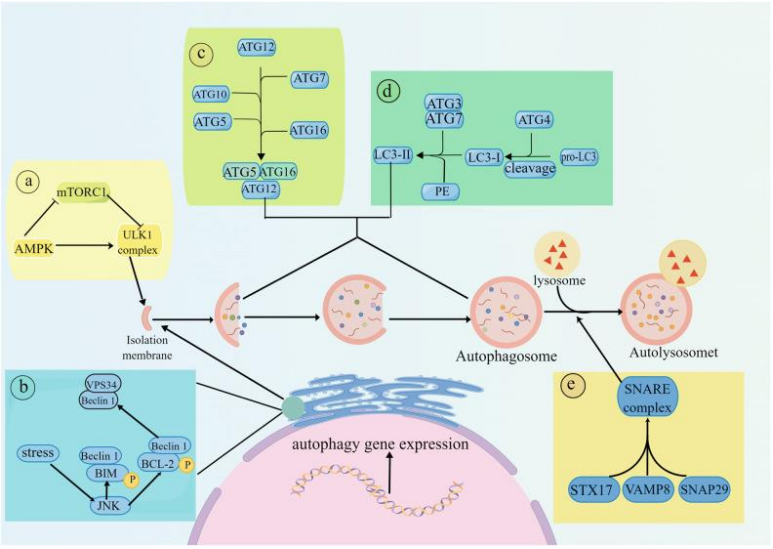

Figure 7. Mechanism of autophagy.

Autophagy, a complex self-degradation process, involves several key steps: a) Signaling pathways, such as AMPK inhibiting mTORC1, initiate autophagy by promoting the formation of the ULK1 complex and the production of autophagic vesicles. b) The Beclin-1/VPS34 complex extends autophagic vesicles, facilitated by JNK activation, which frees Beclin1 to activate VPS34 and promote vesicle extension. c) The ATG12-ATG5 complex polymerizes to form ATG5-ATG12-ATG16L, which fuses with autophagic vesicles to aid in their formation. d) LC3 undergoes processing and is inserted into autophagosomes, with ATG4 cleaving LC3 into LC3-I and subsequent conversion to LC3-II before insertion. e) Autophagosomes and lysosomes fuse to form autolysosomes, facilitated by the formation of a SNARE complex involving STX17, SNAP29, and VAMP8, enabling fusion between lysosomes and autophagosomes[99].

1.2.3. Autophagy in coronaviruses infection

Research has confirmed that autophagy serves as an inducible factor and effector in the immune response against pathogens, acting as a natural defense mechanism to promote the clearance of intracellular pathogens[101]. Autophagy also plays a crucial role in viral replication, transcription, and the pathogenesis of viral infections. In specific, it is reported that autophagy negatively regulates TGEV replication[102] and PGAM5 degrades PDCoV N through autophagy by interacting with the cargo receptor P62 and the E3 ubiquitination ligase STUB1[103]. BST2 suppresses PEDV replication by degrading virus N protein with selective autophagy[104]. Recent studies indicate that some viruses have evolved various strategies to resist, evade, or even exploit cellular autophagy to enhance their own proliferation. PEDV infection activates AMPK and JNK through TAK1 to induce autophagy and enhance virus replication[105]. SARS-CoV-2 ORF3a is a selective inhibition of STING-triggered autophagy to facilitate viral replication[106]. Jiao et. found that the enteric coronavirus nsp2 serves as a

virulence factor by recruiting NBR1 for the autophagic targeting of TBK1, thereby dampening the innate immune response[107]. These studies underscore the crucial role of autophagy in coronavirus infection, providing a new perspective for the prevention and control of coronaviruses.

1.3 Hypoxia inducible 1-α (HIF-1α)

1.3.1. The production mechanism of HIF-1α

HIF-1 is a crucial regulatory factor in oxygen homeostasis and a significant transcription factor under hypoxic conditions. It is known to regulate over a hundred target genes, including various glucose transporters, vascular endothelial growth factor (VEGF), insulin-like growth factor, and erythropoietin[108]. The regulatory scope of HIF-1 encompasses energy metabolism, growth, proliferation, angiogenesis, biosynthesis, and apoptosis. HIF-1 is modulated by cellular oxygen concentration changes and is a key transcription factor in the body's response to hypoxia, maintaining oxygen balance, and mediating the transcriptional activation of hypoxia-related genes[109].

HIF-1 is a heterodimer composed of two subunits: HIF-1α and HIF-1β, with HIF-1α serving as the functional subunit and HIF-1β as the structural subunit[110]. Under normoxic conditions, residues Pro-402 and Pro-564 on HIF-1α can be hydroxylated by prolyl hydroxylases (PHDs)[111]. Consequently, HIF-1α undergoes ubiquitination through the action of an E3 ubiquitin ligase complex, which includes Von Hippel-Lindau (VHL), elongin B/C (EloB/C), Cul2, Rbx1, and E2 ubiquitin-conjugating enzyme, leading to its proteasomal degradation[112]. Under hypoxic conditions, this process is inhibited, allowing HIF-1α levels to stabilize and translocate to the nucleus, where it dimerizes with HIF-1β to form HIF-1. HIF-1 can then bind to hypoxia response elements (HREs) and initiate the transcription of downstream target genes[113] **(Figure 8)**.

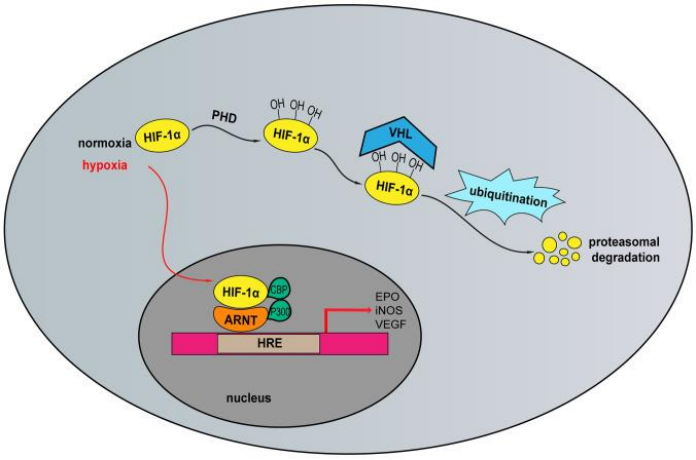

Figure 8. Oxygen-dependent regulation of HIF-1α.

Under normal oxygen conditions, HIF-1α protein undergoes hydroxylation by prolyl

hydroxylases PHD1, PHD2, and PHD3. Once hydroxylated, HIF-1α is targeted for degradation by VHL through the ubiquitin-proteasome pathway. However, in hypoxic conditions, HIF-1α levels increase as it accumulates and translocates to the nucleus. Here, it forms a heterodimeric complex with ARNT, which binds to the promoter region of the HRE. The recruitment of CBP/p300 induces the transcription of downstream target genes[114].

1.3.2. HIF-1α-mediated glycolytic flux

Mammals utilize various mechanisms to maintain metabolic balance under hypoxic conditions. In systemic hypoxia, where oxygen levels and the blood's oxygen-carrying capacity decrease, erythropoietin (EPO) and VEGF are induced, enhancing oxygen delivery and alleviating the oxygen supply-demand imbalance[115-116]. Cellular metabolic pathways sense hypoxia to compensate for reduced oxygen supply. A key cellular adaptation involves shifting from oxidative phosphorylation to glycolysis for ATP production[117]. In hypoxia, genes encoding respiratory chain enzymes decrease, while glycolytic enzyme genes increase or their transcription is upregulated, including aldolase A (ALDA), lactate dehydrogenase A (LDHA), phosphoglycerate kinase 1 (PGK1), pyruvate kinase M2 (PKM2), phosphofructokinase liver type (PFKL), and enolase 1 (ENO1)[118]. In hypoxic cells, HIF-1 binding sites are exposed during transcriptional activation in the promoters of ALDA, LDHA, PGK1, PKM2, PFKL, ENO1, and these enzymes. HIF-1α activates these enzyme genes by binding to these sites, thereby inducing the synthesis of glycolytic enzymes and promoting glycolysis[119-120]. This process generates a large amount of adenosine triphosphate (ATP) through glycolysis to meet the energy metabolic needs of the body. Additionally, it is theorized that glucose transporter 1 (GLUT1) can also be induced by hypoxia. The HIF-1α binding site on the promoter of GLUT1 has been confirmed[121]. This process also starts with HIF-1α inducing the genes of these enzymes, underscoring the critical role of HIF-1α in the induction of glycolysis.

1.3.3. The effect of HIF-1α in virus infection

HIF-1α plays a significant role in viral infections, with studies reporting its promotion of the replication of SARS-CoV-2, HIV-1, and H1N1 infection etc.[122-125]. SARS-CoV-2 infection can induce mitochondrial damage and the production of mitochondrial reactive oxygen species (Mito-ROS) to promote HIF-1α expression. In turn, HIF-1α exacerbates viral infection and inflammatory responses[122]. HIF-1α has also been reported to activate the HIV-1 promoter through a GC-rich binding domain within the long terminal repeat (LTR), thereby increasing viral replication[124]. H1N1 influenza A virus infection activates the HIF-1 signaling pathway in alveolar epithelial cells, promoting host cell glycolysis to support rapid viral replication[123]. However, the role of HIF-1α in porcine coronavirus is still unclear and warrants further investigation.

Chapter 2

Objective

The primary goal of this thesis is to develop and validate novel and potent strategies to combat porcine coronaviruses infections, which pose significant health risks to pigs and lead to considerable economic losses in the global swine industry. This thesis aims to address the urgent need for effective measures by focusing on two critical aspects: preventing viral entry by targeting cell receptors and understanding the mechanisms of virus-induced inflammatory responses to discover new antiviral targets.

APN is a critical host receptor for coronaviruses. Modulating APN expression offers a promising strategy for managing infections by APN-dependent coronaviruses and their variants. Therefore, the initial objective is to find an approach to modulate APN expression. Fortunately, clinical observations have shown that PM, a chemical compound used in feed ingredients, effectively prevents diarrhea and reduces diarrhea-induced mortality in piglets. In addition, our preliminary experiments revealed that PM can inhibit APN expression. However, the mechanisms behind these effects are not yet well understood and warrant further investigation *in vitro* and *ex vivo*. Additionally, we conducted *in vivo* studies in pig models to evaluate the feasibility and safety of using PM for controlling APN-dependent coronavirus entry. This part will provide valuable insights for the preventing of APN-restricted coronaviruses infection. This part refers to Chapter 3.

Excessive inflammation results in severe organ damage and a cascade of associated symptoms, ultimately contributing to high mortality rates of piglets. Despite its profound impact, the underlying mechanism of this inflammatory response remains poorly understood. Therefore, the secondary objective is to elucidate the inflammatory mechanisms associated with porcine coronavirus infections. Utilizing intestinal organoids, we aim to employ a model that accurately reflects the physiological immune responses to viral infections. This part of the study will focus on PRRs, inflammatory pathways and proinflammatory factors involved in TGEV-induced inflammation. We seek to understand key factors that influence inflammatory responses and viral replication. This part will reveal the mechanism of inflammatory responses and provide novel antiviral targets. This part refers to Chapter 4 and 5.

Chapter 3

Potassium molybdate blocks APN-dependent coronavirus entry by degrading receptor via PIK3C3-mediated autophagy

Foreword

In our clinical practice, we observed that addition of potassium molybdate (PM) to the feed could dramatically reduce diarrhea and diarrhea-related mortality in piglets. However, the underlying mechanisms remain elusive and merit further investigation.

In the following article, we conducted the effect of PM on porcine coronaviruses *in vitro and ex vivo*. Furthermore, the mechanism of PM controlling porcine coronaviruses infection, especially TGEV and PRCV, was further explored. Lastly, *in vivo* experiments further confirmed PM with a concentration of no cytotoxicity negatively regulates TGEV infection in piglets.

This chapter has been adapted from the article:

Zhang Y[#]**,** Zhang N[#], Zhang Y, Yang L, Yang N, Cai Y, Tan C, Zhao J, Li W, Liu Y, Rui X, Wu J, Fu Y, Liu G[*]. Potassium Molybdate blocks APN-dependent coronavirus entry by degrading receptor via PIK3C3-mediated autophagy. **Journal of Virology**. (Accepted).

Summary

Swine enteric coronaviruses pose a significant challenge to the global pig industry, inflicting severe diarrhea and high mortality rates among piglets and resulting in substantial economic losses. Despite numerous efforts, there remains an urgent need for an effective countermeasure against these coronaviruses. In clinical observations, feed ingredients of potassium molybdate (PM), a chemical oxidant, has demonstrated efficacy in preventing diarrhea and mortality in piglets. However, the underlying mechanisms remain elusive and merit further investigation. In this study, we revealed that PM effectively inhibited the infection of both APN-dependent coronaviruses, transmissible gastroenteritis virus (TGEV), and porcine respiratory coronavirus (PRCV), both *in vitro* and *ex vivo*. Specifically, PM were found to block TGEV and PRCV penetration by degrading the cell receptor APN through the upregulation of PIK3C3 expression. In addition, knockdown and knockout of PIK3C3 resulted in the attenuation of PM-induced autophagy, thereby rescuing APN expression and viral infection. Correspondingly, replenishment of PIK3C3 in PIK3C3-null ST cells restored PM-mediated APN degradation and successfully blocked viral entry. Furthermore, our findings demonstrated that PM promoted the assembly of the PIK3C3-BECN1-ATG14 complex, leading to the induced autophagic degradation by upregulating PIK3C3 Ser249 phosphorylation. *In vivo* experiments further confirmed that PM induced PIK3C3-mediated autophagic degradation of APN, thereby limiting the pathogenicity of TGEV. In summary, our study for the first time identified the mechanism by which PM blocked TGEV and PRCV internalization by degrading the cell receptor APN via PIK3C3-mediated autophagy. This study provides valuable insights and potential strategies for the preventing of APN-restricted coronavirus infection.

3.1 Introduction

Coronavirus poses a severe threat to human and animal health, especially due to the prevalence of severe acute respiratory syndrome coronavirus 2 (SARS-CoV-2) in humans and some intestinal and respiratory coronavirus in farming [15, 126]. It has been reported that coronaviruses can be internalized into host cells by four kinds of cell receptors, including angiotensin-converting enzyme 2 (ACE2), aminopeptidase N (APN), dipeptidyl peptidase 4 (DPP4), and carcinoembryonic antigen-related cell adhesion molecule 1 (CEACAM1) [42]; moreover, APN is the main receptor for the majority of alphacoronaviruses (family *Coronaviridae*, order *Nidovirales*), such as transmissible gastroenteritis virus (TGEV), and porcine respiratory coronavirus (PRCV), although porcine APN is not the main functional receptor for porcine epidemic diarrhea virus (PEDV) [127-128]. Specifically, TGEV and PEDV primarily attack small intestinal epithelial cells and cause acute watery diarrhea, vomiting, dehydration, and anorexia, with high morbidity and mortality, particularly in nursing piglets [15, 129]. In addition, PRCV, a naturally occurring spike deletion mutant of TGEV, mainly infects the respiratory tract rather than the intestine and causes coughing, interstitial pneumonia, and lung lesions [130]. Due to the lack of effective approaches for prevention and control, these porcine coronaviruses have resulted in significant financial losses in the swine industry worldwide, suggesting that new antiviral methods are urgently needed.

Previous investigations have reported that a great variety of medicines are proposed to control porcine coronavirus infection *in vitro*. Specifically, tomatidine and hypericin inhibit alphacoronavirus replication by targeting the 3CL protease [131-132], while Griffithsin blocks porcine coronavirus attachment and internalization by binding to the viral spike protein [133-134]. Most of these medicines are extremely difficult to apply in clinical therapy because they are mostly derived from plants and are easily decomposed in complex environments *in vivo* [135]. It has been reported that potassium molybdate (PM or K_2MoO_4), a chemical oxidant, is hydrolyzed to potassium ions and molybdate anions, which are both inherent transition metals and are involved in many metabolic pathways throughout life, like oxidative stress etc. [78, 136-137]. This means that PM is more likely to adapt to the body's environment and fulfill its biological function significantly. Based on the prophylactic effect of PM in diarrhea of piglets from clinical practice, the underlying mechanism is worth further elucidation.

Autophagy is an intracellular catabolic process in which damaged organelles and proteins are degraded to maintain cellular homeostasis [138-139]. In addition, autophagy is a very complicated process in which many autophagy-related genes and complex formations are involved, such as the negative regulation of mammalian target of rapamycin (mTOR), Unc-51-like autophagy activating kinase 1 (ULK1) complex activation, class III phosphoinositide 3-kinase (PtdIns3K) complex formation and the generation of double-vesicle autophagosomes and autolysosomes with digestive functions [140-141]. During this process, the PtdIns3K complex is important for the initiation of autophagy and includes phosphatidylinositol 3-kinase catalytic subunit type 3 (PIK3C3), Beclin-1 (BECN1) and autophagy-related gene 14 (ATG14) [142-144]. Furthermore, the binding of PIK3C3, BECN1, and ATG14 generates a phagophore-

specific pool of phosphatidylinositol-3-phosphate (PtdIns3P), leading to the nucleation of the phagophore to induce autophagy [145]. Recent work has shown that autophagy can suppress porcine coronavirus infection in different cell types, but the specific molecular mechanism involved remains unclear [102, 146].

In this study, we discovered for the first time that the PM blocks TGEV and PRCV entry by degrading the receptor APN in different types of models and in the small intestine of piglets. Detailed mechanistic investigations revealed that this degradation was achieved by PIK3C3-mediated autophagy. Thus, our study proposes a novel antiviral strategy to target viral cell receptors and provides insight into blocking APN-dependent coronavirus entry.

3.2 Materials and methods

3.2.1. Cell culture and viruses

Swine testicular cells (ST cells), Vero-E6 cells, PK-1, human embryonic kidney 293T cells (HEK-293T cells), baby hamster Syrian kidney-21 cells (BHK-21 cells) and A549 cells were maintained in Dulbecco's modified Eagle's medium (DMEM) (Sigma–Aldrich, USA, D6429) supplemented with 10% fetal bovine serum (Invigentech, Brazil, A6901). The cells were incubated at 37 °C in a humidified incubator with 5% CO_2. The TGEV Miller, PRCV, PEDV LJX01/2014 and PDCoV strains were maintained in our laboratory, and their titers were $10^{7.25}$ $TCID_{50}$/ml, 10^{6} $TCID_{50}$/ml, $10^{6.25}$ $TCID_{50}$/ml and 10^{6} $TCID_{50}$/ml respectively.

3.2.2. Porcine intestinal 3D organoid culture

Porcine ileum crypts were isolated from pigs and cultured in Matrigel (Corning, USA, 356231) and Organoid Growth Medium (OGM) (Stem Cell, Canada, 06010) containing 10 μM ATP-competitive inhibitor of Rho-associated kinases (Y-27632; CST, USA, 72302) according to the manufacturer's protocol [147].

3.2.3. Establishment of apical-out porcine intestinal organoids

Porcine 3D ileum organoids coated with Matrigel for 1 week were dissociated by incubation in 5 mM cold EDTA buffer on a rotating platform for 1 h at 4 ℃. After that, the organoids were harvested by centrifugation at 250 × g for 5 min, washed with ice-cold DMEM/F12 (Sigma–Aldrich, USA, D0697), and cultured in ultralow-attachment 24-well tissue culture plates (Corning, USA, 3473) in OGM supplemented with 10 μM Y-27632 at 37 °C with 5% CO_2 according to the protocol. The apical-out organoids were generated after 3 days[147].

3.2.4. Porcine intestinal organoid monolayer culture

The 3D ileum organoids were collected using ice-cold DMEM/F12 medium and centrifuged at 250 × g for 5 min after culture for 5 days. The organoid pellet without Matrigel was generated by washing twice with ice-cold DMEM/F12 medium. TrypLE Express (Gibco, USA, 12605-010) was used to disassociate organoids into single cells for 5 min at 37 °C. Single cells or small fragments were resuspended in OGM supplemented with 10 μM Y-27632 and seeded into 48-well plates according to the

manufacturer's protocol [148]. The monolayers reached confluency after 3 days of culture and were used for the follow-up experiment.

3.2.5. Antibodies and reagents

Rabbit pAb against APN (A5662) and rabbit pAb against SQSTM1/P62 (A7758) were obtained from ABclonal. Rabbit mAbs against LC3B (3868), rabbit mAb against ACE2 (4355S), rabbit mAb against P-PIK3C3 (Ser249) (13857), rabbit mAb against P-BECN1 (Ser15) (84966), rabbit mAb against P-ATG14 (Ser29) (92340), rabbit mAb against Flag (D6 W5B) (14793) and mouse mAb against Myc (9B11) (2276) were obtained from Cell Signaling Technology. Rabbit pAb against PIK3C3 (13723-1-AP), rabbit pAb against BECN1 (11306-1-AP), and rabbit pAb against ATG14 (19491-1-AP); mouse mAb against His (66005-1); rabbit pAb against GAPDH (10494-1-AP); and coralite 488-conjugated goat anti-rabbit IgG (H+L) were obtained from Proteintech. Rabbit mAb against CEACAM1 (ab108397), rabbit mAbs against DPP4 (ab215711), goat anti-rabbit IgG H&L (Alex Fluor 594, ab150080) and goat anti-mouse IgG H&L (Alex Fluor 647, ab150115) were obtained from Abcam. TGEV-N and PRCV-N were gifts from Prof. Li Feng (Harbin Veterinary Research Institute, Chinese Academy of Agricultural Sciences). PEDV N was generated in our laboratory. Potassium molybdate was obtained from Sigma–Aldrich. 3-Methyladenine (3-MA) (HY-19312), MG-132 (HY-13259), Z-VAD-FMK (HY-16658B), SBI-0206965 (HY-16966) and 3BDO (HY-U00434) were obtained from MedChemExpress.

3.2.6. Plasmid construction, small interfering RNA (siRNA), and Transfection

The coding sequences of porcine PIK3C3 (NM_001012956.2), BECN1 (NM_001044530.1) and ATG14 (XM_001924990.5) were amplified from the cDNA of ST cells and cloned and inserted into pCMV-Myc, pCDNA3.1-Flag, and pCDNA3.4-His, respectively. The pCMV-Myc-PIK3C3 mutant was constructed by site-directed mutagenesis. RFP and LC3B were cloned and inserted into pEGFP-C1 to construct RFP-EGFP-LC3B plasmids for monitoring autophagic flux. pCMV-HA-APN (pigs) was stored in our laboratory. All plasmids were transfected with Lipofectamine 3000 transfection reagents (Thermo Fisher Scientific, USA, L3000015). Four siRNAs targeting PIK3C3 were designed and synthesized by GenePharma. The sequences of primers used were as follows: PIK3C3-1, 5'-GGACUAUACCAAGAAACAUTT-3'; PIK3C3-2, 5'-GCCAAUGGAUGUAGAGGAUTT-3'; and PIK3C3-3, 5'- GCUCGUCCAAGCUC UCAAATT-3'; and PIK3C3-4 (5'-GCUGGAUAUUGCGUGAUUATT-3'). All siRNAs targeting PIK3C3 were transfected with GP-transfect-Mate according to the manufacturer's instructions.

3.2.7. Histopathological and immunofluorescence analysis

Small intestinal tissues were collected, fixed for 24 h in 10% formalin, dehydrated according to the standard protocol, embedded in paraffin, and subjected to hematoxylin and eosin staining by standard procedures. For immunofluorescence analysis, the organoid monolayers or ST cells were fixed with 4% paraformaldehyde for 20 min and then permeabilized with 0.1% Triton X-100 (Beyotime, China, ST797)

for 20 min at 37 °C. Organoid monolayers or ST cells were blocked with 5% BSA (Biofroxx, Germany, 4240GR100) for 1 h and then labeled with primary antibodies overnight at 4 °C. After rinsing, the sections were incubated with secondary antibodies for 1 h at room temperature. Next, 4',6-diamidino-2-phenylindole (DAPI; Beyotime, China, C1006) was used to stain the nuclei. After washing, the organoid monolayers or ST cells were visualized using confocal laser-scanning microscopy (Zeiss LSM 900, Germany). Apical-out porcine intestinal organoids or small intestine tissues were stained with primary and secondary antibodies and visualized using confocal laser-scanning microscopy (Zeiss LSM 900, Germany) according to the manufacturer's protocol [147].

3.2.8. RNA extraction and real-time quantitative PCR

Total RNA was extracted using RNAiso reagent (TaKaRa, Japan, 9109) and reverse transcribed into cDNA using HiScript Q RT SuperMix for qPCR (Vazyme, China, R223-01), both of which followed the manufacturer's recommendations. The TGEV and PRCV virus copy numbers were detected by the TaqMan probe-based RT–qPCR method developed previously in our laboratory [149]. Relative qPCR was also performed using ChamQ SYBR qPCR master mix (Vazyme, China, Q311-02), and the results were calculated via the $2^{-\Delta\Delta CT}$ method. The primers and probes used in this study are listed in **Table 1**.

Table 1 Primers for real-time PCR

Names	Primer	Sequence (5'-3')
TGEV N	Forward	TGCCATGAACAAACCAAC
	Reverse	GGCACTTTACCATCGAAT
	Probe	HEX-TAGCACCACGACTACCAAGC-BHQ1*a*
PRCV N	Forward	TGCCATGAACAAACCAAC
	Reverse	GGCACTTTACCATCGAAT
	Probe	HEX-TAGCACCACGACTACCAAGC-BHQ1a
GAPDH	Forward	CATCCATGACAACTTCGGCA
	Reverse	GCATGGACTGTGGTCATGAGTC

3.2.9. Coimmunoprecipitation (co-IP) and western blot

Cotransfected cells were washed with cold PBS twice and lysed with NP40 lysis buffer (Beyotime, China, P0013F) supplemented with 1 mM PMSF (Beyotime, China, ST506) and phosphatase inhibitors (Beyotime, China, P1096). Lysis buffer containing cells was added to 20 μl of protein A+G agarose beads (Beyotime, China, P2055) and IgG (Santa Cruz, USA, 2025) on a rotating device for 4 h at 4 °C to remove nonspecific proteins, after which the mixture was centrifuged at 2500 rpm for 5 minutes. The supernatant was harvested, and anti-Flag/Myc/His/IgG antibodies were added to the samples on a rocking platform overnight at 4 °C. Subsequently, 40 μl of protein A+G agarose beads was added to the supernatant containing the antibody, which was incubated for 4 h at 4 °C on a rotating device. After washing with lysis

buffer three times, the immunoprecipitates were collected by centrifugation, and the supernatant was discarded. Immunoprecipitated proteins were detected by western blotting. For the western blot, the proteins were separated by SDS–PAGE and transferred onto a PVDF membrane (GE, USA, 10600023). The membranes were blocked in 5% nonfat milk at room temperature for 2 h and then incubated with specific primary antibodies overnight. Subsequently, the membrane was incubated with the secondary antibody for 1 h at room temperature. Finally, the proteins on the membranes were visualized with WesternBright ECL (Advansta, USA, K-12045-D50).

3.2.10. CRISPR–Cas9 for PIK3C3 knockout in ST cell lines

Porcine PIK3C3-specific sgRNAs targeting the second exon sequence (GTAAGAACTTCGTATAAGGC) were designed (http://crispor.tefor.net/) and cloned and inserted into the pSpCas9(BB)-2A-Puro (PX459) vector. The recombinant vectors were transfected into ST cells by Lipofectamine 3000 followed by puromycin (2 μg/ml) selection for 5 days. Monoclonal cells were chosen and identified for further experiments. The knockout level of PIK3C3 in ST cells was determined by Sanger sequencing and western blotting [150].

3.2.11. Pig experiments

Neonatal pigs spontaneously delivered from sows did not receive colostrum and were confirmed to be negative for TGEV by RT-qPCR and enzyme-linked immunosorbent assay. They were kept into animal house for one day and fed with milk replacer in Biosafety Level 3 Laboratory (BSL-3). For the cytotoxicity and pharmacokinetic parameters of the PM, three piglets were orally administered PM (100 mg/kg), and the serum was collected by venipuncture at 0, 1, 2, 4, 6, 8, 10, 12, 16 and 24 h after oral administration of PM for cytotoxicity assays and pharmacokinetic parameter determination. For antiviral animal experiments, piglets were randomly separated into four groups: the mock group (3), TGEV group (3), TGEV-PM-therapy group (3) and TGEV-PM-prevention group (3). For the TGEV group, neonatal pigs were orally administered 1.245×10^8 PFU TGEV Miller for 24 h. In addition, piglets in the TGEV-PM therapy group were orally infected with 1.245×10^8 PFU TGEV Miller and then treated with PM (100 mg/kg). For the TGEV-PM-prevention group, three neonatal pigs were orally pretreated with PM (100 mg/kg) for 24 h and subsequently inoculated with 1.245×10^8 PFU TGEV Miller for 24 h. The body weights of all piglets were recorded, and anal swabs were collected every 12 h. At 24 hpi, all pigs were euthanized, and intestinal tissues were collected for RT–qPCR, western blot, IFA and pathological examination. All animals were handled in strict accordance with good animal practice according to the Animal Ethics Procedures and Guidelines of the People's Republic of China, and the study was approved by The Animal Administration and Ethics Committee of Lanzhou Veterinary Research Institute, Chinese Academy of Agricultural Sciences (Permit No. LVRIAEC-2020-030).

3.2.12. Statistical analysis

All data were analyzed using GraphPad Prism 8.0 software (GraphPad, La

Jolla, CA, USA) by one or two-way analysis of variance. Differences between the two groups are indicated as *, $P \leq 0.05$; **, $P \leq 0.01$; ***, $P \leq 0.001$; ns, not significant. Every experiment was performed with three biological replicates, and the results were recorded as the mean ± SD.

3.3 Results

3.3.1. PM inhibits TGEV and PRCV infection in ST cells

To evaluate whether PM regulates porcine coronavirus infection, including TGEV, PRCV, PDCoV and PEDV, a cytotoxicity assay of different concentrations of PM was first performed with a Cell Counting Kit 8 (Sigma–Aldrich, USA, 96992). PM at concentrations less than 30 mM did not exhibit significant cytotoxicity in ST cells compared to $CoCl_2$, which was used as a positive control **(Fig. 9A)**. Next, the effect of PM on porcine coronavirus infection was analyzed. The experimental workflow is shown in **Fig. 9B**. The results showed that the PM effectively restricted TGEV infection, PRCV infection and PDCoV infection **(Fig. 9C, 9D and Supplemental Fig. S1A)**. The immunofluorescence staining results demonstrated similar trends for both TGEV and PRCV infections **(Fig. 9E and F)**. However, the PM was unable to repress PEDV infection in Vero-E6 cells according to the $TCID_{50}$ and western blot results **(Fig. 9G)**. These results indicated that PM is a potential antiviral agent for TGEV and PRCV infection but not for PEDV infection.

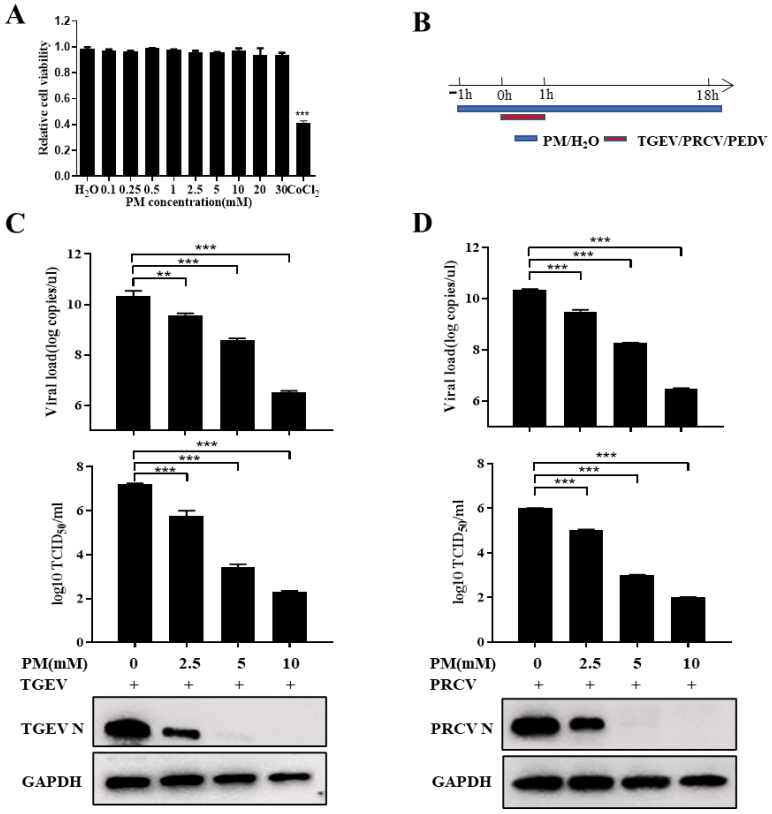

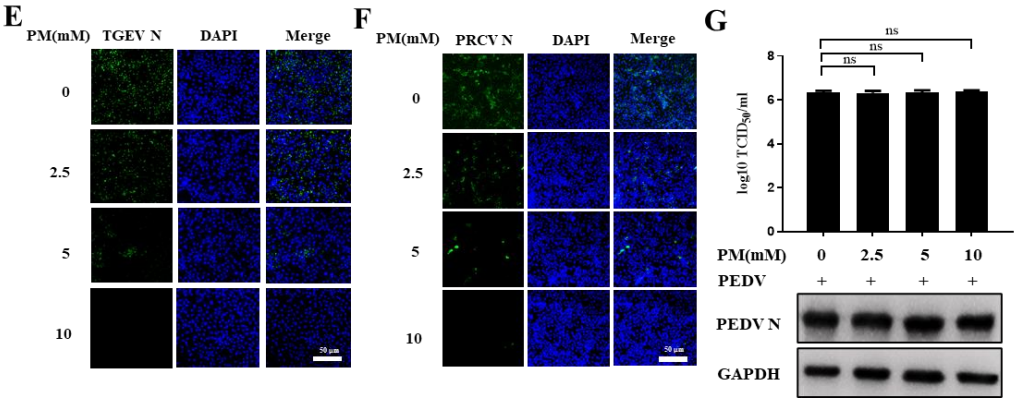

Figure 9.PM inhibits TGEV and PRCV infection in ST cells.

(A) A cytotoxicity assay of PM in ST cells. ST cells were incubated with different concentrations of PM for 24 h, which was tested by Cell Counting Kit 8. (B) Time course for PM inhibiting TGEV or PRCV or PEDV infection assay. (C-F) The ST cells, pretreated with PM at the indicated concentrations for 1 h were infected with TGEV Miller (0.1 MOI) or PRCV (0.1 MOI) for 1 h and were again treated with PM at 37 °C for 17 h. The cell samples were collected and examined by RT-qPCR, $TCID_{50}$, western blot (C and D), and IFA (E and F), Scale bar: 50 μm. (G) Vero-E6 cells were treated with indicated PM and infected with PEDV LJX 01/2014 according to time course of Fig. 1B, which detected by $TCID_{50}$ and western blot. Results are presented as mean ± SD of data from three independent experiments **, $P \leq 0.01$; ***, $P \leq 0.001$.

3.3.2. PM restricts TGEV and PRCV infection ex vivo

To further investigate the *ex vivo* antiviral activity of PM, a porcine intestinal organoid culture system and a physiological model mimicking the gut environment for swine enteric virus infection were used in this study [147-148]. First, porcine intestinal crypts from the ileum were isolated and cultured in Matrigel, and intestinal 3D organoids were formed after culture for 4 days (Supplemental Fig. S2A). Next, an intestinal organoid monolayer was established and observed via optical microscopy, and the presence of ZO-1 on the outer membrane indicated that apical-out organoids were successfully generated according to IFA detection (Supplemental Fig. S2B). A cytotoxicity assay of different concentrations of PM was performed and revealed that PM at concentrations less than 30 mM did not cause significant cytotoxicity to intestinal organoids **(Fig. 10A)**. Then, the two organoid models were treated with different concentrations of PM before TGEV infection. As depicted in **Fig. 10B to D**, treatment with PM significantly inhibited TGEV infection in the intestinal organoid monolayer in a dose-dependent manner **(Fig. 10B and C)**. Moreover, RT–qPCR, $TCID_{50}$, and western blot analysis of the apical-out organoids also revealed that the PM markedly inhibited TGEV infection **(Fig. 10D)**. In addition, the same phenotypes were found in the PRCV-infected organoid monolayer and apical-out organoids **(Fig. 10E to G)**. These results suggested that the PM effectively suppressed TGEV and PRCV infection in porcine intestinal organoids.

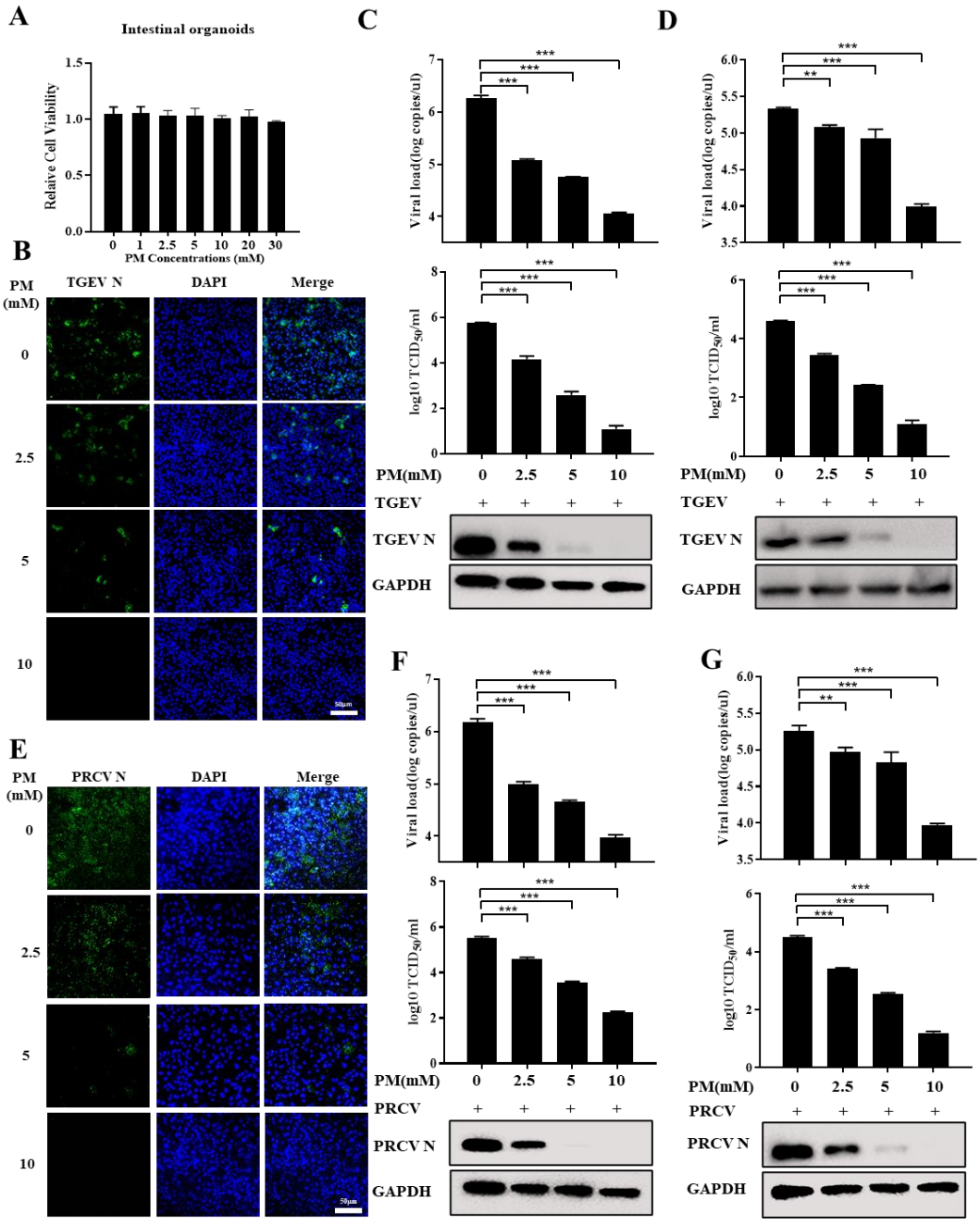

Figure 10.PM restricts TGEV and PRCV infection in porcine intestinal organoids.

(A) Intestinal organoids were incubated with different concentrations of PM for 24 h, which was tested by Cell Counting Kit 8. (B and C) The intestinal organoids monolayer was treated

with indicated PM and infected with TGEV Miller (0.1 MOI) for 24 h, which was measured by IFA (B), Scale bar: 50 μm, RT-qPCR, $TCID_{50,}$ and western blot (C). (D) Apical-out intestinal organoids were treated with indicated PM and infected TGEV Miller (1 MOI) for 48 h, which was determined by RT-qPCR, $TCID_{50,}$ and western blot. (E and F) The intestinal organoids monolayer was treated with different concentrations of PM and infected with PRCV for 24 h, which was determined by IFA (E), Scale bar: 50 μm, RT-qPCR, $TCID_{50,}$ and western blot (F). (G) Apical-out intestinal organoids were treated with indicated PM and infected PRCV (1 MOI) for 48 h, which was detected by RT-qPCR, $TCID_{50,}$ and western blot. Results are presented as mean ± SD of data from three independent experiments **, $P \leq 0.01$; ***, $P \leq 0.001$.

3.3.3. PM inhibits TGEV and PRCV infection via a synergistic effect on potassium ions and molybdate

It has been reported that PM (K_2MoO_4) is a chemical compound that is synthesized from potassium ions and molybdate [78]. To clarify whether the inhibitory effects of PM on TGEV and PRCV are ion-mediated or compound-mediated, the effects of potassium chloride and sodium molybdate on TGEV infection were assessed. RT–qPCR determined that neither potassium chloride nor sodium molybdate was able to suppress TGEV infection **(Fig. 11A and B)**. Notably, cotreatment with both potassium chloride and sodium molybdate had antiviral effects similar to those of PM on TGEV and PRCV infection **(Fig. 11C and D)**. These results suggested that the PM restricts TGEV and PRCV infection via synergistic effects between potassium ions and molybdate.

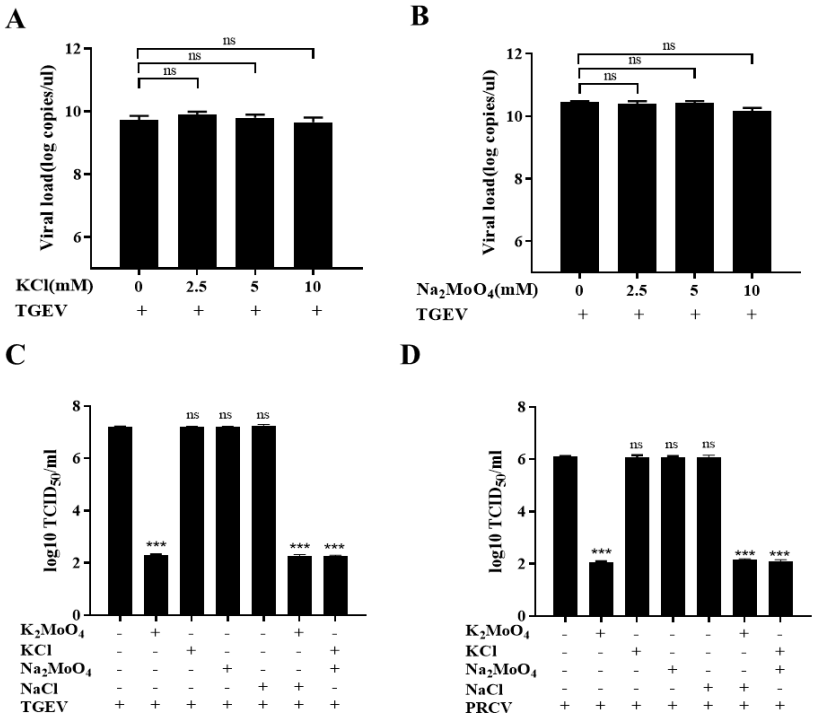

Figure 11.PM inhibits TGEV and PRCV infection by potassium ion and molybdate synergy.

(A and B) The ST cells, pretreated with potassium chloride (KCl) or sodium molybdate (Na_2MoO_4) at the indicated concentrations for 1 h were infected with TGEV Miller (0.1 MOI) for 1 h and were again treated with KCl or Na_2MoO_4 at 37 °C for 17 h. The cell samples were measured by RT-qPCR. (C and D) ST cells were treated with PM (K_2MoO_4, 10 mM), KCl (20 mM), Na_2MoO_4 (10 mM), sodium chloride (NaCl, 10 mM), K_2MoO_4 (10 mM), and NaCl (20 mM) as well as Na_2MoO_4 (10 mM) and KCl (20 mM) for 1 h and then infected with TGEV Miller (0.1 MOI) or PRCV (0.1 MOI) for 17 h, which was determined by $TCID_{50}$. Results are presented as mean ± SD of data from three independent experiments ***, $P \leq 0.001$; ns, no significance.

3.3.4. PM dampens TGEV and PRCV infection mainly by blocking viral entry

To characterize how PM dampens TGEV and PRCV infection, a time-of-drug-addition assay was performed. First, we found that PM was unable to directly prevent early inactivation of TGEV **(Fig. 12A and Supplemental Fig. S3A)**. The next experiment was undertaken to determine which step of TGEV infection was inhibited by PM treatment[151-154]. The effect of PM on the adsorption, internalization, replication, and release processes of TGEV throughout the life cycle was evaluated in ST cells. As shown in **Fig. 12B to F** and **Supplemental Fig. S3B**, PM treatment was uninfluential in virus adsorption and release **(Fig. 12B, 12F and S3B)** but significantly inhibited TGEV entry **(Fig. 12C and 12D)** and moderately restricted viral replication **(Fig. 12E)**. The same results were also demonstrated for PRCV infection (Supplemental **Fig. S4A and B)**. Interestingly, the TGEV replication process was also restricted by PM treatment **(Fig. 12E)**, but the effect on replication was not as significant as that on entry. Overall, these findings suggest that the PM inhibits TGEV and PRCV infection mainly by blocking viral entry.

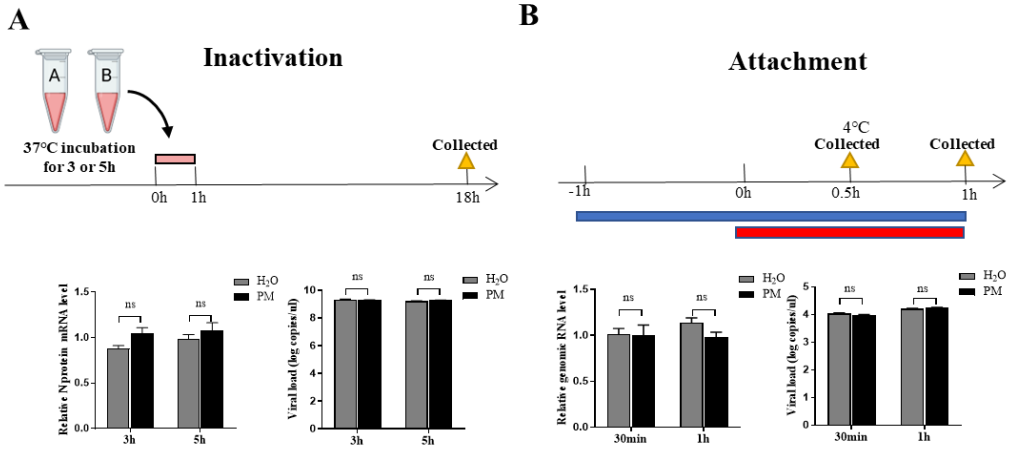

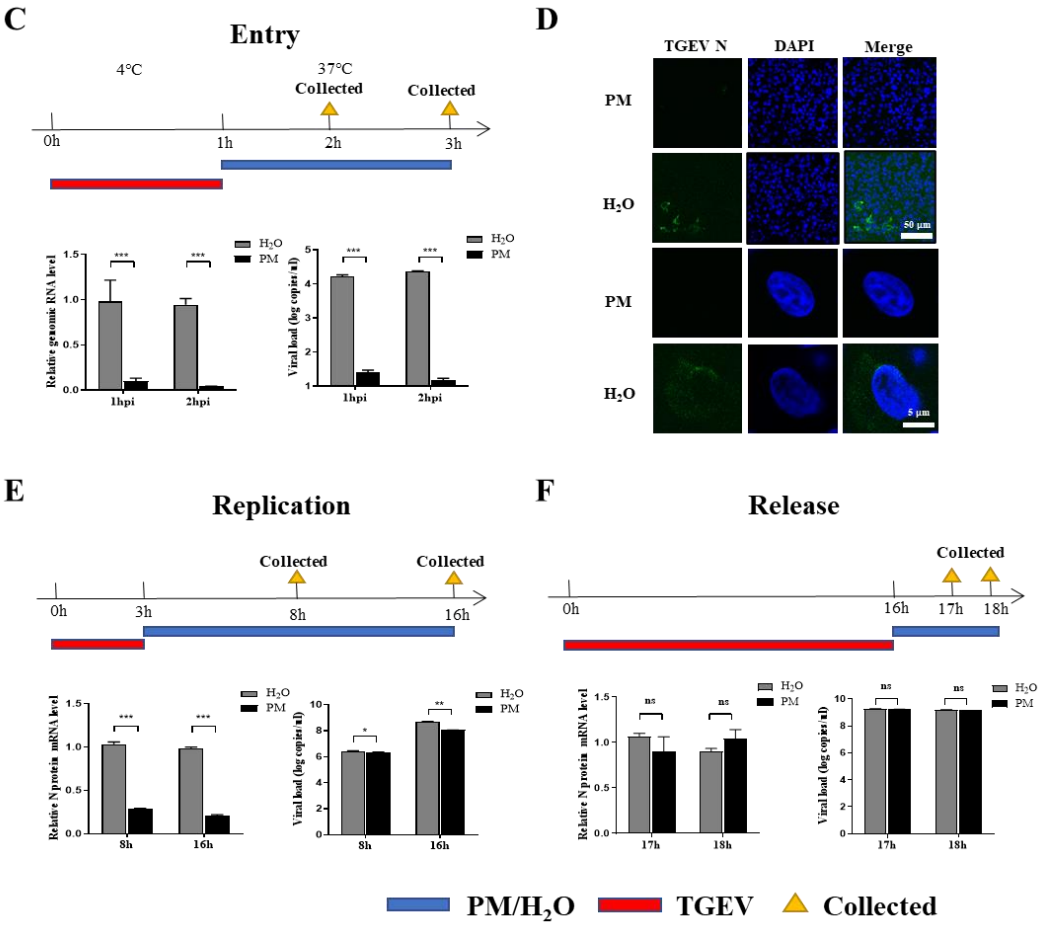

Figure 12.PM dampens TGEV infection by mainly blocking viral entry.

(A) Inactivated assay. A: TGEV (0.1 MOI) + PM (10 mM) or B: TGEV (0.1 MOI) + H2O were mixed and incubated at 37 °C for 3 h and 5 h respectively and then the mixtures were added into ST cells. After incubation at 37°C for another 1 h, culture supernatants were replaced with fresh culture medium for 17 h at 37°C. After washing with PBS, the mRNA levels and viral load of TGEV N protein were measured by RT-qPCR (B) Adsorption assay. ST cells were pretreated with PM (10 mM) or H_2O (blue bar) for 1 h at 37 °C, and then the media were replaced by a mixture of PM (10 mM) or H_2O and TGEV (5 MOI, red bar) for 0.5 h or 1 h at 4 °C. After washing with PBS, the genomic RNA levels and viral load of TGEV N protein were measured by RT-qPCR. (C and D) Penetration assay. ST cells were infected with 5 MOI TGEV (red bar) for 1 h at 4 °C and were then treated with PM (10 mM) or H_2O (blue bar) for 1 h or 2 h at 37 °C after washing with PBS. The cell samples were washed using sodium citrate buffer and tested through RT-qPCR (C) and IFA (D) Scale bar: 50 μm /5 μm. (E) Replication assay. ST cells infected with 5 MOI TGEV (red bar) were incubated at 37 °C for 3 h and washed with sodium citrate buffer. Then, cells were treated with PM (10 mM) or

H_2O (blue bar) for 5 h or 13 h. The cells were harvested and examined by RT-qPCR. (F) Release assay. ST cells were infected with 5 MOI TGEV (red bar) for 16 h and then PM (10 mM) or H_2O (blue bar) was added to the cells for 1 h or 2 h. qRT-PCR was used to test the mRNA levels and viral load of the virus in the supernatant. Results are presented as mean ± SD of data from three independent experiments ***, $P \leq 0.001$; ns, no significance.

3.3.5. PM blocks TGEV and PRCV infection by decreasing APN expression

It has been reported that APN is the main cell receptor for TGEV and PRCV internalization but is not the functional cell receptor for PEDV entry [42, 127]. According to our above results, PM blocked the penetration of both TGEV and PRCV but not that of PEDV, and we hypothesized that the PM degraded the APN receptor and resulted in the restriction of TGEV and PRCV infection. To test this hypothesis, ST cells were treated with PM and harvested at different time points for western blot and IFA analysis. The results showed that PM decreased APN expression in ST cells **(Fig. 13A and B)**. To further explore the relationship between APN expression and TGEV or PRCV infection, ST cells were treated with PM and then infected with TGEV or PRCV. The results demonstrated that PM can reduce APN expression to inhibit TGEV and PRCV infection **(Fig. 13C and Supplemental Fig. S5A)**. Furthermore, as depicted in **Fig. 13D to I**, intestinal organoid monolayers and apical-out intestinal organoids were used to confirm these findings. Clearly, PM decreased *ex vivo* APN expression in the absence or presence of TGEV at different time points, as shown by western blotting **(Fig. 13D, 13F, 13G and 13I)** and IFA detection **(Fig. 13E and 13H)**. To further confirm the effect of PM on APN degradation and TGEV inhibition, an APN plasmid was overexpressed followed by TGEV and PM treatment in ST cells. The results demonstrated that overexpression of APN rescued TGEV from PM-mediated restriction, which indicated that PM blocks TGEV entry by decreasing APN expression **(Fig. 13J)**. In addition, to explore whether the PM degrades APN in different species, HEK-293T and BHK-21 cells were treated with PM for 8 h and 16 h. The results showed that the PM also decreased human and mouse-derived APN expression **(Supplemental Fig. S6A and B)**. To determine whether intracellular, extracellular and membrane receptors were affected by PM treatment, retinoic acid-inducible gene 1 (RIG-I), toll-like receptor 4 (TLR4), angiotensin-converting enzyme 2 (ACE2), dipeptidyl peptidase-4 (DPP4) and carcinoembryonic antigen-related cell adhesion molecule 1 (CEACAM1) were detected. The results demonstrated that PM treatment did not affect RIG-I, TLR4, ACE2 or CEACAM1 expression **(Supplemental Fig. S7A to S7D)** but could inhibit DPP4 expression **(Supplemental Fig. S7E)**. These results demonstrated that the PM blocked TGEV and PRCV entry by decreasing APN expression.

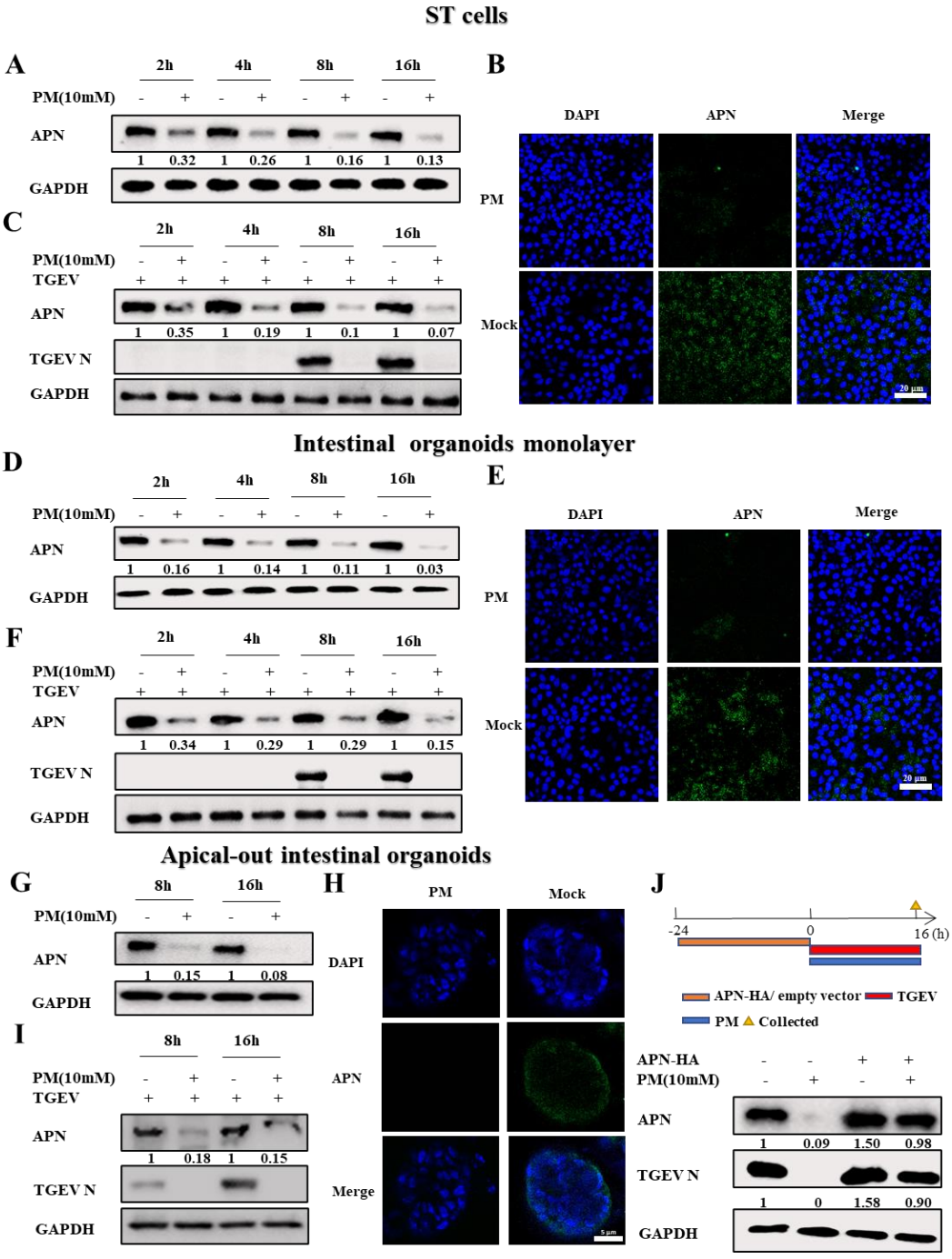

Figure 13.PM blocks TGEV infection by degrading APN expression.

(A, D, and G) ST cells (A) or intestinal organoids monolayer (D) or apical-out intestinal

organoids (G) were treated with PM (10 mM) at 2 h, 4 h, 8 h, and 16 h, which was collected and determined by western blot. (B, E, and H) ST cells (B) or intestinal organoids monolayer (E) or apical-out intestinal organoids (H) were treated with PM (10 mM) at 16 h, which was measured by IFA, Scale bar: 20 μm. (C, F, and I) ST cells (C) or intestinal organoids monolayer (F) or apical-out intestinal organoids (I) were treated with PM (10 mM) and infected with 0.1 MOI TGEV at 2 h, 4 h, 8 h, and 16 h. The cell samples were harvested and detected by western blot. (J) ST cells were transfected with empty vector or pCMV-HA-APN (pig) plasmids for 24 h, which was treated with H_2O or PM and then infected with 0.1 MOI TGEV for 16 h. The cell samples were detected by western blot. All western blot results were calculated by Image J. All experiments were performed in triplicate.

3.3.6. PM degrades APN via the autophagy–lysosome pathway

To elucidate the molecular mechanism responsible for APN degradation by PM, potential pathways were screened by using pathway inhibitors. As indicated in **Fig. 14A**, the degradation of APN by PM was reversed by 3-MA (an autophagy inhibitor) but not by MG132 (a protease inhibitor) or Z-VAD-FMK (a caspase inhibitor) **(Fig. 14A)**, suggesting that PM degrades APN expression via the autophagy–lysosome pathway. Further investigation revealed that, compared with that in the control group, p62 was consumed, and more of the autophagosome protein LC3-II was generated from LC3-I with the degradation of APN **(Fig. 14B)**. Furthermore, precise measurement of autophagic flux is of paramount importance for understanding autophagy induction, so the effect of PM on autophagic flux was determined by the RFP-EGFP-LC3B sensor. The results demonstrated that increased RFP signals (autolysosomes) and merge signals (autophagosomes) were observed in response to PM treatment **(Fig. 14C)** and were quantified by ImageJ **(Fig. 14D)**. In addition, the PM-treated ST cells formed more autophagosomes (yellow arrow) and autolysosomes (white asterisk) than the H_2O-treated cells, as measured via transmission electron microscopy analysis and quantified per area **(Fig. 14E and F)**. Collectively, these results indicated that PM decreased APN expression via the activation of autophagy.

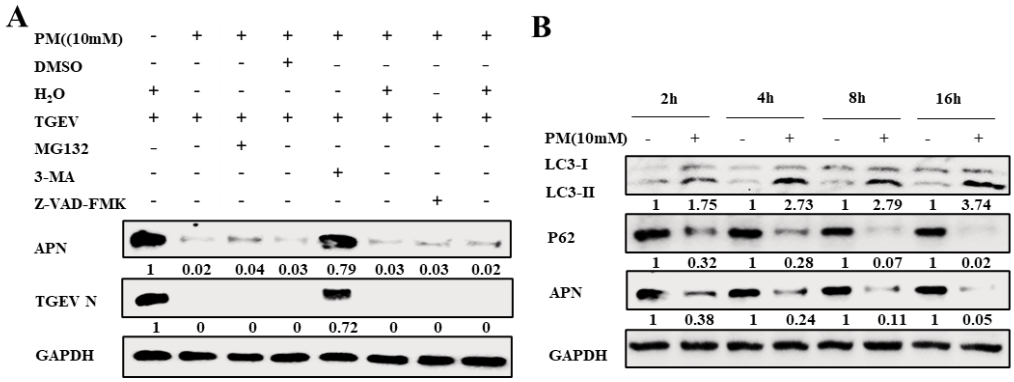

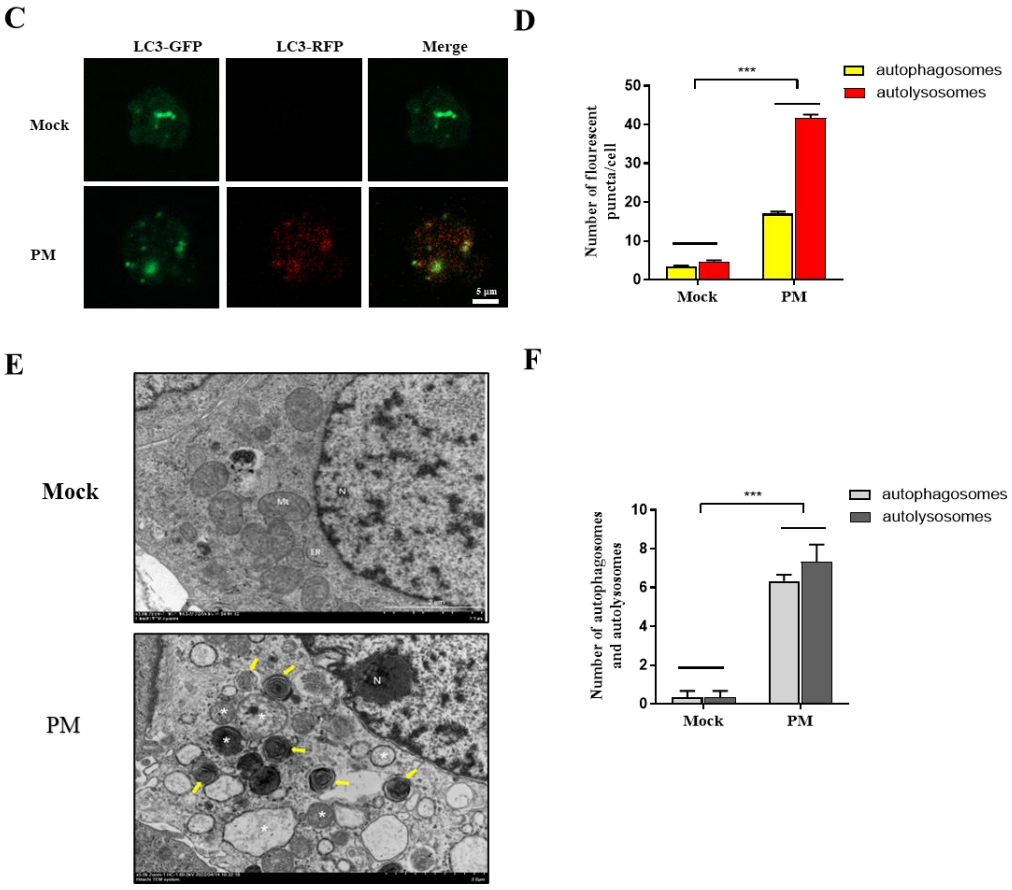

Figure 14.PM degrades APN by autophagy-lysosome pathway.

(A) ST cells were treated with PM (10 mM) and infected with TGEV (0.1MOI) in the presence and absence of MG132 (20 μM), 3-MA (20 mM), and Z-VAD-FMK (20 μM) for 16 h. The APN expression and TGEV N were detected by western blot. (B) ST cells were treated with PM (10 mM) at 2 h, 4 h, 8 h, and 16 h, autophagy markers P62 and LC3, and APN were measured by western blot. (C) ST cells were transfected with RFP-EGFP-LC3B for 12 h and then treated with PM (10 mM) or H_2O for 36 h. The fluorescence of GFP and RFP was detected by confocal microscopy, Scale bar: 5 μm. (D) Quantification of autophagosomes (Merge) and autolysosomes (RFP) from C using Image J software. (E) ST cells were treated with PM or H_2O for 24h. The autophagosomes (yellow arrow) and autolysosomes (asterisk) were detected by transmission electron microscope, Scale bar: 2 μm. (F) The number of autophagosomes (yellow arrow) and autolysosomes (asterisk) was quantified. All western blot results were calculated by Image J. Results are presented as mean ± SD of data from three independent experiments ***, $P \leq 0.001$.

3.3.7. PM degrades APN expression by activating PIK3C3-mediated autophagy

The induction of autophagy includes many important processes, including mTOR inhibition, formation of the ULK complex, and the PtdIns3K complex **(Fig. 15A)**. The potential pathways involved in PM-induced autophagy were further screened. As shown in **Fig. 15B**, treatment with 3-MA (a PtdIns3K complex inhibitor) reversed the changes in APN expression after PM treatment. However, SBI0206965 (a ULK complex inhibitor) and 3BDO (an mTOR activator) cannot abolish the degradation of APN after PM treatment. In addition, to further determine the effect of PM on the PtdIns3K complex, the main elements involved in this complex, PIK3C3, BECN1, and ATG14, were measured. The results showed that the PM activated PIK3C3 expression, rather than BECN1 or ATG14 expression, to induce autophagy and decreased APN expression, but these effects were abolished by the addition of 3-MA **(Fig. 15C)**. To further confirm this phenotype, small interfering RNAs (siRNAs) targeting PIK3C3 were constructed and screened. The results showed that siRNA-4 markedly downregulated PIK3C3 expression **(Fig. 15D)**. Additionally, knockdown of PIK3C3 reduced autophagy and rescued APN degradation after PM treatment **(Fig. 15E)**. Furthermore, PIK3C3 KO STs were constructed and identified by sequencing **(Fig. 15F)** and western blotting **(Fig. 15G)**. **Fig. 15H** clearly shows that, compared with those in WT ST cells, PM-induced autophagy and degradation of APN were abolished in PIK3C3 KO ST cells **(Fig. 15H)**. In addition, ectopic expression of PIK3C3 in KO ST cells recovered PIK3C3-mediated autophagy and inhibited APN expression compared to that in the control group after PM treatment **(Fig. 15I)**. These results suggested that the PM activated PIK3C3-mediated autophagy to reduce APN expression.

A

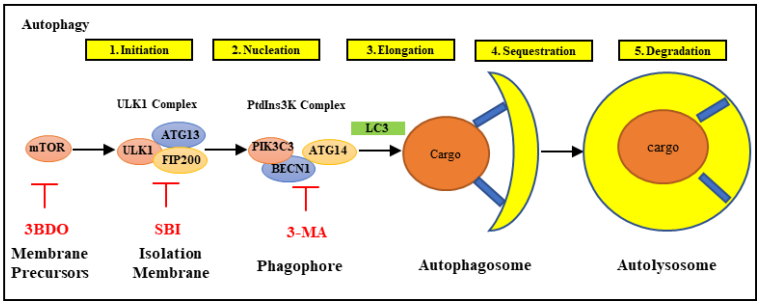

B

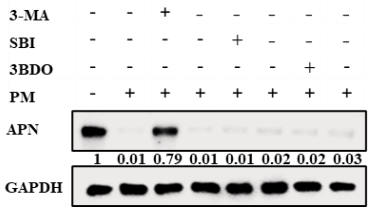

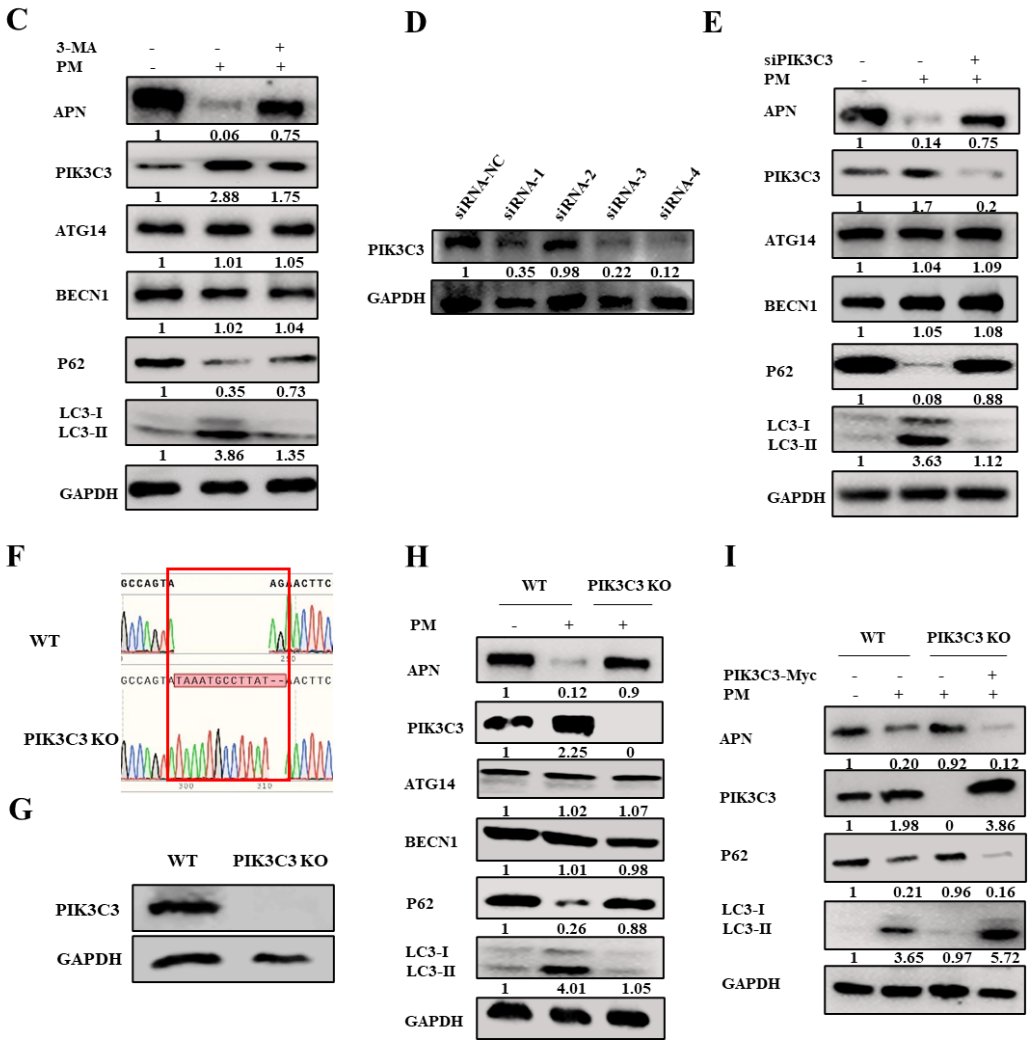

Figure 15.PM degrades APN expression via activating PIK3C3-mediated autophagy.

(A) Graphical representation for autophagy and the targets of different autophagy inhibitors. (B) ST cells were treated with PM (10 mM) in the presence and absence of 3-MA (20 mM), SBI0206965 (20 μM), and 3BDO (30 μM) for 16 h, and the APN expression was detected by western blot. (C) ST cells were treated with PM (10 mM) in the presence and absence of 3-MA (20 mM) for 16 h, and the APN, PIK3C3, ATG14, BECN1, P62, and LC3 were measured by western blot. (D) ST cells were transfected with PIK3C3 siRNA-1, PIK3C3 siRNA-2, PIK3C3 siRNA-3, PIK3C3 siRNA-4, and NC siRNA for 24 h, the PIK3C3 expression was detected by western blot. (E) ST cells were transfected with PIK3C3 siRNA-4 or NC siRNA for 24 h and then treated with PM (10 mM) for 16 h. The APN, PIK3C3, ATG14, BECN1, P62, and LC3 were detected by western blot. (F) Sequencing diagram for WT ST cells and PIK3C3

KO ST cells. (G) PIK3C3 was detected by western blot in WT ST cells and PIK3C3 KO ST cells. (H) WT ST cells and PIK3C3 KO ST cells were treated with PM (10 mM) for 16 h and then the APN, PIK3C3, ATG14, BECN1, P62, and LC3 were detected by western blot. (I) WT ST cells and PIK3C3 KO ST cells were transfected with pCMV-Myc and pCMV-Myc-PIK3C3 respectively for 24 h and treated with PM (10 mM) for 16 h. The APN, PIK3C3, P62, and LC3 were detected by western blot. All western blot results were calculated by Image J. All experiments were performed in triplicate.

3.3.8. PM promotes PIK3C3-BECN1-ATG14 complex assembly by enhancing PIK3C3 Ser249 phosphorylation

The PtdIns3K complex is a critical component of the initiation of autophagy. On the basis of the above results, we hypothesized that PM regulates PtdIns3K complex formation to induce autophagy. To verify this hypothesis, interactions between components of the PtdIns3K complex were investigated via coimmunoprecipitation (co-IP). As expected, the interaction between exogenously expressed Myc-PIK3C3 and Flag-BECN1 increased after PM treatment **(Fig. 16A)**. However, the interaction between Flag-BECN1 and His-ATG14 was not affected by PM treatment **(Fig. 16B)**, indicating that PIK3C3 is a specific target for PM treatment. The PtdIns3K complex is formed and activated mainly by phosphorylating PIK3C3 at Ser249, BECN1 at Ser15 (human)/Ser14 (murine), and ATG14 at Ser29[155]. The detailed effects of PM on the PIK3C3-BECN1-ATG14 complex were further evaluated. ST cells were co-transfected with Myc-PIK3C3, Flag-BECN1, or His-ATG14 for 12 h and treated with PM for 36 h, followed by immunoprecipitation with Myc, Flag, or His antibodies. The results demonstrated that the interaction of Myc-PIK3C3, Flag-BECN1, and His-ATG14 was promoted in all IPs by upregulation of PIK3C3 Ser249 phosphorylation after PM treatment **(Fig. 16C to 16E)**, indicating that the phosphorylation of PIK3C3 at Ser249 was crucial for PM to promote PIK3C3-BECN1-ATG14 complex assembly. Confocal microscopy analysis confirmed that PM enhanced the colocalization of Myc-PIK3C3, Flag-BECN1, and His-ATG14 in ST cells **(Fig. 16F)**, and the number of merged fluorescent spots representing the PIK3C3-BECN1-ATG14 complex was significantly higher than that in the mock group **(Fig. 16G)**. To further confirm the effect of PIK3C3 Ser249 on the promotion of PIK3C3-BECN1-ATG14 assembly, a Myc-PIK3C3 mutant with Ser249A was constructed, co-transfected into ST cells with Flag-BECN1 and His-ATG14 for 12 h, and then treated with PM for 36 h. The results illustrated that the assembly of the PIK3C3-BECN1-ATG14 complex by PM treatment was attenuated by mutant PIK3C3 Ser249A **(Fig. 16H)**. Collectively, these results suggested that PM promoted PIK3C3-BECN1-ATG14 complex assembly by increasing PIK3C3 Ser249 phosphorylation.

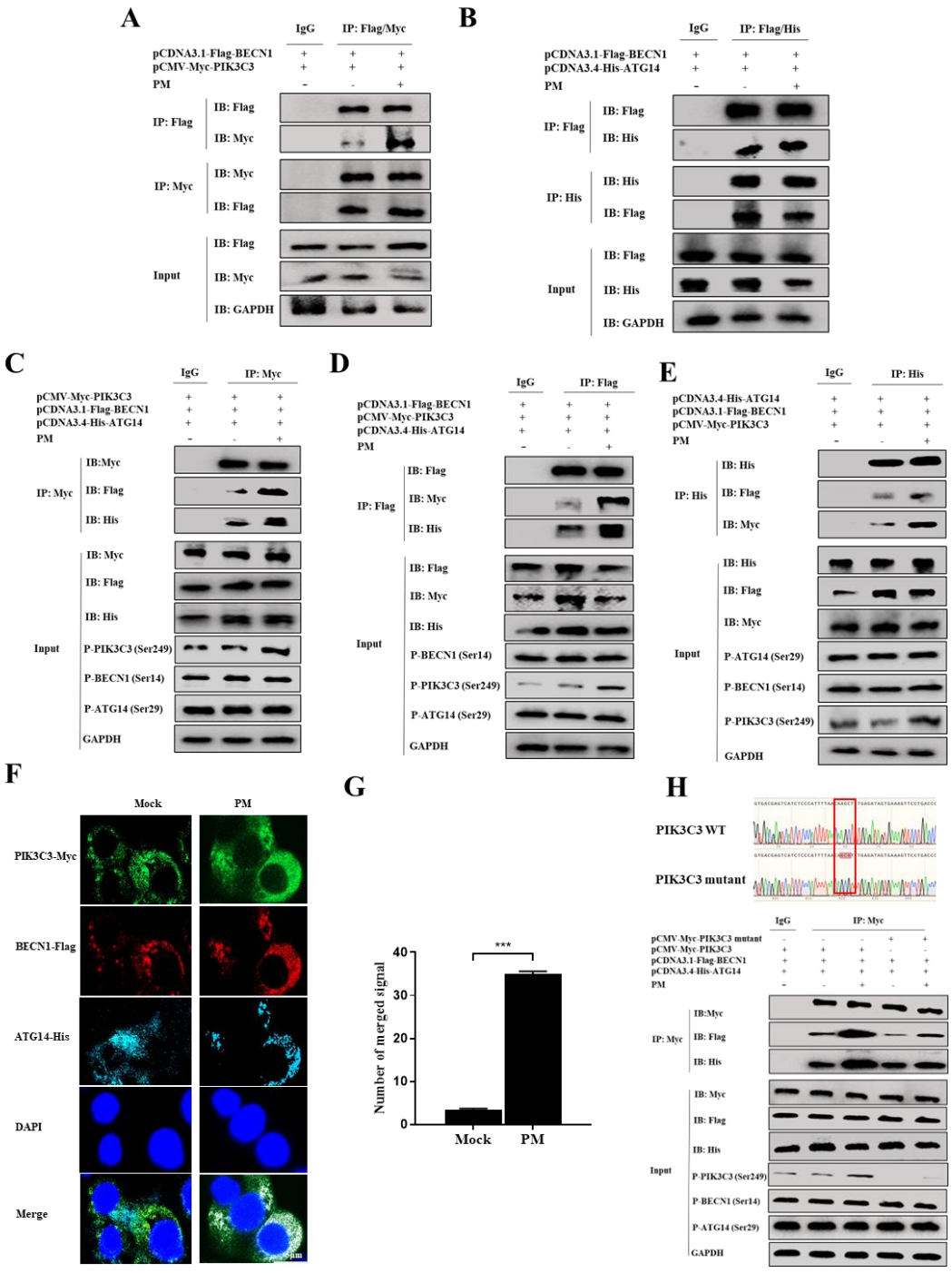

Figure 16.PM promotes PIK3C3-BECN1-ATG14 complex assembly by enhancing

PIK3C3 Ser249 phosphorylation.

(A) ST cells were transfected with pCMV-Myc-PIK3C3 and pCDNA3.1-Flag-BECN1 for 12 h and then treated with PM (10 mM) for 36 h. The Co-ip was carried out by Flag or Myc Ab, followed by Western blot analysis. (B) ST cells were transfected with pCDNA3.1-Flag-BECN 1 and pCDNA3.4-His-ATG14 for 12 h and treated with PM (10 mM) for 36 h. The Co-ip was performed with Flag or Myc Ab, followed by western blot detection. (C-E) ST cells were transfected with pCMV-Myc-PIK3C3, pCDNA3.1-Flag-BECN1, and pCDNA3.4-His-ATG14 for 12 h, and PM (10 mM) was added to the cells for 36 h. Then Co-ip was performed with a Myc, Flag, and His Ab individually, and all IPs, input, and phosphorylation of PIK3C3 (Ser249), BECN1 (Ser14), and ATG14 (Ser29) were detected by western blot. (F) ST cells were transfected with pCMV-Myc-PIK3C3, pCDNA3.1-Flag-BECN1, and pCDNA3.4-His-ATG14 for 12 h, and PM (10 mM) was added to the cells for 36 h, which detected by IFA, Scale bar: 20 μm. (G) Quantification of PIK3C3-BECN1-ATG14 complex (merged signal) from F using Image J software. (H) ST cells were transfected with pCMV-Myc-PIK3C3 or pCMV-Myc-PIK3C3 mutant, pCDNA3.1-Flag-BECN1 and pCDNA3.4-His-ATG14 for 12 h and then treated with PM (10 mM) for 36 h. Then Co-ip was performed with a Myc, Flag, and His Ab individually, and all IPs, input, and phosphorylation of PIK3C3 (Ser249), BECN1 (Ser14), and ATG14 (Ser29) were detected by western blot. Results are presented as mean ± SD of data from three independent experiments ***, $P \leq 0.001$.

3.3.9. PM represses TGEV and PRCV infection by degrading APN via PIK3C3-mediated autophagy

The above investigations demonstrated that the PM activated PIK3C3-mediated autophagy to reduce APN expression. Therefore, it is rational to hypothesize that PM dampens TGEV and PRCV infection by degrading APN via PIK3C3-mediated autophagy. As expected, we initially found that knockdown of PIK3C3 reduced PM-induced autophagy and rescued APN expression and TGEV infection **(Fig. 17A)**. $TCID_{50}$ and RT–qPCR results also validated the recovery of TGEV infection in PIK3C3-knockdown ST cells **(Fig. 17B)**. Furthermore, TGEV or PRCV N and APN expression in PIK3C3 KO ST cells were significantly restored after PM compared to those in WT ST cells **(Fig. 17C and Supplemental Fig. S8A)**. The decrease in TGEV or PRCV mRNA levels and viral titers induced by PM treatment was reversed in PIK3C3 KO ST cells **(Fig. 17D, Supplemental Fig. S8B and S8C)**. Furthermore, ectopic expression of PIK3C3 in KO ST cells restored PM-mediated APN degradation and inhibited TGEV or PRCV infection by reinducing autophagy **(Fig. 17E and Supplemental Fig. S8D)**. $TCID_{50}$ and RT–qPCR confirmed the inhibitory effects of TGEV **(Fig. 17F)** and PRCV infection **(Supplemental Fig. S8E and F)** by PM treatment after replenishment of PIK3C3 in KO ST cells, indicating that the PM restricted TGEV and PRCV infection by degrading APN via PIK3C3-mediated autophagy.

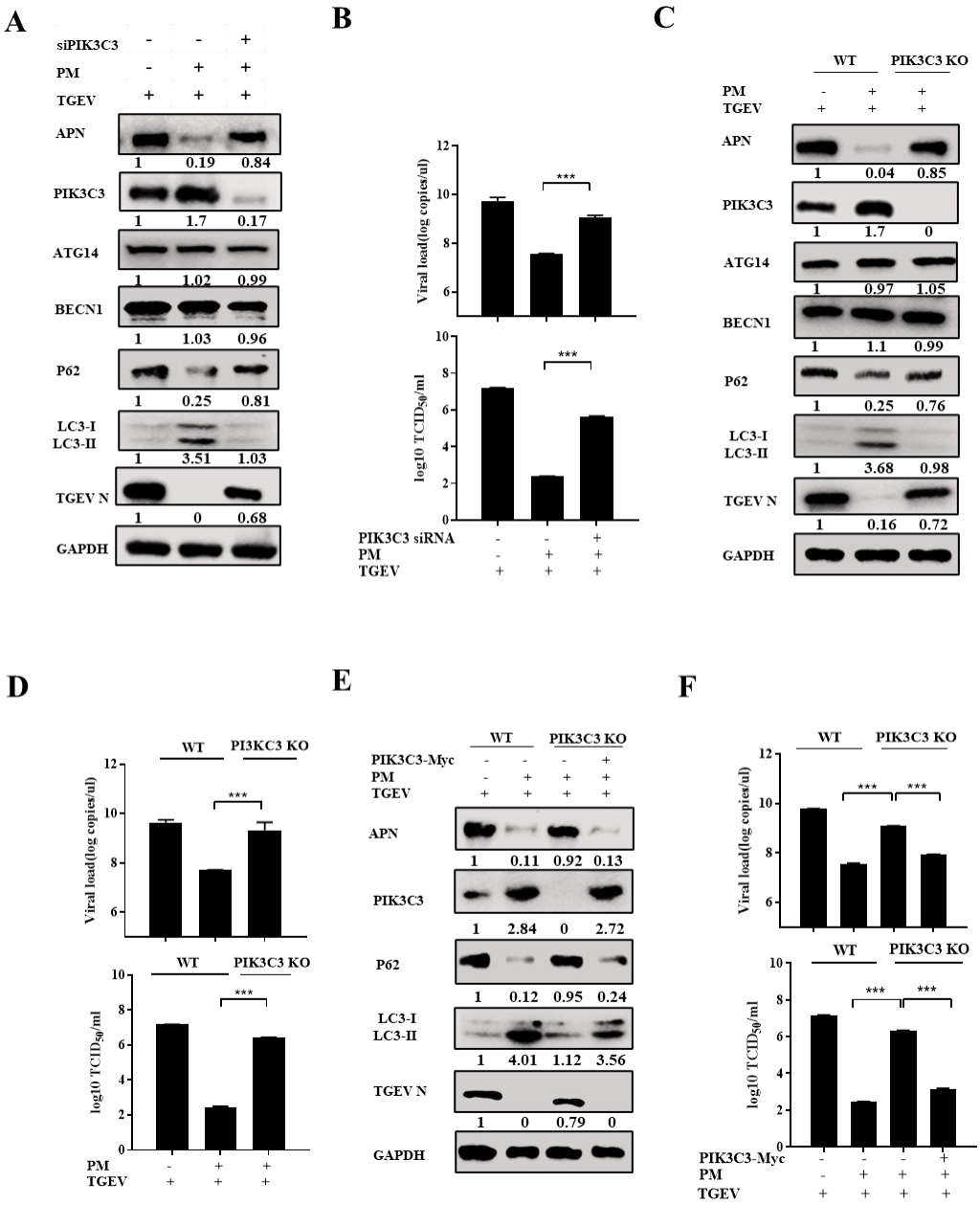

Figure 17. PM represses TGEV infection by degrading APN via PIK3C3-mediated autophagy.

(A-B) ST cells transfected with PIK3C3 siRNA-4 or NC siRNA for 24 h were treated with PM (10 mM) and infected with TGEV (0.1 MOI) for 16 h. The APN, PIK3C3, ATG14, BECN1, P62, TGEV N, and LC3 were measured by western blot (A), and viral titers and TGEV N mRNA levels were determined by $TCID_{50}$ and RT-qPCR (B). (C-D) WT ST cells and PIK3C3

KO ST cells were treated with PM (10 mM) and infected with TGEV (0.1 MOI) for 16 h. Then the APN, PIK3C3, ATG14, BECN1, P62, TGEV N, and LC3 were detected by western blot (C), and viral titers and TGEV N mRNA levels were determined by $TCID_{50}$ and RT-qPCR (D) respectively. (E-F) WT ST cells and PIK3C3 KO ST cells transfected with pCMV-Myc and pCMV-Myc-PIK3C3 respectively for 24 h were treated with PM (10 mM) and infected with TGEV (0.1 MOI) for 16 h. The APN, PIK3C3, P62, TGEV N, and LC3 were detected by western blot (E). $TCID_{50}$ and RT-qPCR (F) were performed to detect viral titers and TGEV N m RNA level. All western blot results were calculated by Image J. Results are presented as mean ± SD of data from three independent experiments ***, $P \leq 0.001$.

3.3.10. Oral administration of PM reduces TGEV pathogenicity via autophagic degradation of APN in piglets

Given the above *in vitro* and *ex vivo* results, neonatal pigs were used to evaluate the therapeutic and preventive efficacy of PM against TGEV infection *in vivo.* First, the cytotoxicity of PM was evaluated at different times by detecting key biochemical indicators. The results demonstrated that oral administration of PM did not affect aminotransferase (AST), creatine kinase (CK) or Creatinine (CREA) levels at different times **(Supplemental Fig. S9A)**, which indicated that PM (100 mg/kg) is a safe concentration in piglets. To further confirm the frequency of orally administered PM, pharmacokinetic parameters were calculated. The results illustrated that the t1/2 of PM was approximately 12 h **(Table 2 and Supplemental Fig. S9B)**. Therefore, the oral administration of PM every 12 h is the optimal frequency for maintaining the activation of PM.

Next, we determined the therapeutic and prophylactic efficacy of PM against TGEV infection in piglets. The piglets in the different groups were treated with PM or DMEM every 12 h and then inoculated with TGEV individually by oral administration **(Fig. 18A)**. We monitored body weight and collected anal swabs every 12 h. The animals in the TGEV group lost more weight and had higher viral shedding than those receiving PM **(Supplemental Fig. S10A, Fig. 18B)**. To further determine the effect of PM on TGEV-induced damage to the small intestine, each segment of the small intestine was paraffin embedded, followed by slicing and staining with hematoxylin and eosin (H&E). As expected, PM treatment alone did not have any impact on the small intestine, and, strikingly, PM almost completely reversed TGEV-induced villous atrophy of small intestinal segments despite preventive or therapeutic treatment **(Supplemental Fig. S10B and S10C)**. Moreover, inflammatory infiltration and intestinal villus shedding were improved in the PM treatment group compared with those in the TGEV infection group. Mechanistically, via RT–qPCR and western blot detection, the TGEV burden and APN and P62 expression throughout the small intestine were substantially lower, and PIK3C3 expression was significantly higher in the PM-therapy and PM-prevention groups than in the control group **(Fig. 18C)**. The IFA results also showed that APN expression and TGEV N protein expression were almost entirely inhibited upon PM treatment **(Fig. 18D)**. Overall, our data demonstrated that PM induced PIK3C3-mediated autophagic degradation of APN in response to TGEV infection in a therapeutic and prophylactic manner *in vivo.*

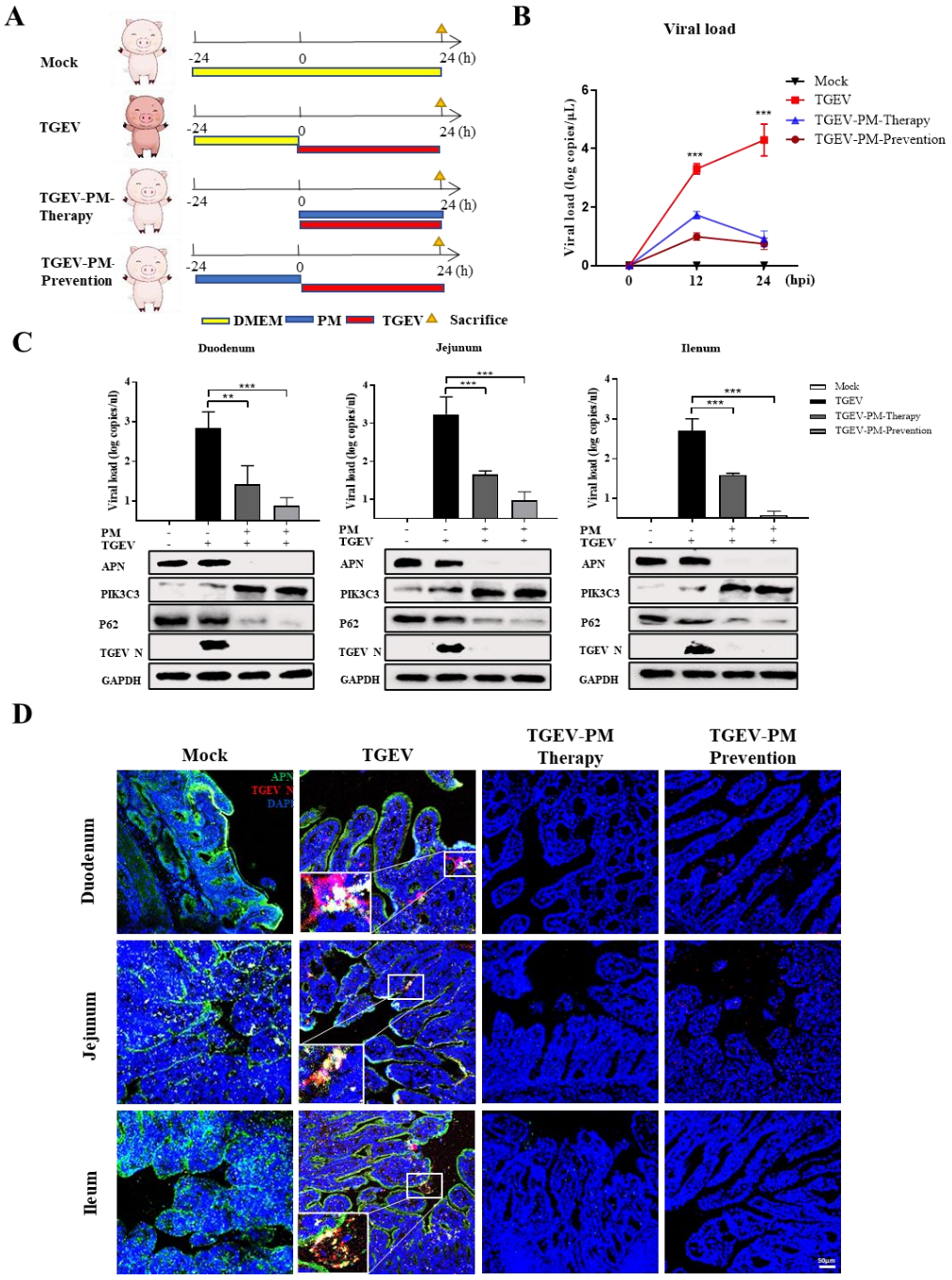

Figure 18. Oral administration of PM reduces TGEV pathogenicity by autophagic degradation of APN in piglets.

(A) Experimental schemes for testing therapeutic and prophylactic efficacy of PM treatment

against TGEV challenge in four groups of piglets. (B) Viral shedding was measured by RT-qPCR every 12 h postinfection. (C) TGEV genome copy numbers of duodenum, jejunum and ileum were detected by RT-qPCR and APN, PIK3C3, P62 and TGEV N in small intestine were determined by western blot from piglets sacrificed at 24 h pi. (D) IFA of TGEV N and APN in different segments of small intestine from piglets sacrificed at 24 hpi. Scale bar: 50 μm. Results are presented as mean ± SD of data from three independent experiments **, $P \leq 0.01$; ***, $P \leq 0.001$.

Table 2 Pharmacokinetic parameters of PM

Parameter	Unit	Mean ± SD
$AUC_{(0-t)}$	mg/L*h	975.253±33.380
$AUC_{(0-\infty)}$	mg/L*h	1341.054±21.475
$MRT_{(0-t)}$	h	10.735±0.155
$MRT_{(0-\infty)}$	h	19.027±1.388
$t_{1/2z}$	h	11.784±0.954
T_{max}	h	7.333±2.309
CLz/F	L/h/kg	0.074±0.001
Vz/F	L/kg	1.267±0.093
C_{max}	mg/L	62.645±0.677

3.4 Discussion

In recent years, the outbreak and prevalence of coronavirus have posed major threats to human health and the livestock industry. In addition to vaccines and neutralizing antibodies, diverse small molecule drugs that target virus functional receptors are promising therapeutic options. Wang et al. reported that diltiazem blocks SARS-CoV-2 attachment and penetration by decreasing ACE2 expression in different types of cell lines and mouse lungs [156]. Moreover, inhibitors of the cell receptor DPP4 could modulate the pathogenesis of MERS-CoV infection and serve as potential therapeutics [157]. In our study, we first found that PM significantly inhibited invasion of TGEV and PRCV but not that of PEDV. Despite the unknown underlying mechanisms involved, we inferred that PM may play an inhibitory role by modulating the TGEV and PRCV receptors.

APN, a member of the M1 zinc metallopeptidase family, is a multifunctional metalloenzyme expressed in many cells and a cell receptor that mainly mediates alphacoronavirus invasion [128, 158]. A previous study reported that TGEV and PRCV invade host cells through the binding of APN to their spike proteins [128]. However, it has been reported that PEDV entry into Vero-E6 cells and porcine small intestine epithelial cells is APN independent and that APN-KO piglets are protected from TGEV but not from PEDV infection [49, 159]. In the present study, PM dampened TGEV and PRCV infection *in vitro* and *ex vivo* mainly by blocking their internalization but

not by blocking PEDV internalization. Because of the same functional receptor for TGEV and PRCV, we speculated that APN was involved in this effect. As expected, PM significantly inhibited porcine-derived APN expression to block APN-restricted coronavirus penetration in ST cells, porcine intestinal organoid monolayers, apical-out intestinal organoids and piglets. Furthermore, the overexpression of APN can obviously ameliorate TGEV infection, which means that APN degradation is a dominant factor in the effectiveness of PM treatment against TGEV infection. Notably, PM degraded human and mouse-derived APN receptors, implying that PM may inhibit human and mouse APN-dependent coronavirus infection. It is noteworthy that PM does not exhibit a degradative effect on pattern recognition receptor RIG-I and TLR4, as well as coronavirus receptors ACE2 and CEACAM1, excluding DPP4, which is the cell receptor for MERS-CoV and SARS-CoV-2[160]. These findings suggested that PM may pose potential in impeding MERS-CoV and SARS-CoV-2 infections by targeting DPP4 for degradation, nonetheless this possibility needs to be further explored.

Transition metals such as potassium (K), manganese (Mn), and zinc (Zn), which are necessary for all forms of life, have been reported to restrict many viral infections [161]. Specifically, manganese activates antiviral innate immunity via the cGAS-STING pathway against DNA virus infection [162]. Zinc restricts coronavirus replication and arterivirus RNA polymerase activity [163] and was even used as a drug for asymptomatic or mild coronavirus disease 2019 (COVID-19) infection in a randomized controlled trial [164]. Furthermore, silver nanoparticles were also indicated to be antiviral materials against nonenveloped and enveloped viruses [165]. Copper has recently been reported to orchestrate broad-spectrum virus resistance by regulating the SPL9-miR528-AO pathway [166]. A recent study showed that cerium molybdates have antiviral activity against the bacteriophage Φ6 and SARS-CoV-2, but the detailed underlying mechanisms are unclear [167]. Thus, the PM-mediated antiviral phenomenon has been poorly studied, and the underlying mechanisms have also been elucidated. Interestingly, neither potassium ions nor molybdate, which are the main elements of PM, had a significant effect on TGEV infection, while the synergistic effect of potassium ions and molybdate suppressed TGEV and PRCV infection, suggesting that only potassium ions and molybdate synergy or PM compounds have a vital inhibitory effect on TGEV and PRRSV infection.

Three canonical pathways, the autophagy–lysosome pathway, proteasome pathway, and apoptotic pathway, are involved in protein degradation [168-169]. In the present study, PM decreased APN expression to block APN-restricted coronavirus penetration via the autophagy–lysosome pathway, which indicated that PM-mediated autophagy regulates coronavirus infection [102]. Specifically, autophagy has been reported to negatively regulate TGEV infection, but the underlying mechanism has not been further explored. Here, the PM induced autophagy to degrade TGEV cell receptors through PIK3C3-mediated autophagy, which may explain why autophagy inhibited TGEV infection. In addition, the phosphorylation of PIK3C3, BECN1, and ATG14 has been reported to be critical for PtdIns3K complex assembly and the initiation of autophagy [170-171]. Our results suggest that PM can enhance the PIK3C3-BECN1-ATG14 interaction by inducing PIK3C3 Ser249 phosphorylation, but molecular docking revealed that PM cannot directly bind PIK3C3. Despite the lack of studies on

the underlying mechanisms, we speculate that PM plays a role in several aspects of this process. First, due to molybdate being the active site of several molybdenum-requiring enzymes, PM may function in the metabolism of purines, hormone biosynthesis, and protein synthesis, thus mediating PIK3C3 expression [172-174]. Second, molybdate is a kind of phosphatase substrate, and inactivating alkaline phosphatase enzymes may be one strategy for increasing PIK3C3 Ser249 phosphorylation [175-176]. Based on our data, we infer that PM may regulate the protein conformation of PIK3C3 to increase its expression and activation; however, these findings need to be further verified. In addition, knockdown and knockout of PIK3C3 partially reversed viral replication, suggesting that other pathways might be involved in the restriction of TGEV and PRCV entry by PM. The Kv1.3 ion channel was revealed to restrict hepatitis C virus (HCV), dengue virus (DENV) and Zika virus (ZIKV) entry by inhibiting endosome acidification-mediated viral membrane fusion[177]. Therefore, we speculate that the Kv1.3 ion channel may also be involved in blocking TGEV and PRCV entry via the synergistic effect of potassium ions with molybdate during PM treatment, but this possibility needs to be further explored. In addition, autophagic degradation always occurs in the cytoplasm[145], but why APN, a membrane protein, can be degraded is still unclear. Endosomes, PAK1-mediated cytoskeleton rearrangement and SUMOylation have been proven to be involved in the autophagic degradation of membrane proteins[178-180]. We hypothesize that these mechanisms may mediate the autophagic degradation of APN, although Co-IP detection revealed that PIK3C3 can precipitate with APN (data not shown). However, further studies are needed to understand this phenomenon in detail.

In conclusion, our research is the first to reveal that PM blocks APN-dependent coronavirus entry by degrading receptors via PIK3C3-mediated autophagy **(Fig. 19)**. These findings indicate that PM could be considered an inhibitor of current and emerging APN-dependent coronaviruses in humans and animals. Our study provides novel insight into the degradation of cell receptors on viruses through autophagic pathways to block receptor-dependent virus entry.

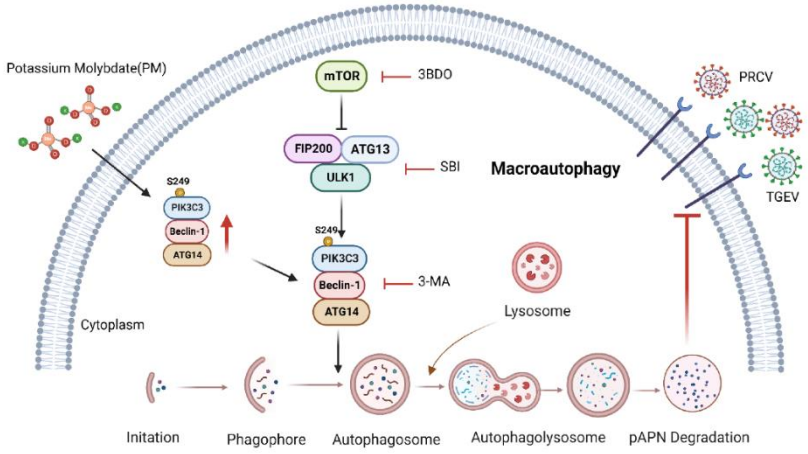

Figure 19. The schematic diagram of PM blocking APN-dependent coronavirus entry by

degrading receptor via PIK3C3-mediated autophagy.

PM promoted PIK3C3-BECN1-ATG14 complex assembly by enhancing PIK3C3 Ser249 phosphorylation to induce autophagy, which degraded cell receptor APN to block APN-dependent coronavirus entry. The diagram was created in BioRender.com.

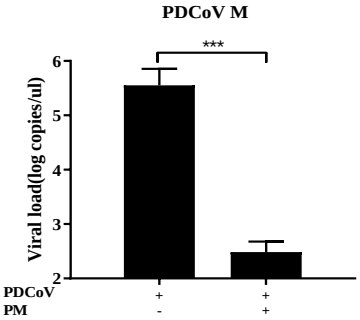

Supplementary Figure 1. PM inhibits PDCoV infection.

(A) The PK1 cells, pretreated with PM (10mM) concentrations for 1 h were infected with PDCoV (0.1 MOI) for 1 h and were again treated with PM at 37 °C for 17 h. The cell samples were collected and examined by RT-qPCR. Results are presented as mean ± SD of data from three independent experiments ***, P≤ 0.001.

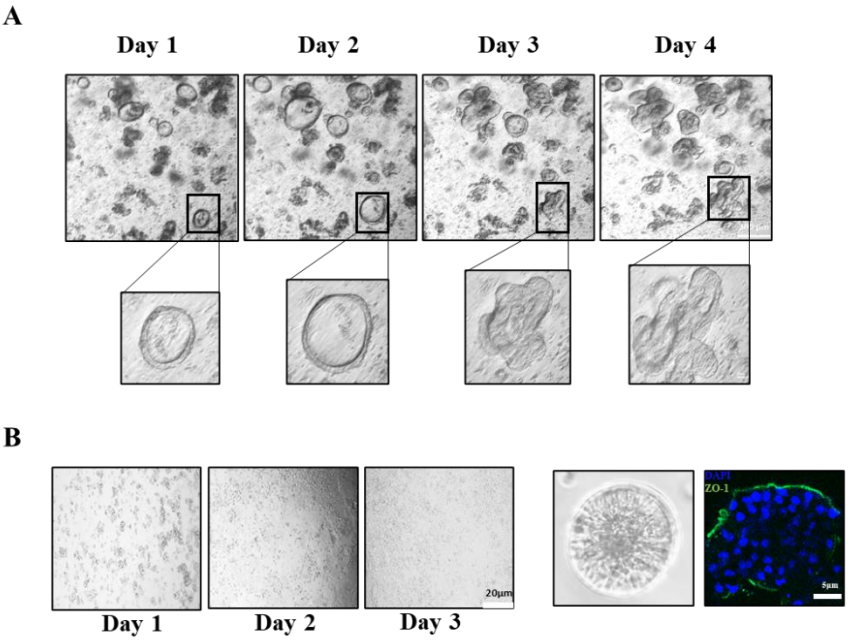

Supplementary Figure 2. Establishment of intestinal organoids monolayer and apical-out intestinal organoids.

(A) Isolation of porcine intestinal crypts cultured for 1-4 days. (B) Generation of intestinal organoids monolayer and apical-out porcine intestinal organoids were successfully established with ZO-1 in the outer membrane of organoids by IFA detection, Scale bar: 5 μm.

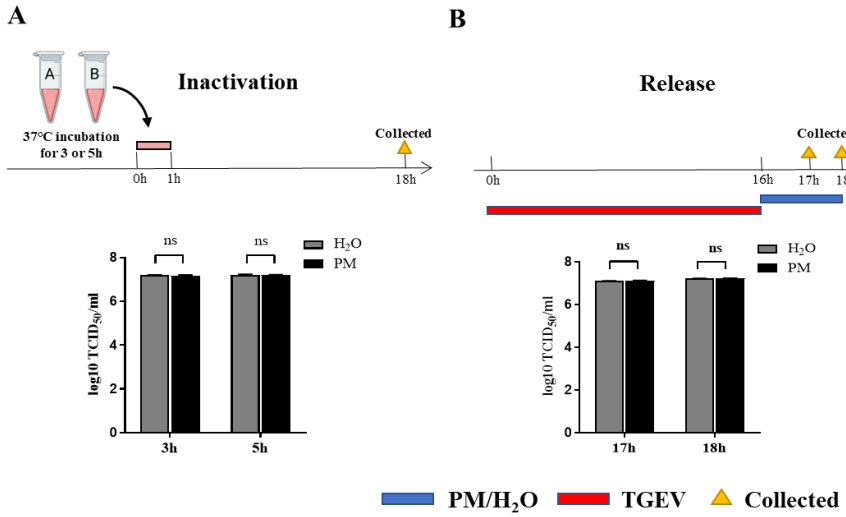

Supplementary Figure 3.PM cannot inactivate TGEV and affect viral release

(A) Inactivated assay. A: TGEV (0.1 MOI) + PM (10 mM) or B: TGEV (0.1 MOI) + H_2O were mixed and incubated at 37 °C for 3 h and 5 h respectively and then the mixtures were added into ST cells. After incubation at 37°C for another 1 h, culture supernatants were replaced with fresh culture medium for 17 h at 37°C. After washing with PBS, the mRNA levels and viral load of TGEV N protein were measured by $TCID_{50.}$ (B) Release assay. ST cells were infected with 0.1 MOI TGEV (red bar) for 16 h and then PM (10 mM) or H_2O (blue bar) was added to the cells for 1 h or 2 h. $TCID_{50}$ was used to test the viral titers in supernatant. Results are presented as mean ± SD of data from three independent experiments ns, no significant.

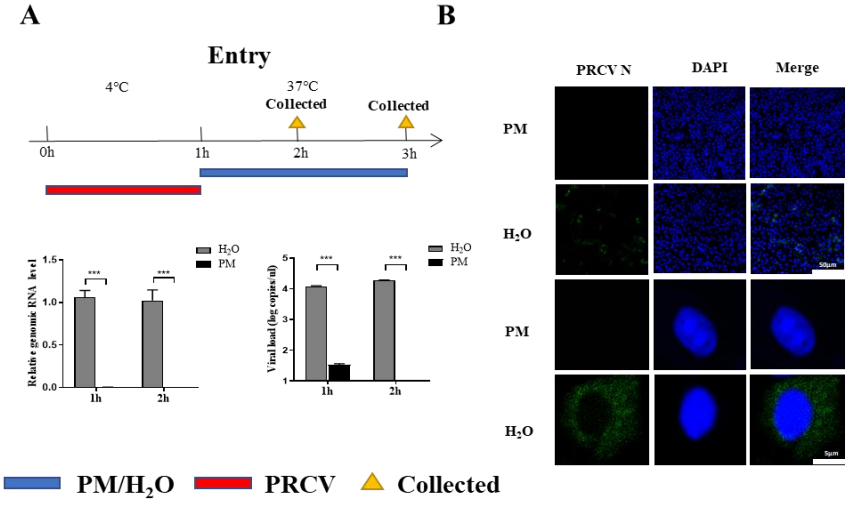

Supplementary Figure 4.PM blocks PRCV internalization.

(A and B) Entry assay. ST cells were infected with 0.1 MOI PRCV for 1 h at 4 °C, and were then treated with PM (10 mM) or H_2O for 1 h or 2 h at 37 °C. The cells samples were washed using sodium citrate buffer and detected by RT-qPCR (A) and IFA (B), Scale bar: 50 μm /5 μm. Results are presented as mean ± SD of data from three independent experiments ***, $P \leq 0.001$.

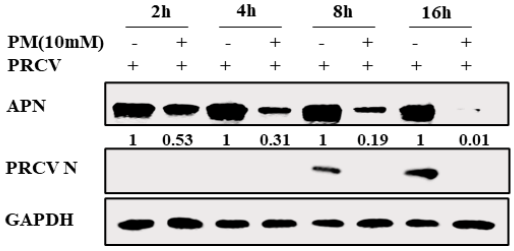

Supplementary Figure 5. PM blocks PRCV infection by degrading APN expression.

(A) ST cells were treated with PM (10 mM) and infected with 0.1 MOI PRCV at 2 h, 4 h, 8 h and 16 h. The cell samples were harvested and determined by western blot. All western blot results were calculated by Image J. All experiments were performed in triplicate.

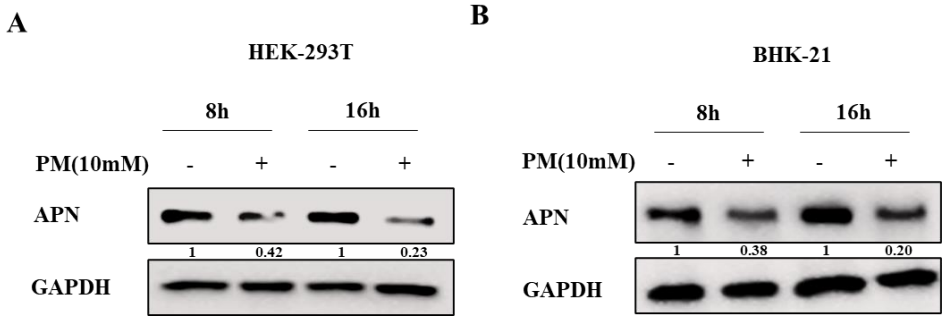

Supplementary Figure 6. PM degrades human and mouse-derived APN expression.

(A and B) HEK-293T cells (A) and BHK-21 cells (B) were treated with PM (10 mM) for 8 h or 16 h respectively, APN expression was measured by western blot. All western blot results were calculated by Image J. All experiments were performed in triplicate.

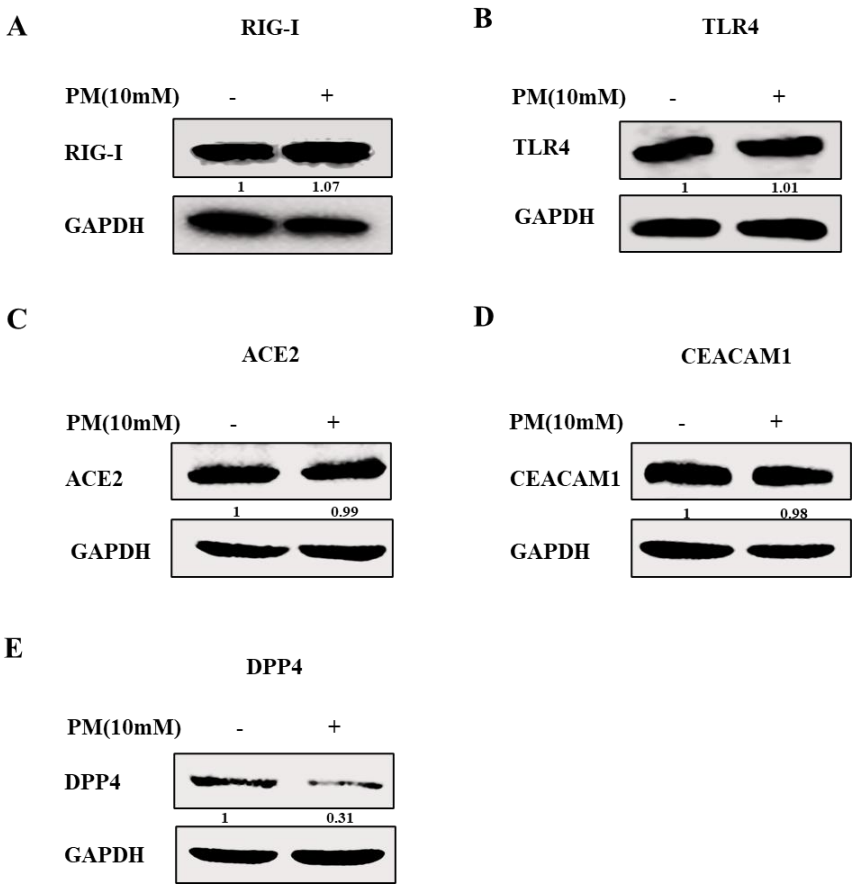

Supplementary Figure 7. PM cannot affect RIG-I, TLR4, ACE2, CEACAM1, but not DPP4 expression.

(A and B) ST cells were treated with PM (10 mM) for 16 h, RIG-I (A) and TLR4 (B) expression were detected by western blot. (C) 293T cells were treated with PM (10 mM) for 16 h, ACE2 (C) expression was determined by western blot. (D-E) A549 cells were treated with PM (10 mM) for 16 h, CEACAM1 (D) and DPP4 (E) expression were measured by western blot. All western blot results were calculated by Image J. All experiments were performed in triplicate.

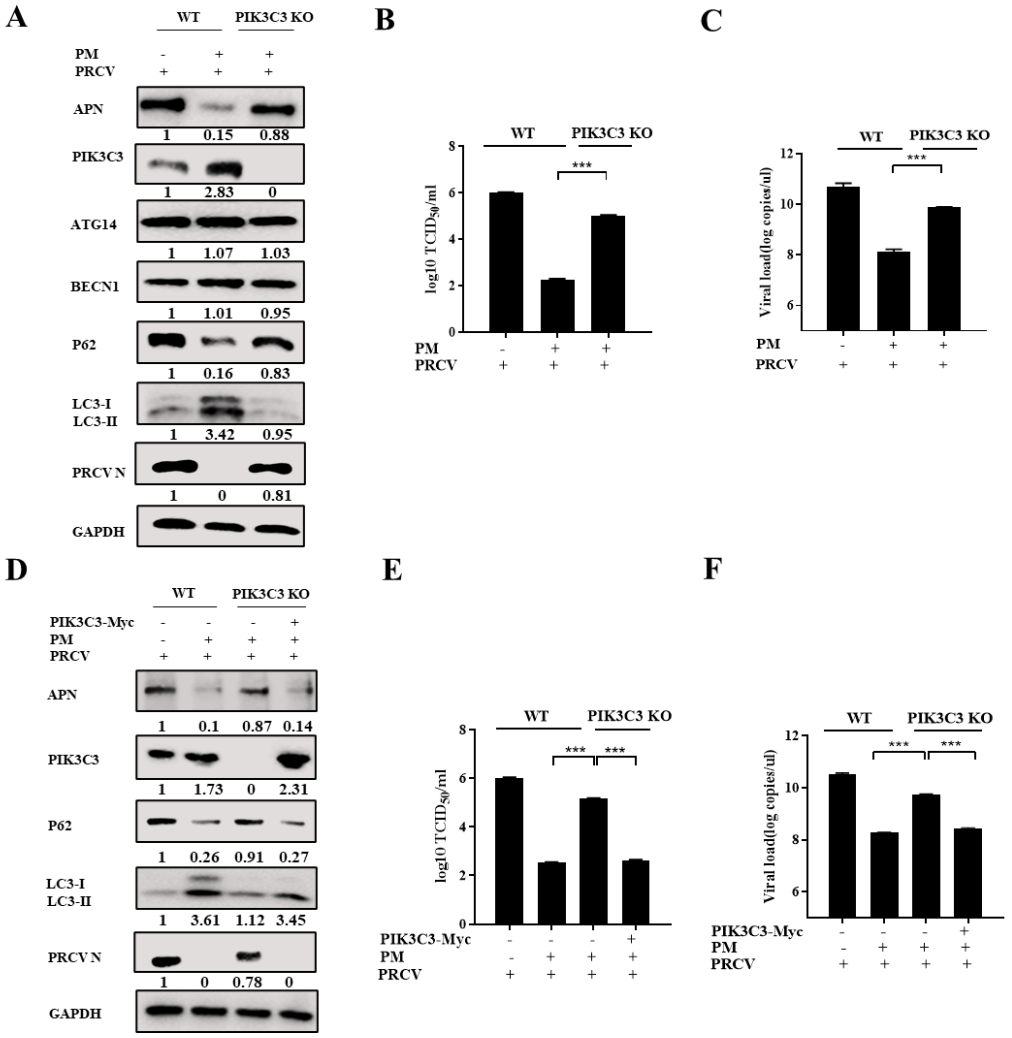

Supplementary Figure 8. PM inhibits PRCV infection by degrading APN via PIK3C3-mediated autophagy.

(A-C) WT ST cells and PIK3C3 KO ST cells were treated with PM (10 mM) and infected with PRCV (0.1 MOI) for 16 h. Then the APN, PIK3C3, ATG14, BECN1, P62, PRCV N and LC3 were detected by western blot (A), and viral titers and PRCV N mRNA level were determined by $TCID_{50}$ (B) and RT-qPCR (C). (D-F) WT ST cells and PIK3C3 KO ST cells transfected with pCMV-Myc and pCMV-Myc-PIK3C3 respectively for 24 h were treated with PM (10 mM) and infected with PRCV (0.1 MOI) for 16 h. The APN, PIK3C3, P62, PRCV N and LC3 were determined by western blot (D). $TCID_{50}$ (E) and RT-qPCR (F) were performed to detect viral titers and PRCV N m RNA level. All western blot results were calculated by Image J. Results are presented as mean ± SD of data from three independent experiments ***, $P \leq 0.001$.

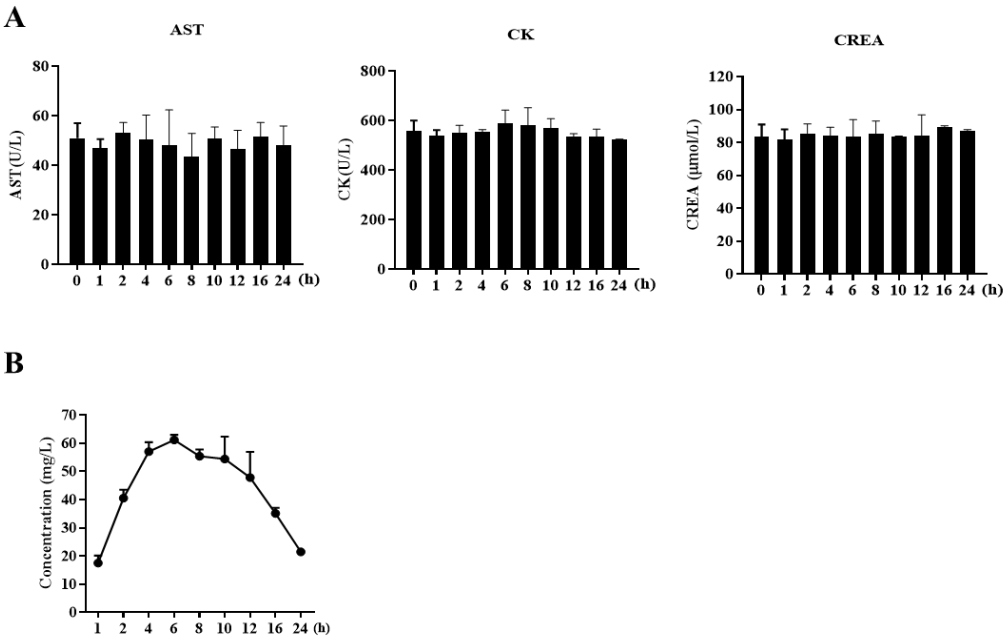

Supplementary Figure 9. Cytotoxicity assay and t1/2 detection of PM in piglets.

(A) The serum of piglets orally administered PM were collected at 1, 2, 4, 6, 8, 10, 12, 16 and 24 hours respectively and AST, CK and CREA level in those sera were measured by biochemical parameters. (B) PM concentrations at indicated times in piglets were determined by ICP-MS. Results are presented as mean ± SD of data from three independent experiments ns, no significant.

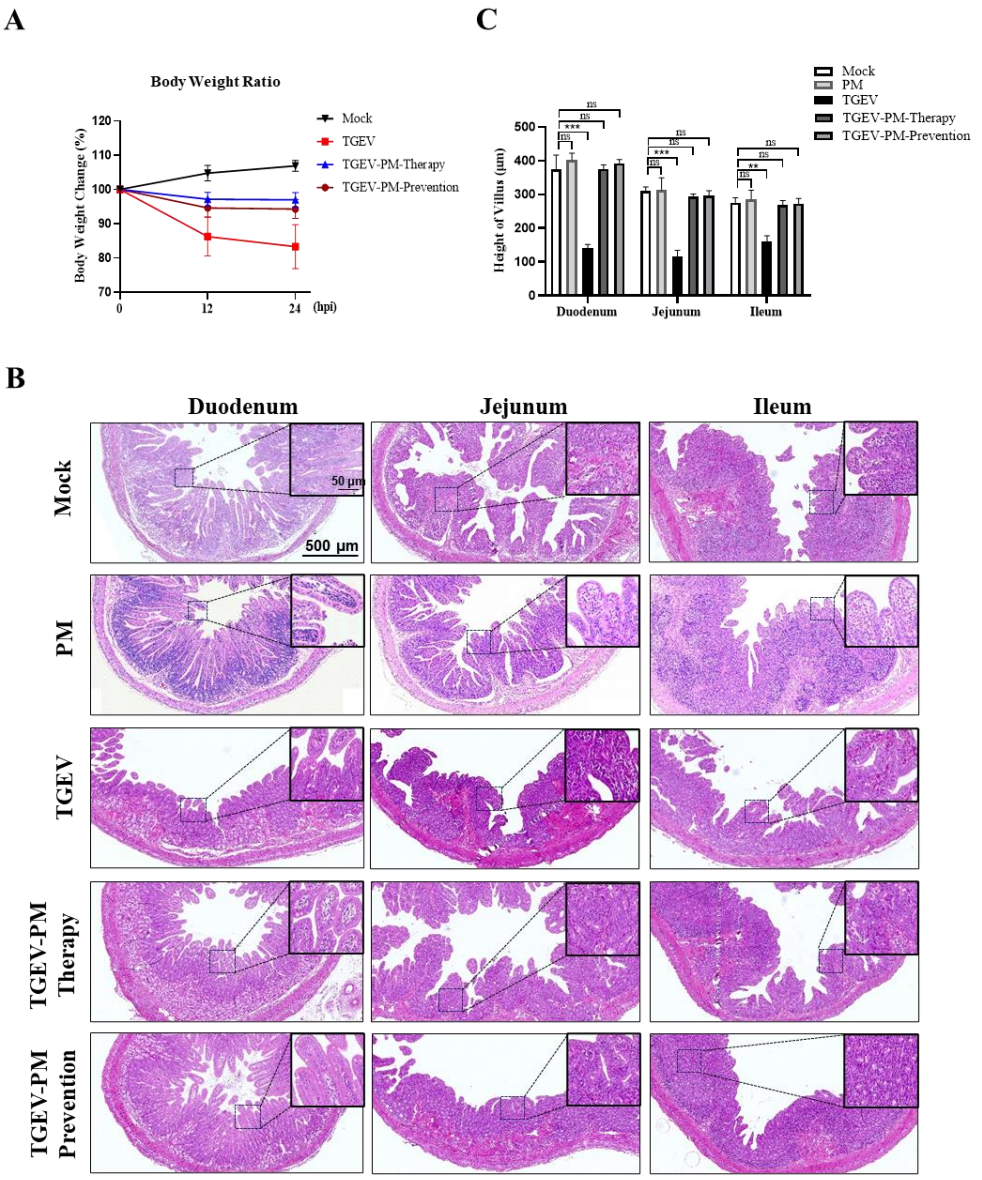

Supplementary Figure 10. PM reduces TGEV induced weight loss and intestinal damage.

(A) The body weight of piglets in each group was recorded every 12 h and calculated as %. (B) HE staining of three segments of small intestine from piglets sacrificed at 24 hpi. Scale bar: 500 or 50 μm. (C) Height of Villus for B was calculated by Image J. Results are presented as mean ± SD of data from three independent experiments **, $P \leq 0.01$; ***, $P \leq 0.001$.

Chapter 4

Transmissible gastroenteritis virus induces inflammatory responses via RIG-I/NF-κB/HIF-1α/Glycolysis axis in intestinal organoids and *in vivo*

Foreword

Excessive inflammation can cause severe damage to target organs, leading to a range of related symptoms, and is a significant factor in the high mortality rate of piglets. However, the underlying mechanism remains unclear. Consequently, in Chapter 4, we concentrated on investigating the inflammation induced by porcine coronaviruses.

In our recently published article in May 2024, we investigated the mechanisms underlying TGEV-induced inflammation. We began by utilizing apical-out porcine intestinal organoids to explore the infection and inflammatory responses triggered by TGEV. In this organoid model, we identified the key pattern recognition receptors (PRRs), inflammatory pathways, and pro-inflammatory factors involved in TGEV-induced inflammation. Subsequent pig experiments corroborated these findings, demonstrating the same trends observed in the organoids model.

This chapter has been adapted from the article:

Zhang Y, Yang N, Li Y, Tan C, Cai Y, Rui X, Liu Y, Fu Y*& Liu G*. Transmissible gastroenteritis virus induces inflammatory responses via RIG-I/NF-κB/HIF-1α/glycolysis axis in intestinal organoids and *in vivo*. **Journal of Virology**. 2024 May 23:e0046124.

Summary

Transmissible gastroenteritis virus (TGEV)-induced enteritis is characterized by watery diarrhea, vomiting, and dehydration, and has high mortality in newborn piglets, resulting in significant economic losses in the pig industry worldwide. Conventional cell lines have been used for many years to investigate inflammation induced by TGEV, but these cell lines may not mimic the actual intestinal environment, making it difficult to obtain accurate results. In this study, apical-out porcine intestinal organoids were employed to study TEGV-induced inflammation. We found that apical-out organoids were susceptible to TGEV infection, and the expression of representative inflammatory cytokines was significantly upregulated upon TGEV infection. In addition, retinoic acid-inducible gene I (RIG-I) and the nuclear factor-kappa B (NF-κB) pathway were responsible for the expression of inflammatory cytokines induced by TGEV infection. We also discovered that the transcription factor hypoxia-inducible factor-1α (HIF-1α) positively regulated TGEV-induced inflammation by activating glycolysis in apical-out organoids, and pig experiments identified the same molecular mechanism as the *ex vivo* results. Collectively, we unveiled that the inflammatory responses induced by TGEV were modulated via the RIG-I/NF-κB/HIF-1α/glycolysis axis *ex vivo* and *in vivo.* This study provides novel insights into TGEV-induced enteritis and verifies intestinal organoids as a reliable model for investigating virus-induced inflammation.

4.1 Introduction

Transmissible gastroenteritis virus (TGEV), a member of the genus *Alphacoronavirus* (family *Coronaviridae*, order *Nidovirales*), is a single-stranded, positive-sense RNA virus [53]. TGEV primarily attacks small intestinal epithelial cells and causes acute watery diarrhea, vomiting, dehydration, and anorexia, with high morbidity and mortality, particularly in nursing piglets [15]. Enteritis caused by TGEV results in high mortality in piglets less than 2 weeks old [129], suggesting that the inflammation of the small intestine might be instrumental in the pathogenesis of TGEV infection. Wang et al. reported that TGEV nonstructural protein 2 (Nsp2) contributes to inflammation via NF-κB activation in ST cells and IPEC-J2 cells [78]. However, ST cells and IPEC-J2 cells are immortalized single-cell lines, which may not reveal the actual inflammatory responses occurring *in vivo*. Therefore, a more physiological culture system is urgently needed for investigating TGEV-induced inflammation.

Intestinal organoids were differentiated from $Lgr5^+$ stem cells and first reported from mice in 2009 [181]. Intestinal organoids include many intestinal cell types, such as stem cells, goblet cells, Paneth cells, enterocytes etc., and can better mimic the real gut environment [181]. Recently, our laboratory developed an apical-out porcine intestinal organoid culture system and intestinal organoid monolayer to explore virus–host interactions and found that TGEV can infect organoid models and induce immune responses effectively [147-148]. Apical-out organoids, which are a three-dimensional (3D) culture model, are reported to be more likely to benefit viral infection and the differentiation of intestinal cell types, suggesting that they are a more physiological model for exploring inflammatory responses to TGEV infection [147].

Inflammatory responses are critical effectors of host responses against pathogen invasion, but excessive inflammatory responses can be harmful [182]. Coronavirus triggers inflammatory responses through a complex signal cascade [183]. In detail, pattern recognition receptors (PRRs) are appointed to sense pathogen-associated molecular patterns (PAMPs) [184]. PRRs related to coronavirus mainly include Toll-like receptor 3 (TLR3), Toll-like receptor 7 (TLR7), Toll-like receptor 8 (TLR8), retinoic acid-inducible gene I (RIG-I), and melanoma differentiation-associated gene 5 (MDA5), which all recruit adaptor molecules to mediate the signaling cascade [185]. Specifically, the Toll-like receptors recruit TIR-domain-containing adaptor-inducing IFN-β (TRIF) and myeloid differentiation primary response gene (MyD88) to activate downstream pathways. Meanwhile, RIG-I and MDA5 belong to the RIG-like receptors (RLRs), which interact with mitochondrial antiviral signaling protein (MAVS) to deliver the signal [186-187]. The production of inflammatory cytokines can be induced through the activation of various pathways such as NF-κB and mitogen-activated protein kinases (MAPK)-activating protein 1 (AP-1) pathways [74]. The classical NF-κB activation cascade is initiated by stimulus-induced ubiquitinated degradation of IκBα, releasing NF-κB dimers and promoting their nuclear translocation [188]. The AP-1 pathway is composed of JUN, FOS, or ATF (activating transcription factor) subunits, and activation of the pathway is characterized by the phosphorylation of JUN [189].

In this study, apical-out intestinal organoids were established to explore TGEV-

induced inflammation. Using this model, we found that, TGEV can effectively infect apical-out organoids and induce the production of inflammatory cytokines, such as tumor necrosis factor-α (TNF-α), interleukin-6 (IL-6), interleukin-8 (IL-8), interleukin-1β (IL-1β), and interleukin-18 (IL-18). In addition, we found that RIG-I, but not MDA5, can positively activate the NF-κB pathway to regulate TGEV-induced inflammation. Furthermore, hypoxia-inducible factor-1α (HIF-1α) was demonstrated to regulate TGEV-induced inflammation by activating glycolysis downstream of the RIG-I–NF-κB pathway. Finally, animal experiments showed the same molecular mechanism for TGEV-induced inflammation. Collectively, TGEV induces inflammatory responses via the RIG-I/NF-κB/HIF-1α/glycolysis axis in apical-out intestinal organoids and pigs.

4.2 Materials and methods

4.2.1. Cell culture, virus, and animals

ST cells for $TCID_{50}$ detection were maintained in DMEM (Sigma-Aldrich, USA, D6429) with 10% fetal bovine serum (Invigentech, Brazil, A6901). The cells were incubated at 37 °C in a humidified incubator with 5% CO_2. The TGEV Miller strain was maintained in our laboratory and the titer was $10^{7.25}$ $TCID_{50}$/mL. Porcine intestines for crypts isolation were obtained from Luoniushan Co., Ltd (Hainan Province, China).

4.2.2. Porcine intestinal 3D organoids culture

Porcine ileum crypts were isolated from pigs and cultured in Matrigel (Corning, USA, 356231) and OGM (Stem Cell, Canada, 06010) containing 10 μM ATP-competitive inhibitor of Rho-associated kinases (Y-27632; CST, USA, 72302) according to a published protocol [147].

4.2.3. Establishment of apical-out porcine intestinal organoids

Porcine 3D ileum organoids cultured with Matrigel for 5 days were dissociated by incubation with 5 mM cold EDTA buffer on a rotating platform for 1 h at 4 ℃. The organoids were then harvested by centrifugation at 250 *g* for 5 min, washed with ice-cold DMEM/F12 (Sigma-Aldrich, USA, D0697), and cultured in ultralow-attachment 24-well tissue culture plates (Corning, USA, 3473) in OGM supplemented with 10 μM Y-27632 at 37 ℃ and 5 % CO_2. According to the previously published protocol, the apical-out organoids were generated after 3 days [147].

4.2.4. Virus infection on apical-out organoids

Apical-out organoids were harvested from culture suspension by centrifugation at 250 *g* for 5 min and inoculated with the TGEV Miller strain (multiplicity of infection = 10) for 1 h at 37 °C. The virus residue was removed and washed three times with DMEM/F12 for centrifugation. The organoids were incubated in OGM in a 37 °C incubator supplied with 5% CO_2. Cells and supernatant were collected at indicated times for determination of viral load and inflammatory responses.

4.2.5. Histopathological and immunofluorescence analysis

Porcine ileum samples were collected, fixed for 24 h in 10% formalin, dehydrated according to the standard protocol, embedded in paraffin, and subjected to H&E staining by standard procedures. For IFA, apical-out porcine intestinal organoids were fixed with 4% paraformaldehyde for 20 min and then were blocked and permeabilized with 10 mM phosphate buffer (with 3% bovine serum albumin [Biofroxx, Germany, 4240GR100] and 1% Triton X-100 [Beyotime, China, ST797]) for 12 h at 4 °C. The apical-out organoids were labeled with primary antibodies for 24 h at 4 °C. After rinsing, secondary antibodies were incubated for 24 h at 4 °C. Next, 4', 6-diamidino-2-phenylindole (DAPI; Beyotime, China, C1006) was used to stain with the nucleus. After washing, the apical-out organoids were visualized using confocal laser-scanning microscopy (Zeiss LSM 900, Germany).

4.2.6. Nuclear and cytoplasmic extraction, Western blotting, and lactate measurement

Apical-out organoids were collected by NP40 containing PMSF per 20 μL of cell pellet and lysed to nuclear extract and cytoplasmic extract according to the manufacturer's recommendations (Nuclear and Cytoplasmic Protein Extraction Kit, Beyotime, China, P0027). For the Western blot, proteins were separated by sodium dodecyl sulfate-polyacrylamide gel electrophoresis (SDS-PAGE) and transferred onto a polyvinylidene fluoride (PVDF) membrane (GE, USA, 10600023). The membranes were blocked in 5% nonfat milk at room temperature for 2 h and incubated with specific primary antibodies overnight (see **Table 3** for antibodies). Subsequently, the secondary antibody was incubated with the membrane for 1 h at room temperature. Finally, the proteins on the membranes were visualized with WesternBright ECL (Advansta, USA, K-12045-D50) [150, 153]. The lactate level in supernatant or serum was determined by using a lactate assay kit (Dojindo, China, L256) according to the manufacturer's instructions.

Table 3. List of antibodies used in this study

Antibody	Type	Supplier	Product Number
ZO-1	Rabbit	Invitrogen	**PA5-85256**
Sox9	Rabbit	CST	82630
Villin	Mouse	Santa Cruz	SC-58897
CGA	Mouse	Santa Cruz	sc-393941
Muc2	Rabbit	Abcam	ab134119
LYZ	Rabbit	Invitrogen	PA5-16668
P65	Rabbit	proteintech	10745-1-AP
P-JUN	Rabbit	proteintech	28891-1-AP
P-P65	Rabbit	CST	3033
LaminB1	Rabbit	proteintech	12987-1-AP
IκBα	Rabbit	proteintech	10268-1-AP
RIG-I	Rabbit	proteintech	20566-1-AP
HIF-1α	Rabbit	proteintech	20960-1-AP

GAPDH	Rabbit	Proteintech	10494-1-AP

4.2.7. RNA extraction, real-time quantitative PCR, and protein microarray

Total RNA was extracted using RNAiso reagent (TaKaRa, Japan, 9109) and reverse transcribed into cDNA using HiScript Q RT SuperMix for qPCR (Vazyme, China, R223-01), both following the manufacturer's recommendations. The TGEV virus copy number was detected by the TaqMan probe-based RT-qPCR developed previously in our laboratory [149]. The relative qPCR was performed using the ChamQ SYBR qPCR master mix (Vazyme, China, Q311-02) and calculated with the $2^{-\Delta\Delta CT}$ method. The primers and probes used in this study are listed in **Table 4**. For protein microarray, samples of intestinal contents and serum were detected by Quantibody Porcine Cytokine Array 1 (Raybiotech, USA, QAP-CYT-1).

Table 4. Primers for real-time qPCR

Names	**Primer or probe**	**Sequence (5'-3')**
	Forward	TGCCATGAACAAACCAAC
TGEV N	Reverse	GGCACTTTACCATCGAAT
	Probe	HEX-TAGCACCACGACTACCAAGC-BHQ1*a*
TNF-α	Forward	GTCTCAAACCTCAGATAAG
	Reverse	GTTGTCTTTCAGCTTCAC
IL-8	Forward	TCCTGCTTTCTGCAGCTCTC
	Reverse	GGGTGGAAAGGTGTGGAATG
IL-6	Forward	AATGCTCTTCACCTCTCC
	Reverse	TCACACTTCTCATACTTCTCA
IL-1β	Forward	AGAGGGACATGGAGAAGCGA
	Reverse	GCCCTCTGGGTATGGCTTT
IL-18	Forward	CGATGAAGACCTGGAATCGG
	Reverse	CATCATGTCCAGGAACACTTCTCTG
RIG-I	Forward	AGAGCAGCGGCGGAATC
	Reverse	GGCCATGTAGCTCAGGATGAA
IFN-α	Forward	CTGCTGCCTGGAATGAGAGCC
	Reverse	TGACACAGGCTTCCAGGTCCC
IFN-β	Forward	CCACCACAGCTCTTTCCATGA
	Reverse	TGAGGAGTCCCAGGCAACT
IFN-λ1	Forward	CCACGTCGAACTTCAGGCTT
	Reverse	ATGTGCAAGTCTCCACTGGT
MDA5	Forward	TCCGGGAAACAGGCAACTC
	Reverse	CAAAGGATGGAGAGGGCAAGT
TLR3	Forward	GAGCAGGAGTTTGCCTTGTC
	Reverse	GGAGGTCATCGGGTATTTGA
TLR7	Forward	TCTGCCCTGTGATGTCAGTC
	Reverse	GCTGGTTTCCATCCAGGTAA
TLR8	Forward	CTGGGATGCTTGGTTCATCT
	Reverse	CATGAGGTTGTCGATGATGG
HIF-1α	Forward	GGCGCGAACGACAAGAAAAA

	Reverse	GTGGCAACTGATGAGCAAGC
NLRP3	Forward	GAGCCAGAATGGGACAATGCAAAT
	Reverse	CTTTCTTTTTCTTACAAATAGAG
NLRP6	Forward	CGGGACAATCCCCTAGGACT
	Reverse	CCTCCCTCCTCGTTCCAAGT
HMGB1	Forward	ACATCCTGGCCTGTCCATTG
	Reverse	TCGTATTTTTCCTTCAGCTTCGC
NEK7	Forward	GGCTGATTCCTGAGAGAACTGT
	Reverse	AGCCGGCTTTATATCTCGGTG
VEGF	Forward	CAAGATCCGCAGACGTGTAA
	Reverse	CAACGCGAGTCTGTGTTTCT
PKM2	Forward	TTCGCATCTTTCATCCGTAA
	Reverse	CGCCCAATCATCATCTTCT

4.2.8. Pig experiments

Neonatal pigs spontaneously delivered from sows did not receive colostrum and were confirmed to be negative for TGEV by RT-qPCR and enzyme-linked immunosorbent assay. They were kept into animal house for one day and fed with milk replacer in Biosafety Level 3 Laboratory (BSL-3). The piglets were randomly separated into three groups: mock (3 pigs), TGEV (3), and TGEV-BAY87 (3). For the TGEV group, piglets were orally infected 1.245×10^8 PFU TGEV for 24 h. For the TGEV-BAY87 group, piglets were orally administered BAY87 (10 mg/kg) every 12 h from 0 h to 48 h and orally infected with 1.245×10^8 PFU TGEV for 24 h. At 24 hpi, all pigs were euthanized, and intestinal tissues were collected for RT-qPCR, Western blot, and pathological examination. ALT and AST in serum were detected by biochemical parameters (HITACHI, Japan, 3110).

4.2.9. Ethics statement

All animals were handled in strict accordance with good animal practice according to the Animal Ethics Procedures and Guidelines of the People's Republic of China. The study was approved by The Animal Administration and Ethics Committee of Lanzhou Veterinary Research Institute, Chinese Academy of Agricultural Sciences (Permit No. LVRIAEC-2020-030).

4.2.10. Statistical analysis

All data were analyzed using GraphPad Prism 8.0 software (GraphPad, La Jolla, CA, USA) by one- or two-way analysis of variance. Differences between two groups are indicated as *, $P \leq 0.05$; **, $P \leq 0.01$; ***, $P \leq 0.001$. Every experiment was performed with three biological replicates, and the results were recorded as the mean ± standard deviation (SD).

4.3 Results

4.3.1. Apical-out porcine intestinal organoids are susceptible to TGEV

Porcine intestinal crypts were isolated from the intestinal follicle-associated epithelium of the ileum according to a previous protocol [147] and were cultured in Matrigel supplemented with organoid growth medium (OGM) **(Fig. S11A)**. The formation of crypt-villus structures was observed from 1 to 5 days **(Fig. S11B)**. To better mimic the physiological environment, apical-out intestinal organoids were established with zonula occludens-1 (ZO-1) in the outer membrane of the organoids, which means that apical-out organoids were successfully generated **(Fig. S11C and D)**. In addition, different intestinal epithelial cell subsets, including absorptive enterocytes (Villin-positive), enteroendocrine cells (CGA-positive), stem cells (SOX9-positive), goblet cells (MUC2-positive), and Paneth cells (LYZ-positive) were successfully detected in the apical-out organoids **(Fig. S11E)**. This finding illustrated that the apical-out organoids possessed complex multicellularity and thus were a more physiologically relevant research model.

To investigate whether the apical-out intestinal organoids were valid for exploring immune responses to viral infection, TGEV was employed to infect the organoids. Reverse transcription-quantitative PCR (RT-qPCR) and a 50% tissue culture infective dose ($TCID_{50}$) assay demonstrated that the apical-out organoids were susceptible to TGEV. The viral load in the supernatant and cells peaked at 48 hours post-infection (hpi) and subsequently decreased by 72 hpi **(Fig. 20A and B)**. The viral titer also peaked at 48 hpi **(Fig. 20C)**. In addition, Western blotting detected the presence of TGEV N protein **(Fig. 20D)**. Consistent with this finding, immunofluorescence assay (IFA) results also showed that apical-out intestinal organoids also detected expression of TGEV N at 48 hpi **(Fig. 20E)**. Collectively, these data illustrated that the apical-out porcine intestinal organoids were susceptible to TGEV.

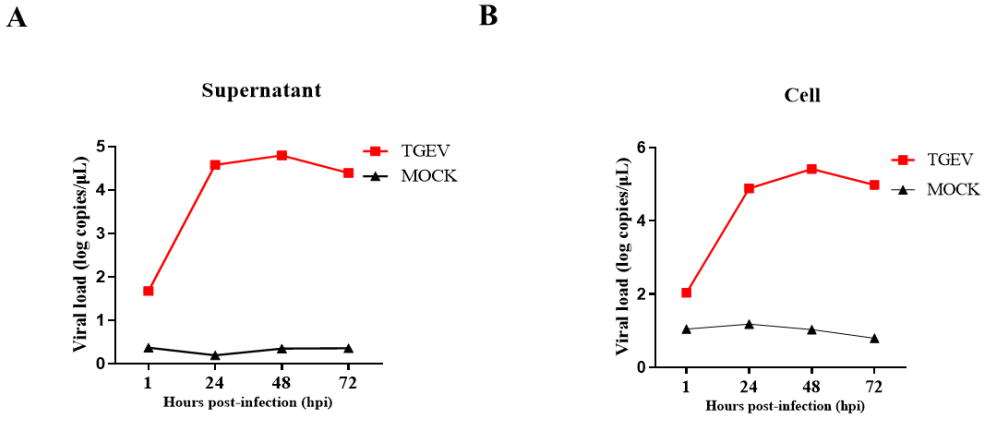

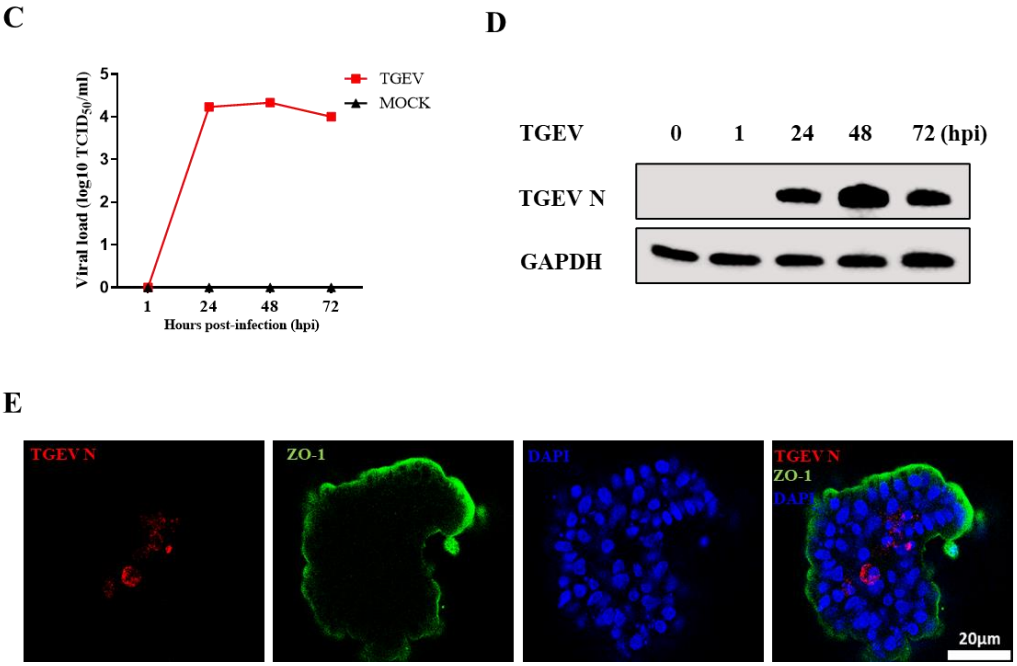

Figure 20. Apical-out porcine intestinal organoids are susceptible to TGEV.

(A–B) Apical-out organoids were inoculated with TGEV, and organoids and supernatant were collected at the indicated times for viral load detection by RT-qPCR. (C–D) TGEV titers and N protein at the indicated times were detected by $TCID_{50}$ and Western blotting, respectively. (E) Apical-out organoids infected with TGEV for 48 h were stained with TGEV N monoclonal antibody; scale bar: 20 μm. All experiments were performed in triplicate.

4.3.2. TGEV infection induces inflammatory responses in apical-out porcine intestinal organoids

To further investigate the inflammatory responses of apical-out organoids upon TGEV infection, the transcription levels of TNF-α, IL-8, IL-6, IL-1β, and IL-18 were evaluated by RT-qPCR. TNF-α and IL-8 mRNA levels peaked at 48 hpi **(Fig. 21A and B)**. Moreover, the TGEV infection significantly activated the transcription of IL-6 and IL-1β at 72 hpi **(Fig. 21C and D)**. Meanwhile, the level of IL-18 mRNA was also upregulated at 24 hpi **(Fig. 21E)**. These data demonstrated that inflammatory responses can be induced by TGEV infection in apical-out organoids.

Next, to determine whether these TGEV-induced inflammatory responses were caused by TGEV protein or by TGEV nucleic acid, the apical-out organoids were infected with UV-inactivated TGEV and TGEV, respectively. The results demonstrated that TGEV, but not UV-inactivated TGEV, could upregulate TNF-α, IL-8, IL-6, and IL-1β mRNA levels **(Fig. 21F)**, indicating that TGEV protein, but not nucleic acid, induced inflammation.

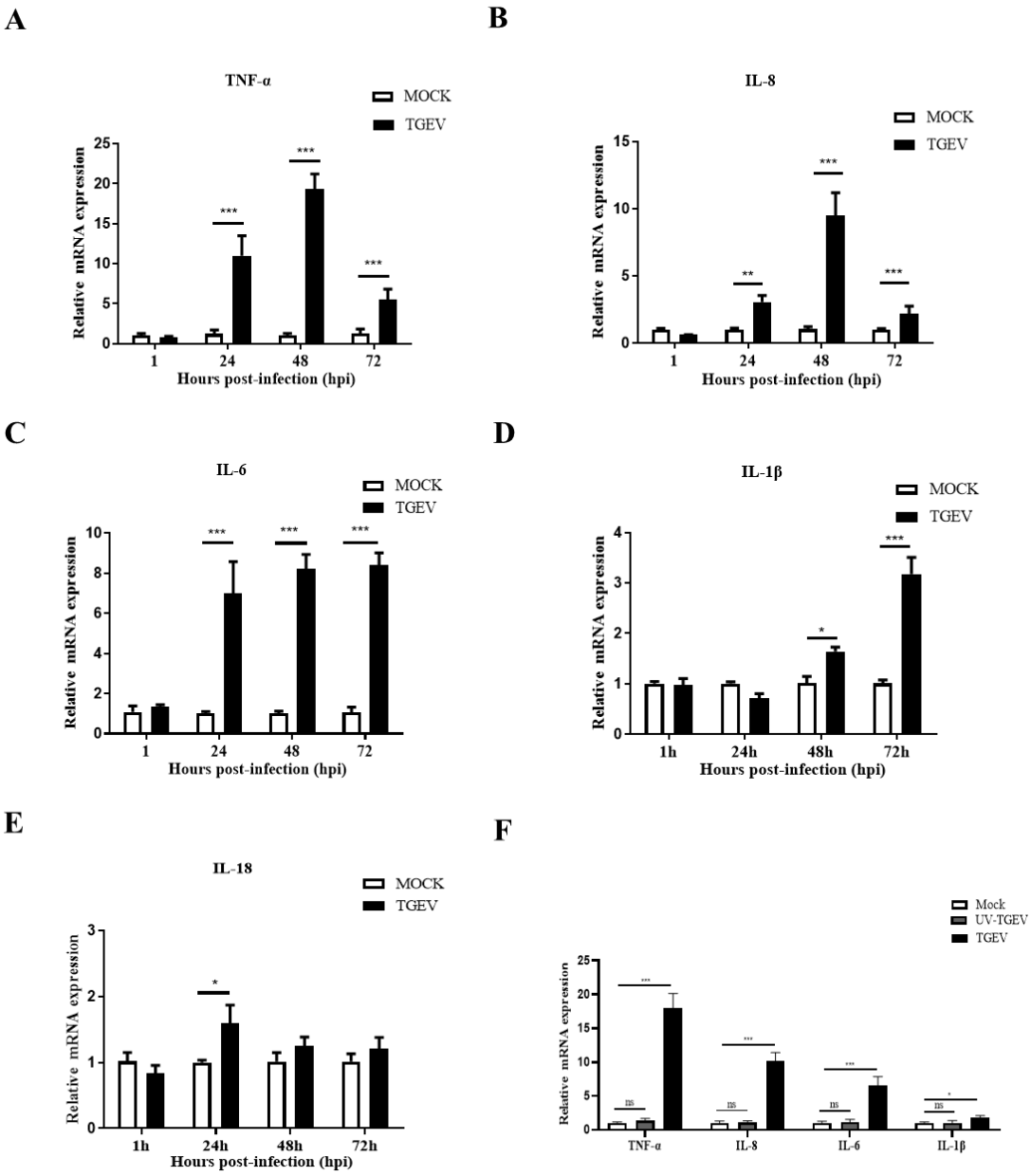

Figure 21. TGEV infection induces inflammatory responses in apical-out porcine intestinal organoids.

(A–E) Transcription levels of TNF-α, IL-8, IL-6, IL-1β, and IL-18 at the indicated times post-TGEV infection were evaluated by RT-qPCR. (F) Transcription levels of TNF-α, IL-8, IL-6, and IL-1β at 48 h after TGEV or UV-inactivated TGEV infection were measured by RT-qPCR. Results are presented as mean ± SD of data from three independent experiments *, $P \leq 0.05$;

**, $P \leq 0.01$; ***, $P \leq 0.001$.

4.3.3. TGEV infection induces inflammatory responses by RIG-I in apical-out porcine intestinal organoids

Activation of various PRRs represents the prime step of the inflammatory response to induce cytokine production. RIG-I, MDA5, TLR3, TLR7, and TLR8 have been reported to be involved in the immune response of coronavirus [185]. To explore which PRRs have critical roles in recognizing viral components and inducing inflammatory response during TGEV infection in apical-out organoids, the expression of PRRs, namely RIG-I, MDA5, TLR3, TLR7, and TLR8, was analyzed using RT-qPCR. The mRNA level of RIG-I was significantly upregulated, whereas no obvious changes in the expression of other PRRs were observed **(Fig. 22A and S12A)**. This trend was confirmed by Western blot analysis **(Fig. 22B)**. To elucidate the function of RIG-I in TGEV-induced inflammation, Cyclo (Phe-Pro), a specific inhibitor of RIG-I activation, was added to mock- or TGEV-infected organoids [190]. As expected, RIG-I activation was suppressed by Cyclo treatment **(Fig. 22C)**, and levels of inflammatory cytokines were also reduced in Cyclo-treated organoids during TGEV infection **(Fig. 22D)**. Furthermore, TGEV infection was enhanced by Cyclo treatment **(Fig. 22E)** and IFN responses were significantly decreased **(Fig. 22F)**. Cyclo exhibited no cytotoxicity at the concentrations used in this study **(Fig. S13A)**.

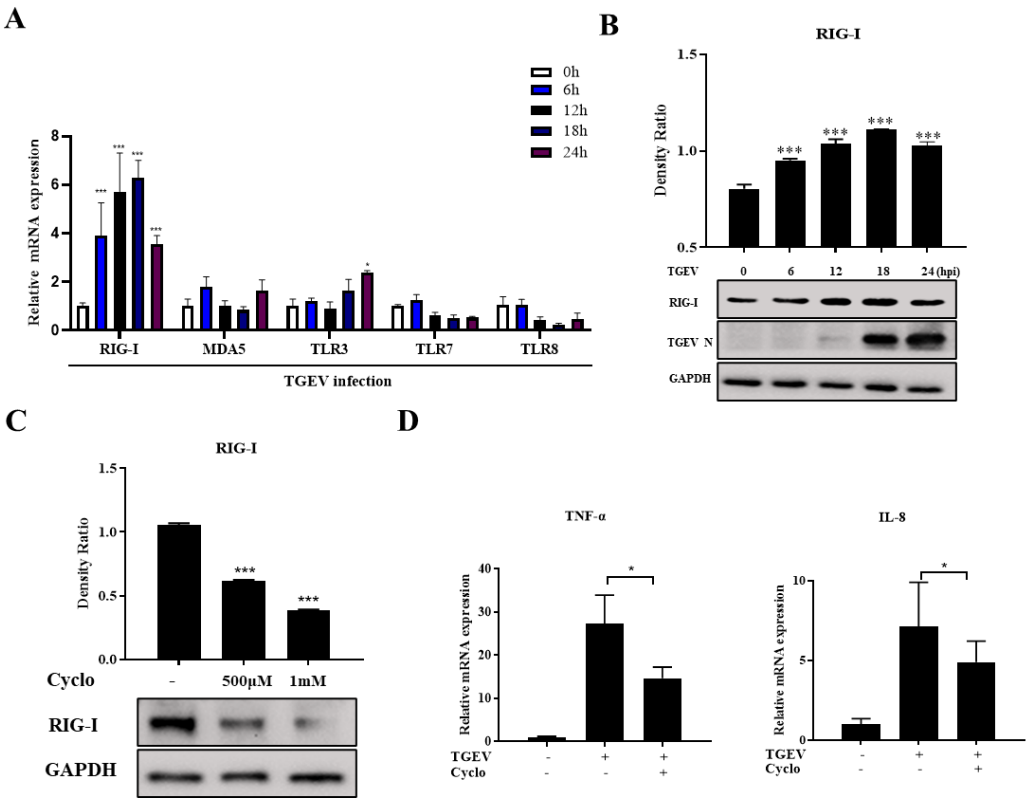

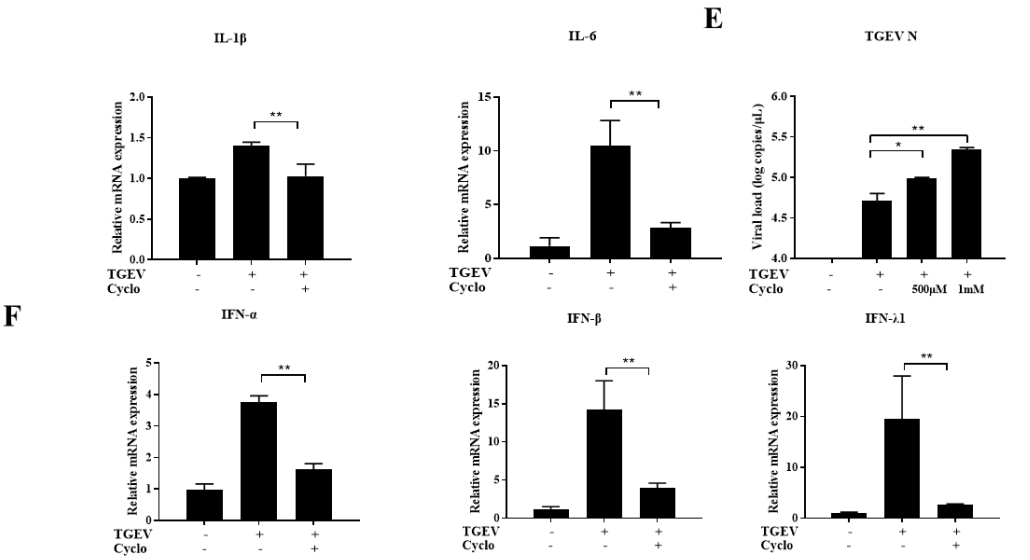

Figure 22.TGEV infection induces inflammatory responses by RIG-I in apical-out porcine intestinal organoids.

(A) Transcription levels of RIG-I, MDA5, TLR3, TLR7, and TLR8 in apical-out organoids at the indicated times post-TGEV infection were evaluated by RT-qPCR. (B) RIG-I expression in apical-out organoids at the indicated times post-TGEV infection was detected by Western blotting and calculated with Image J. (C) Apical-out organoids were treated with 500 μM or 1 mM Cyclo for 48 h, then RIG-I expression was measured by Western blotting and calculated with Image J. (D–F) Apical-out organoids were infected with TGEV followed by Cyclo treatment (1 mM) for 48 h. Subsequently, mRNA levels of TNF-α, IL-8, IL-6, and IL-1β (D), TGEV viral load (E), and mRNA levels of IFN-α, IFN-β, and IFN-λ1 (F) were determined by RT-qPCR. Results are presented as mean ± SD of data from three independent experiments *, $P \leq 0.05$; **, $P \leq 0.01$; ***, $P \leq 0.001$.

4.3.4. TGEV infection triggers inflammatory responses via the NF-κB pathway in apical-out porcine intestinal organoids

To further explore the role of key pathways of inflammatory cytokines during TGEV infection in apical-out intestinal organoids, the activation of NF-κB and AP-1 was determined by Western blotting to detect phosphorylation of P65 and JUN after TGEV infection. The level of phosphorylated P65 was significantly upregulated, whereas the phosphorylation of JUN was slightly increased after TGEV infection, suggesting that TGEV infection can markedly activate the NF-κB pathway **(Fig. 23A and B)**. This result was further confirmed by Western blotting, which showed that nuclear P65 expression and IκBα degradation were promoted by TGEV infection **(Fig. 23A and B)**. In addition, IFA results demonstrated that TGEV induced nuclear translocation of P65 in apical-out organoids at 48 hpi **(Fig. 23C)**.

To further investigate the effect of NF-κB activation on TGEV-induced inflammation, BAY11-7082 (BAY11), which is a specific inhibitor of NF-κB, was

added into mock- or TGEV-infected organoids. This inhibitor did not have any effect on viral load and cytotoxicity in organoids **(Fig. 23D and S3B)**. As expected, mRNA levels of inflammatory cytokines, including TNF-α, IL-8, IL-6, and IL-1β, were reduced in BAY11-treated organoids during TGEV infection **(Fig. 23E)**. This finding indicated that NF-κB signaling plays a critical role in the TGEV-induced inflammatory response in apical-out intestinal organoids.

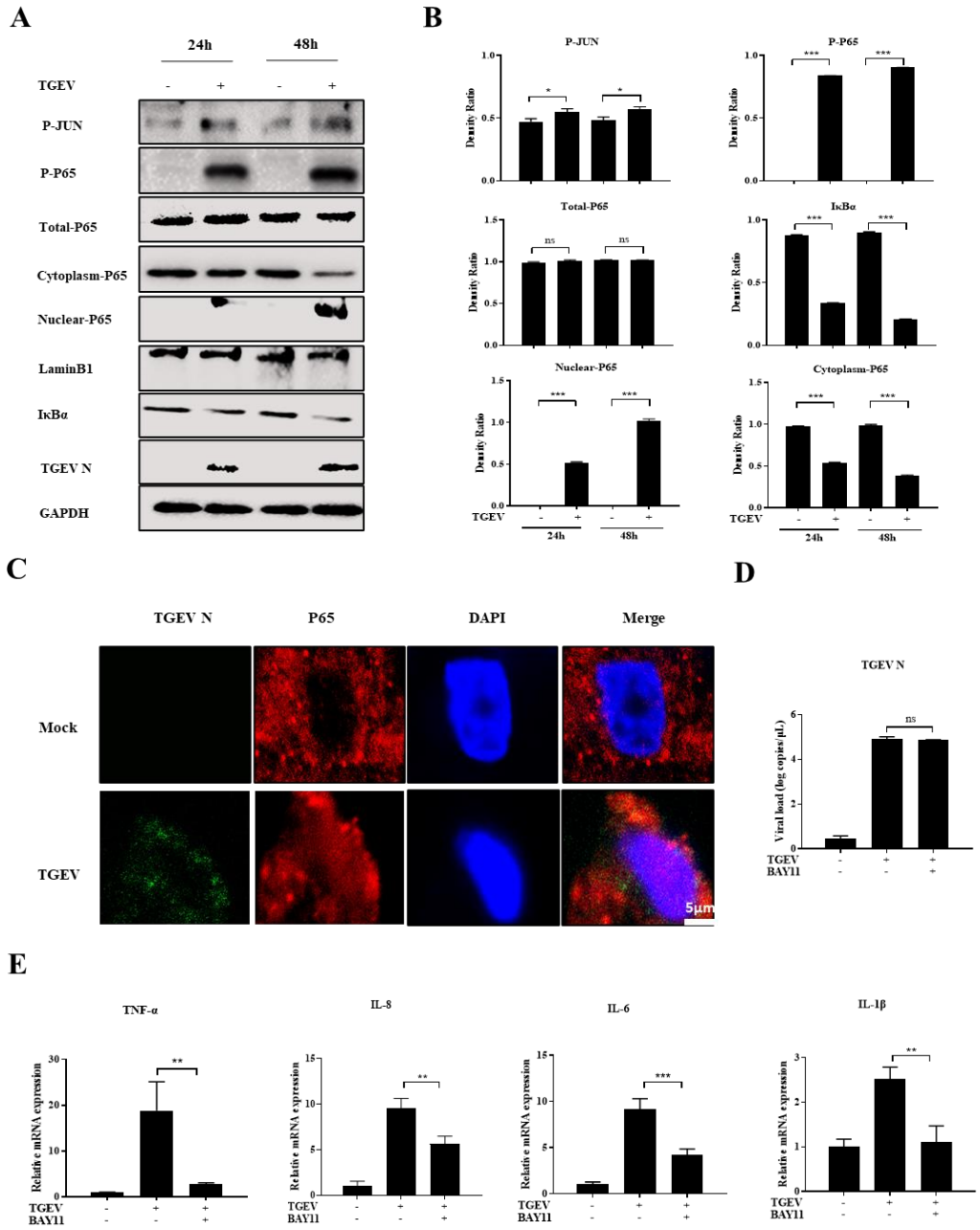

Figure 23. TGEV infection triggers inflammatory responses via the NF-κB pathway in apical-out intestinal organoids.

(A) Apical-out organoids were infected with TGEV for 24 and 48 h, then P-JUN, P-P65, total P65, cytoplasmic P65, nuclear P65, IκBα, and TGEV N were detected by Western blotting. (B) The density ratios of P-JUN, P-P65, total P65, cytoplasmic P65, nuclear P65, and IκBα were calculated with Image J. (C) TGEV-infected or mock-infected apical-out organoids at 48 h were stained with TGEV N and P65 and analyzed by confocal microscopy; scale bar: 5 μm. (D–E) Apical-out organoids were infected with TGEV followed by BAY11 (2 μM) treatment for 48 h. Subsequently, TGEV viral load (D) and mRNA levels of TNF-α, IL-8, IL-6, and IL-1β (E) were detected by RT-qPCR. Results are presented as mean ± SD of data from three independent experiments *, $P \leq 0.05$; **, $P \leq 0.01$; ***, $P \leq 0.001$.

4.3.5. RIG-I controls NF-κB pathway activation upon TGEV infection in apical-out porcine intestinal organoids

PRRs have been reported to regulate the NF-κB pathway to induce inflammation [191]. Therefore, we hypothesized that RIG-I controls NF-κB pathway activation after TGEV infection. To verify this hypothesis, RIG-I, the phosphorylation of P65, nuclear P65, cytoplasmic P65, and IκBα expression was measured after Cyclo treatment. Western blotting showed that when RIG-I activation was repressed by Cyclo, the phosphorylation of P65 and nuclear P65 were reduced and cytoplasmic P65 expression and IκBα degradation were restored compared to the TGEV-infected group **(Fig. 24A and B)**. Furthermore, TGEV-induced nuclear translocation of P65 was abolished by RIG-I inhibition **(Fig. 24C)**. These results illustrated that NF-κB pathway activation can be regulated by RIG-I upon TGEV infection.

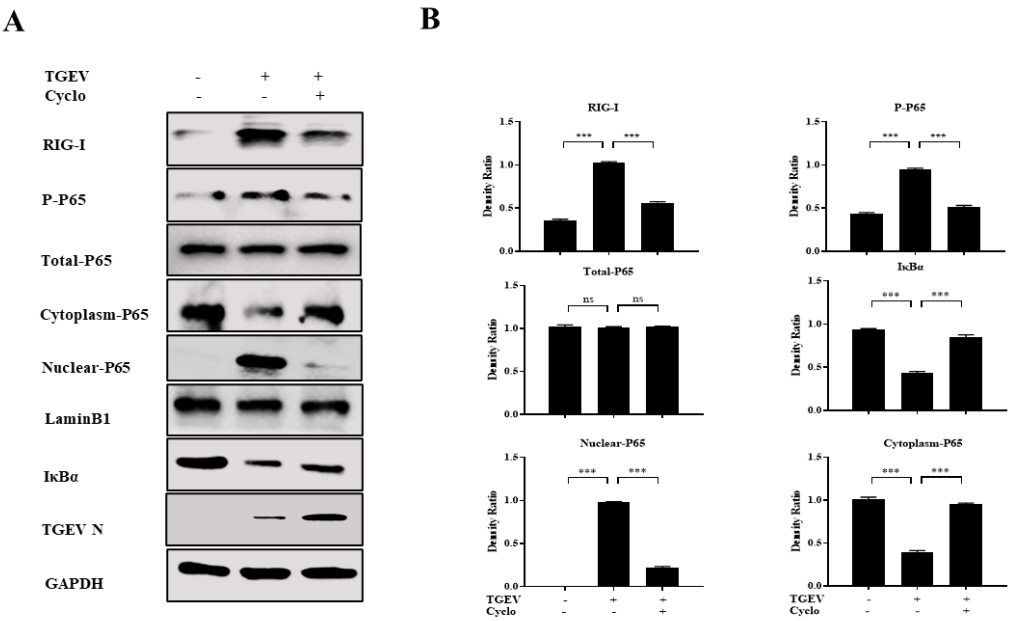

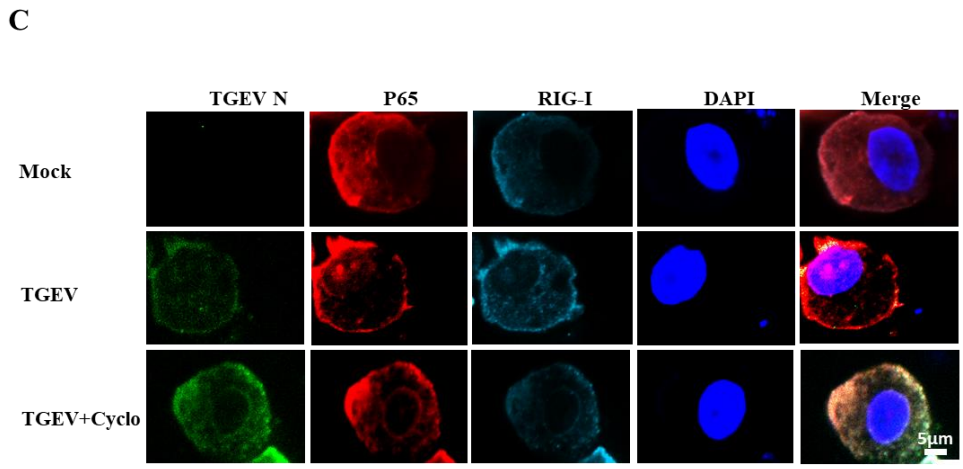

Figure 24. RIG-I controls NF-κB pathway activation upon TGEV infection in apical-out porcine intestinal organoids.

(A) Apical-out organoids were infected with TGEV followed by Cyclo (1 mM) treatment for 48 h, then RIG-I, P-P65, total P65, cytoplasmic P65, nuclear P65, IκBα, and TGEV N were detected by Western blotting. (B) The density ratios of RIG-I, P-P65, total P65, cytoplasmic P65, nuclear P65, and IκBα were calculated using Image J. (C) Apical-out organoids were infected with TGEV followed by Cyclo (1 mM) treatment for 48 h, and then the organoids were stained with TGEV N, P65, and RIG-I and analyzed by confocal microscopy; scale bar: 5 μm. Results are presented as mean ± SD of data from three independent experiments ***, P≤ 0.001; ns, not significant.

4.3.6. HIF-1α positively regulates TGEV-induced inflammation downstream of the RIG-I–NF-κB pathway

The above investigations demonstrated that TGEV induced inflammatory responses via the RIG-I–NF-κB pathway. We hypothesized that key factors participate in TGEV-induced inflammation downstream of the RIG-I–NF-κB pathway. This hypothesis was explored by screening some key proinflammatory proteins related to coronavirus, namely HIF-1α, NOD-like receptor family pyrin domain containing 3 (NLRP3), NOD-like receptor family pyrin domain containing 6 (NLRP6), high mobility group box-1 (HMGB1), and NIMA-related kinase 7 (NEK7). HIF-1α was significantly induced by TGEV infection, but inhibited after downregulation of RIG-I expression and NF-κB pathway by specific inhibitors, respectively, suggesting that the RIG-I–NF-κB pathway positively regulates HIF-1α expression upon TGEV infection **(Fig. 25A and B, Fig. S14A)**. Those inhibitors showed no cytotoxicity at the concentrations used in this study **(Fig. S13 and S14B)**. To further validate the role of HIF-1α on TGEV-induced inflammation, BAY 87-2243 (BAY87, a HIF-1α inhibitor) and $CoCl_2$ (a HIF-1α agonist) were employed. HIF-1α expression was inhibited by BAY87 treatment **(Fig. 25C)**, whereas $CoCl_2$ treatment significantly induced HIF-1α expression **(Fig. 25D)** in apical-out organoids. BAY87 and $CoCl_2$ exhibited no cytotoxicity at the concentrations used in this study (unpublished data). As expected,

TGEV-induced inflammatory cytokines were reduced after BAY87 treatment **(Fig. 25E)**, whereas the same cytokines were promoted by $CoCl_2$ treatment **(Fig. 25F)**, suggesting that HIF-1α positively controls TGEV-induced inflammation. In addition, pharmacological inhibition of HIF-1α could restrict TGEV infection **(Fig. 25G)**, whereas pharmacological upregulation of HIF-1α could promote TGEV infection **(Fig. 25H)**. Together, the proposed molecular mechanism is that TGEV induced inflammation via the RIG-I/NF-κB/HIF-1α axis in apical-out intestinal organoids.

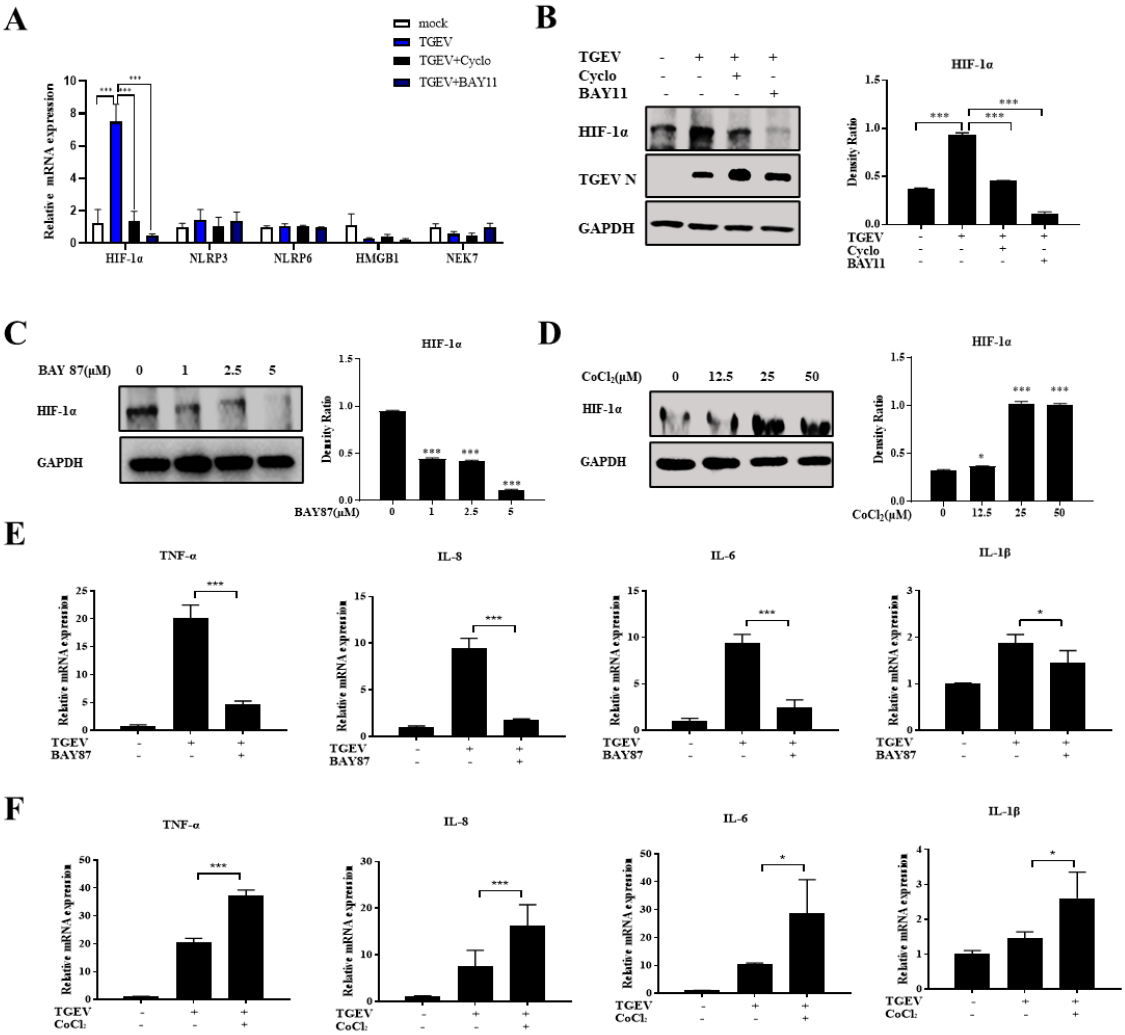

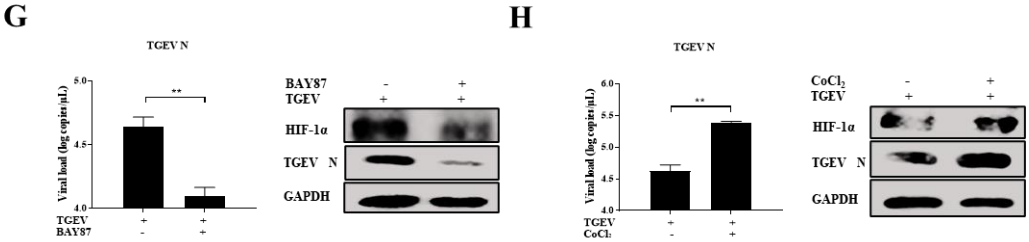

Figure 25. HIF-1α positively regulates TGEV-induced inflammation downstream of the RIG-I–NF-κB pathway.

(A–B) Apical-out organoids were infected with TGEV followed by Cyclo (1 mM) or BAY11 (2 μM) treatment for 48 h. Subsequently, transcription levels of HIF-1α, NLRP3, NLRP6, HMGB1, and NEK7 in the apical-out organoids post TGEV infection were measured by RT-qPCR (A) and HIF-1α protein expression was determined by Western blotting and analyzed using Image J (B). (C–D) Apical-out organoids were treated with the indicated concentrations of BAY87 or $CoCl_2$ for 48 h, then HIF-1α protein expression was detected by Western blotting and analyzed by Image J. (E–F) Apical-out organoids were infected with TGEV followed by BAY87 (5 μM) or $CoCl_2$ (25 μM) treatment for 48 h, then transcription levels of TNF-α, IL-8, IL-6, and IL-1β were determined by RT-qPCR. (G–H) Apical-out organoids were infected with TGEV followed by BAY87 (5 μM) or $CoCl_2$ (25 μM) treatment for 48 h, then TGEV viral load was detected by RT-qPCR, and TGEV N and HIF-1α protein expression was measured by Western blotting. Results are presented as mean ± SD of data from three independent experiments *, $P \leq 0.05$; **, $P \leq 0.01$; ***, $P \leq 0.001$.

4.3.7. TGEV infection triggers inflammatory responses by the RIG-I/NF-κB/HIF-1α pathway in pigs

Given the above results *ex vivo*, we hypothesized that TGEV induces inflammation via the RIG-I/NF-κB/HIF-1α axis *in vivo*. To verify this hypothesis, experiments were performed to evaluate how TGEV induces inflammatory responses in pigs. Groups of pigs were treated with Dulbecco's Modified Eagle's Medium (DMEM) or BAY87 and then inoculated with TGEV individually by oral administration **(Fig. 26A)**. First, RIG-I and MDA5 expression in the ileum of the mock and TGEV groups were measured. TGEV infection significantly upregulated RIG-I expression but not MDA5 expression **(Fig. 26B and S12B)**, which was consistent with *ex vivo* results. In addition, P65 was markedly phosphorylated after TGEV infection, suggesting that the NF-κB pathway is instrumental in TGEV-induced inflammation in pigs **(Fig. 26C)**. Furthermore, HIF-1α expression in the ileum was markedly induced by TGEV infection, but decreased after BAY87 treatment, and this treatment also inhibited TGEV infection *in vivo* **(Fig. 26D, S5A and S15B)**.

To further confirm the relationship between HIF-1α and TGEV-induced inflammation *in vivo*, the expression of TNF-α, IL-8, IL-6, and IL-1β was determined by RT-qPCR and protein microarray. We found that TGEV-induced cytokines in the ileum, intestinal digesta, and serum were downregulated after oral administration of BAY87 in pigs **(Fig. 26E, F, and G)**. In addition, alanine aminotransferase (ALT) and

aminotransferase (AST) were not changed by BAY87 treatment, meaning that oral administration of BAY87 was not cytotoxic in our animal model **(Fig. S16A)**. To further characterize the effect of HIF-1α on inflammatory infiltration caused by TGEV, ileum samples were paraffin-embedded, followed by slicing and staining with hematoxylin and eosin (H&E). Pharmaceutical inhibition of HIF-1α almost reversed the inflammatory infiltration of the ileum **(Fig. 26H)**. These results again suggested that TGEV triggers inflammatory responses predominantly via the RIG-I/NF-κB/HIF-1α axis *in vivo*.

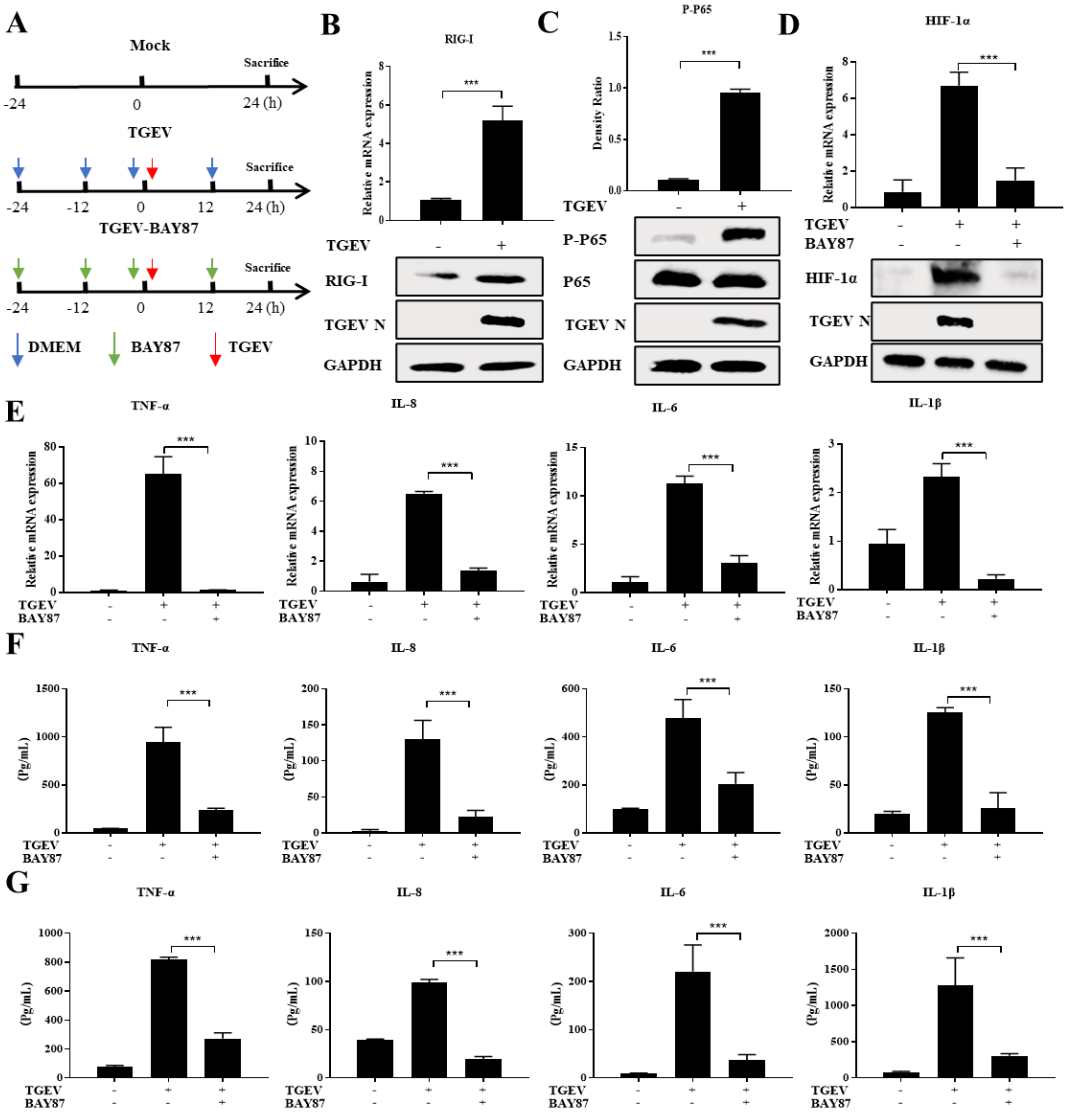

H

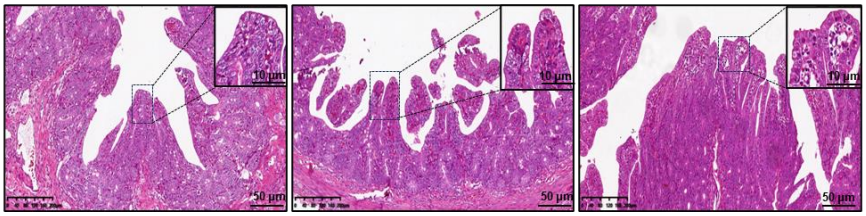

Figure 26. TGEV infection triggers inflammatory responses via the RIG-I/NF-κB/HIF-1α pathway *in vivo.*

(A) Experimental schemes in three groups of piglets. (B) The transcription level of RIG-I in the ileum from piglets sacrificed at 24 hpi was detected by RT-qPCR, and RIG-I and TGEV N protein expression in the ileum were determined by Western blotting. (C) Phosphorylated P65, P65, and TGEV N in the ileum from piglets sacrificed at 24 hpi were detected by Western blotting and analyzed by Image J. (D) The transcription level of HIF-1α in the ileum was detected by RT-qPCR, and HIF-1α and TGEV N in the ileum were measured by Western blotting. (E) The mRNA levels of TNF-α, IL-8, IL-6, and IL-1β in the ileum were determined by RT-qPCR. (F–G) A protein microarray was performed to detect TNF-α, IL-8, IL-6, and IL-1β in intestinal digesta (F) and serum (G). (H) Hematoxylin and eosin staining of ilea from piglets sacrificed at 24 hpi; scale bar: 10 or 50 μm. Results are presented as mean ± SD of data from three independent experiments ***, $P \leq 0.001$.

4.3.8. HIF-1α promotes TGEV-induced inflammatory responses by activating glycolysis

Although HIF-1α was proved to be an indispensable factor in TGEV-induced inflammation, the mechanism of HIF-1α-mediated inflammation upon TGEV infection was unclear and warranted further exploration. HIF-1α is known to positively regulate inflammatory responses mainly by upregulating vascular endothelial growth factor (VEGF) or activating glycolysis [192-193]. Therefore, in this study, VEGF and glycolysis were screened after TGEV infection. The results demonstrated that TGEV infection could not regulate VEGF expression, but could significantly upregulate lactate production and PKM2 expression, which are key markers of glycolysis activation. Moreover, the TGEV-induced lactate production and PKM2 expression were markedly decreased by BAY87 treatment, indicating that HIF-1α can positively regulate TGEV-induced glycolysis *ex vivo* **(Fig. 27A)** and *in vivo* **(Fig. 27B)**. To further verify the effect of HIF-1α-mediated glycolysis on TGEV-induced inflammation, 2-DG (a glycolysis inhibitor) was employed to treat TGEV-infected organoids. As expected, TGEV-induced inflammation was obviously decreased and TGEV infection was also inhibited by pharmaceutical inhibition of glycolysis **(Fig. 27C and D)**. In addition, 2-DG presented no cytotoxicity at the concentrations used in this experiment **(Fig. 27E)**. Collectively, the proposed molecular mechanism is that TGEV induces inflammation via the RIG-I/ NF-κB/HIF-1α/glycolysis axis **(Fig. 28)**.

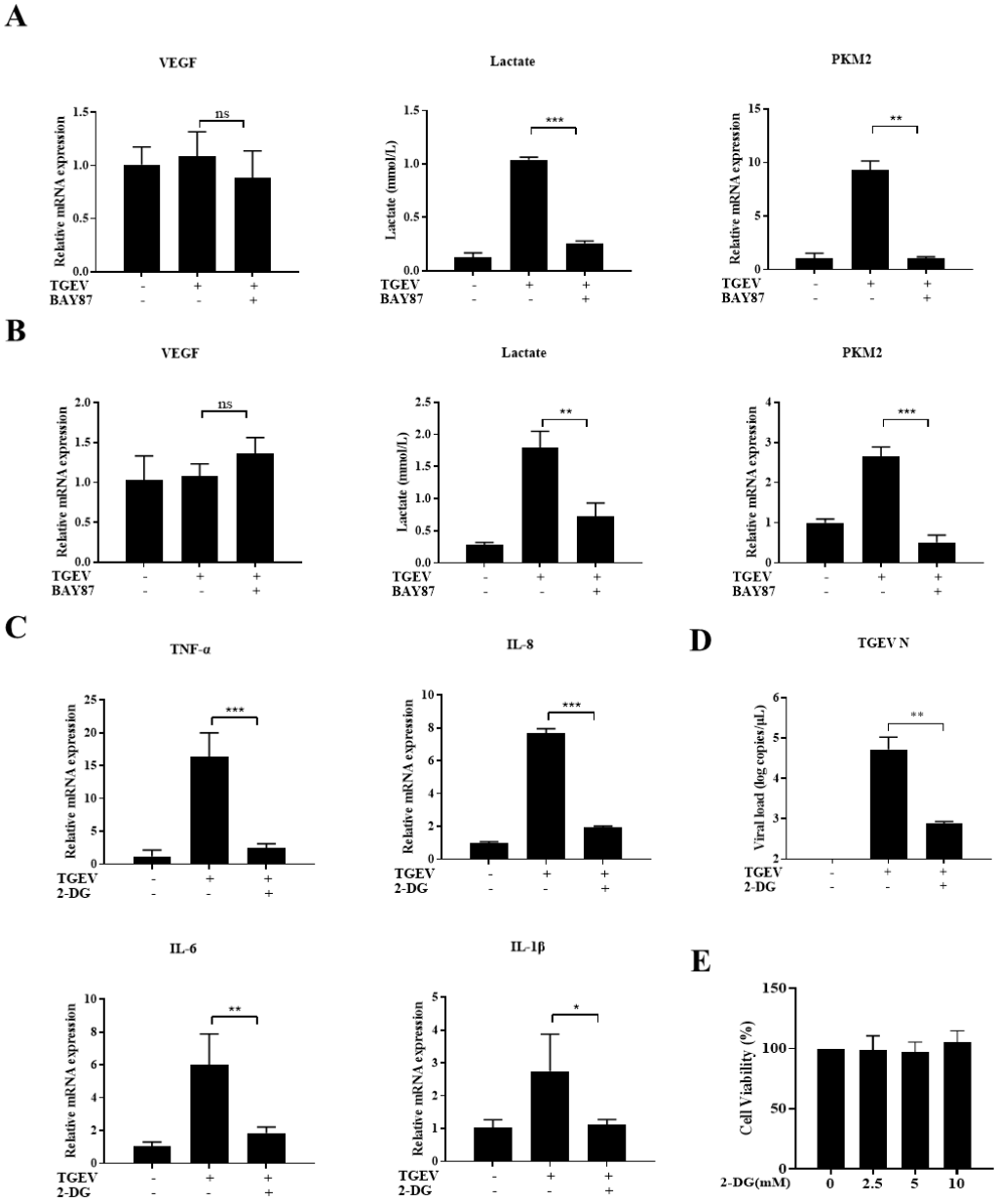

Figure 27. HIF-1α promotes TGEV-induced inflammatory responses by activating glycolysis.

(A) Intestinal organoids were infected with TGEV followed by BAY87 (5 μM) for 48 h, then VEGF and PKM2 mRNA levels, and lactate production were determined by RT-qPCR. (B) Transcription levels of VEGF and PKM2 and lactate production in the ileum were detected by

RT-qPCR. (C–D) Intestinal organoids were infected with TGEV followed by 2-DG (5 mM) for 48 h, then transcription levels of TNF-α, IL-8, IL-6, and IL-1β (C) and TGEV viral load (D) were determined by RT-qPCR. (E) Intestinal organoids were incubated with different concentrations of 2-DG for 48 h and cell viability was assessed using a Cell Counting Kit 8. Results are presented as mean ± SD of data from three independent experiments *, $P \leq 0.05$; **, $P \leq 0.01$; ***, $P \leq 0.001$.

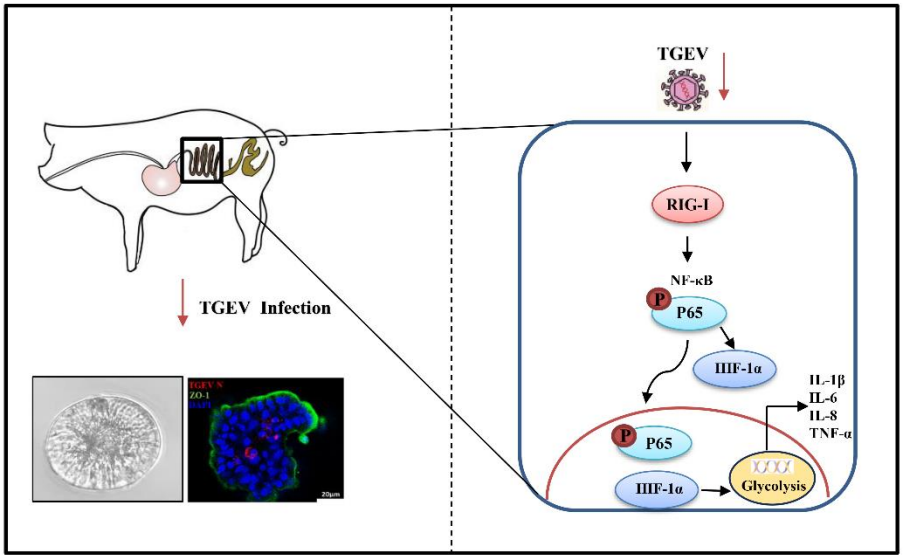

Figure 28. Proposed model of TGEV-induced inflammation via the RIG-I/NF-κB/HIF-1α/glycolysis pathway in intestinal organoids and *in vivo*.

4.4 Discussion

Sensitive cell lines have long been used for viral infections, even though cell lines do not mimic the physiological states in the body. Organoids are more acceptable for the establishment and application of models exploring viral infection and immune responses because the origin and composition of organoids is closer to that of organ systems. Intestinal organoids derived from $Lgr5^+$ stem cells were first proposed in 2009 [181]. Organoids have proved useful in investigations of the production, signaling, and function of innate immunity in response to human enteric viruses, such as human norovirus, rotavirus, and reovirus [194]. Previously, our laboratory developed an apical-out porcine intestinal organoid culture system for swine enteric virus infection and immune response investigations. Apical-out organoids facilitate most enteric virus infections and the differentiation of intestinal cell types, and thus are physiological research models for virus–epithelial interaction investigations [147]. In this study, our results demonstrated that TGEV was able to infect the apical-out intestinal organoids and triggers TGEV-induced inflammatory factors, especially TNF-α, IL-8, and IL-6, which were markedly upregulated. We also found that TGEV protein, but not nucleic

acid, induced inflammation in the apical-out organoids. We infer that TGEV nonstructural protein participates in TGEV-induced inflammation, but further studies are needed to understand the details.

Activation of PRRs is an important strategy utilized by coronaviruses for manipulating inflammatory responses [184]. TGEV infection is reported to trigger inflammation by RIG-I- and MDA5-mediated signaling in ST cells [79]. Here, we found that TGEV induces inflammation by upregulating RIG-I expression in apical-out organoids and pigs, rather than activating MDA5. A potential reason for these discrepancies may be that apical-out organoids are more likely to mimic *in vivo* environments compared to conventional cell lines. Moreover, TGEV infection can be enhanced by Cyclo (a RIG-I inhibitor) treatment, suggesting that RIG-I not only regulates TGEV-induced inflammation but also may affect interferon production which has an antiviral function [195]. Some studies have reported that TGEV induces inflammatory responses by the NF-κB pathway in conventional cell lines [78-79]. Our results provide a similar trend in apical-out organoids and in pigs, indicating that the NF-κB pathway could be a reliable target to control TGEV-induced enteritis. In addition, our results suggested that NF-κB signaling pathway activation had no remarkable effects on TGEV replication, which was consistent with the results of previous studies (4, 22). We infer that NF-κB may play a critical role in many cellular processes to regulate viral replication, including cell proliferation, survival, and differentiation except to inflammation. Therefore, NF-κB not only regulates the expression of HIF-1α but also participates in the regulation of other genes related to viral infection. We infer that there are more host factors involved in the relationship between NF-κB and TGEV infection. Further studies are required to understand this in more detail.

There are many proinflammatory factors involved in coronavirus-induced inflammation. It is reported that HIF-1α promotes SARS-CoV-2 infection and aggravates inflammatory responses in COVID-19 [122]; and HMGB1 enhances porcine epidemic diarrhea virus (PEDV)-induced inflammation by binding to TLR4-induced activation of p38 MAPK [84]. The activation of NLRP3 and NLRP6 inflammasomes also triggers coronavirus-induced inflammatory responses by releasing IL-1β and IL-18 [196-197]. In addition, NLRP3 activation can be mediated by NEK7 downstream of potassium efflux [198]. In this study, we found that HIF-1α expression can be regulated by the RIG-I–NF-κB pathway upon TGEV infection. Moreover, HIF-1α had higher expression in intestinal organoids and tissues compared to conventional cell lines, like ST cells (data not shown). We inferred that HIF-1α may be involved in TGEV-induced inflammation. Our subsequent results demonstrated that HIF-1α was actually a key mediator of TGEV-induced inflammatory responses in intestinal organoids and the porcine ileum, further clarifying that intestinal organoids are more likely to mimic *in vivo* environments than conventional cell lines. However, the detailed molecular mechanism of regulation of NF-κB and HIF-1α remains unclear. We infer that p50 may stabilize HIF-1α protein upon TGEV infection [199], but this theory requires further study.

HIF-1α is reported to positively regulate inflammation by different mechanisms. Codo et al. reported that SARS-CoV-2 stabilized HIF-1α expression, which induced monocyte-derived cytokines by activating glycolysis [193]. HIF-1α also promotes the

H1N1-induced host inflammatory response by regulating glycolysis [200]. In contrast, HIF-1α promotes experimental acute ocular inflammation by stimulating VEGF signaling [192]. In our study, VEGF and glycolysis were screened after TGEV infection or inhibition of HIF-1α to further explore the potential mechanism of HIF-1α promoting TGEV-induced inflammation. We found that HIF-1α facilitated TGEV-induced inflammation by regulating glycolysis. It can actually present novel mechanistic insight for this trend. In addition, similar to HIF-1α, activation of glycolysis can also upregulate TGEV infection. It is reported that H1N1-induced HIF-1α can promote glycolysis to produce lactate which reduces accumulation of the RIG-I–MAVS complex and IFN responses to promote viral infection [200]. We hypothesize that HIF-1α promotion of TGEV infection may be associated with glycolysis and IFN production, and this theory needs to be explored in detail in future studies.

In conclusion, our research is the first to employ apical-out porcine intestinal organoids and pigs for exploring TGEV-induced inflammation and revealed that TGEV induces inflammatory responses via the RIG-I/NF-κB/HIF-1α/glycolysis axis. Our study provides a novel insight into potential therapeutic targets for TGEV-caused swine enteritis and verifies apical-out organoids as a more physiological model for mimicking enteric virus-induced inflammation.

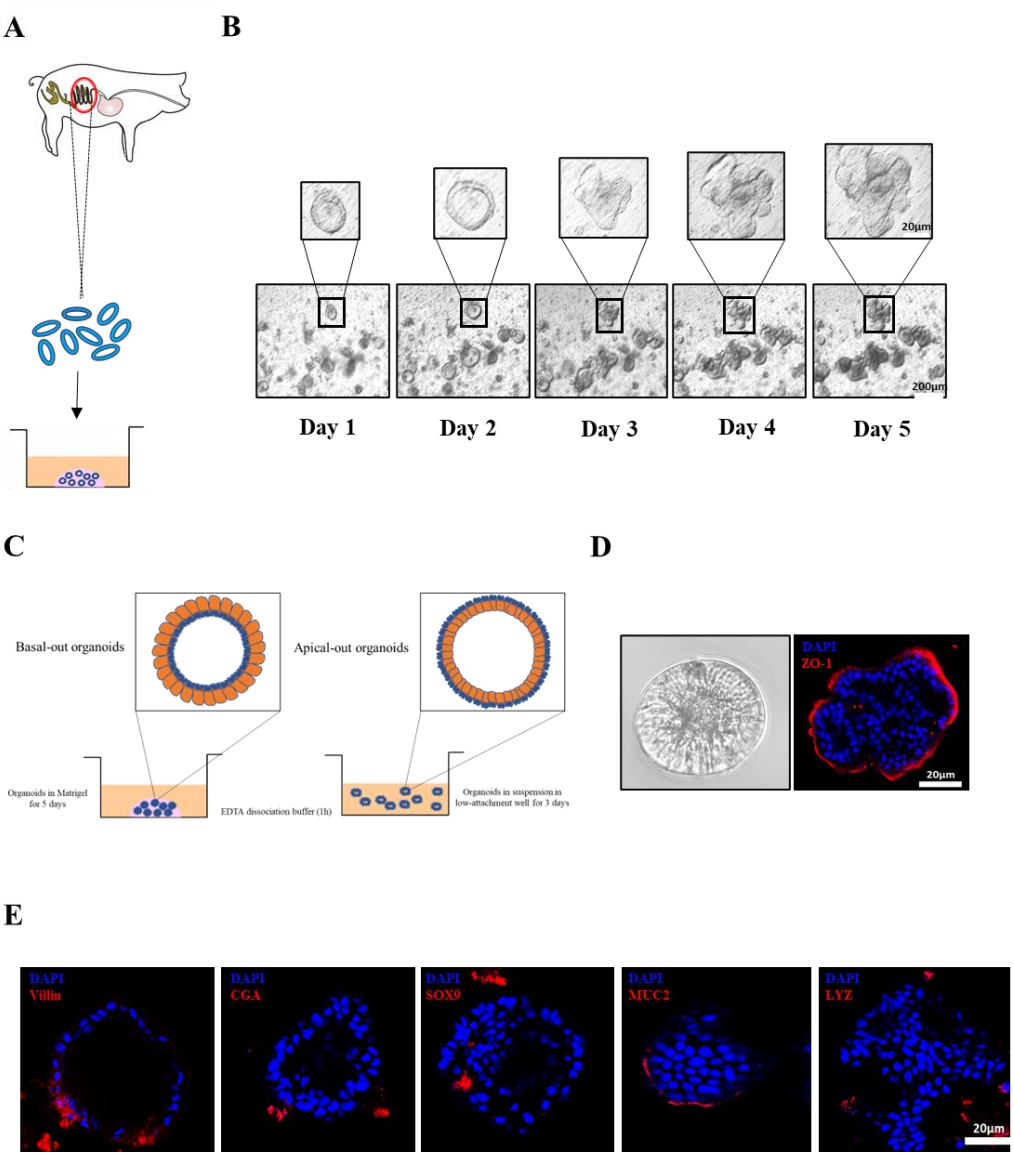

Supplementary Figure 11. Establishment of apical-out porcine intestinal organoids.

(A) Graphical representation for isolation of porcine intestinal crypts. (B) Culture of intestinal organoids from 1 to 5 days; scale bar: 20/200 μm (C) Graphical representation for generation of apical-out organoids (D) Apical-out organoids were stained with ZO-1; scale bar: 20 μm (E) Apical-out organoids was subjected to IFA staining for absorptive enterocytes (Villin), enteroendocrine cells (CGA), stem cells (SOX9), goblet cells (MUC2) and Paneth cells (LYZ) ; scale bar: 20 μm.

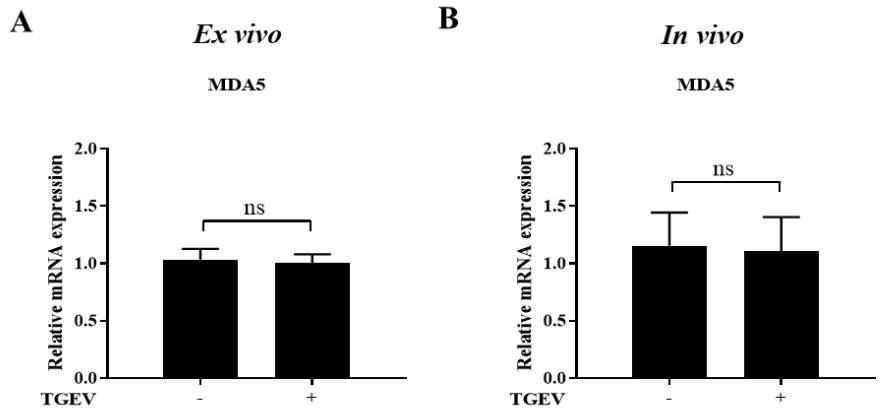

Supplementary Figure 12. TGEV infection can not affect MDA5 expression.

(A)The transcription level of MDA5 in apical-out organoids at 48 h post TGEV infection was evaluated by RT-qPCR. (B) Transcriptional level of MDA5 in ileum was detected by RT-qPCR. Results are presented as mean ± SD of data from three independent experiments ns, no significant.

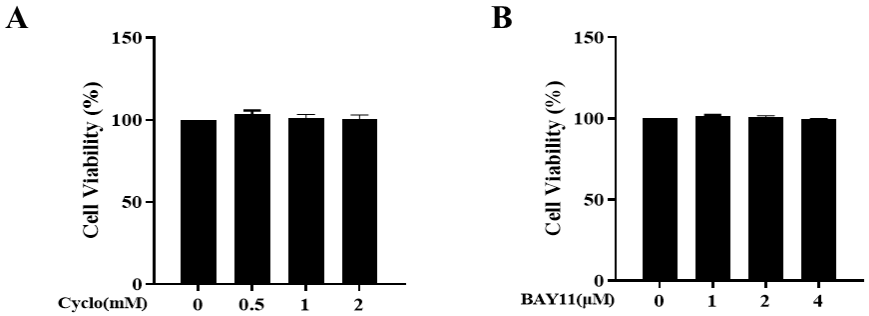

Supplementary Figure 13. Cytotoxicity of Cyclo and BAY11-7082.

(A-B) Intestinal organoids were incubated with different concentrations of Cyclo (A) or BAY11 (B) for 48 h, which was assessed by Cell Counting Kit 8. Results are presented as mean ± SD of data from three independent experiments ns, no significant.

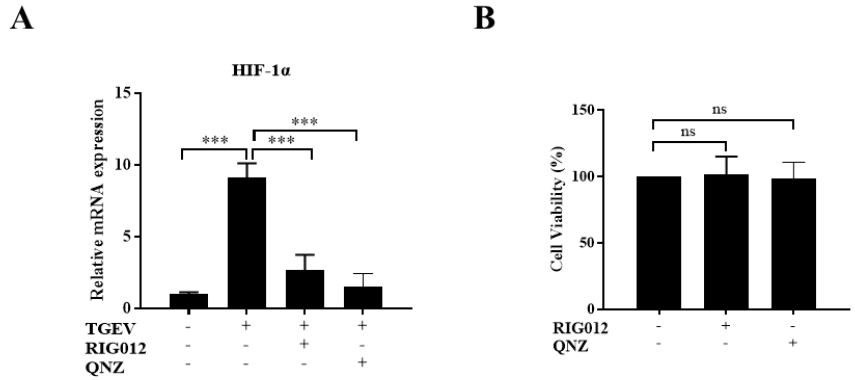

Supplementary Figure 14. RIG-I–NF-κB pathway regulates HIF-1α expression upon TGEV infection.

(A) Intestinal organoids were infected with TGEV followed by RIG012 (5 μM) or QNZ (10 nM) treatment for 48 h. Transcription levels of HIF-1α in the intestinal organoids post TGEV infection were measured by RT-qPCR. (B) Intestinal organoids were incubated with RIG012 (5 μM) or QNZ (10 nM) treatment for 48 h, which was assessed by Cell Counting Kit 8. Results are presented as mean ± SD of data from three independent experiments ns, no significant; ***, $P \leq 0.001$.

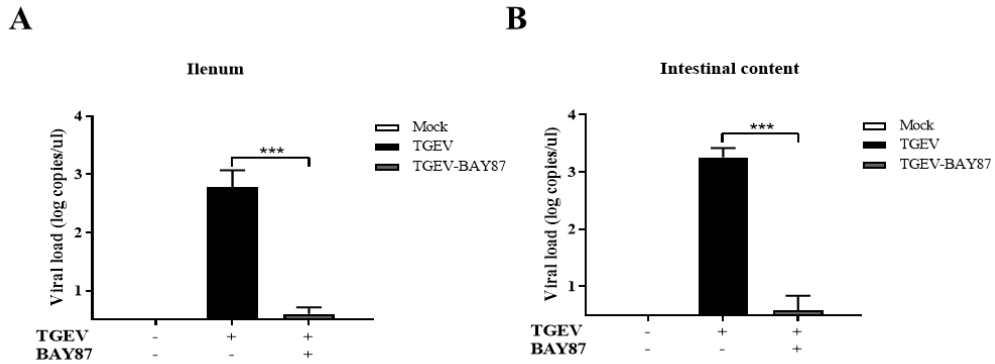

Supplementary Figure 15. Oral administration of BAY87 inhibits TGEV infection in the ileum and intestinal content.

(A-B) TGEV genome copy numbers in the ileum (A) and intestinal content (B) were detected by RT-qPCR. Results are presented as the mean ± SD of data from three independent experiments ***, $P \leq 0.001$.

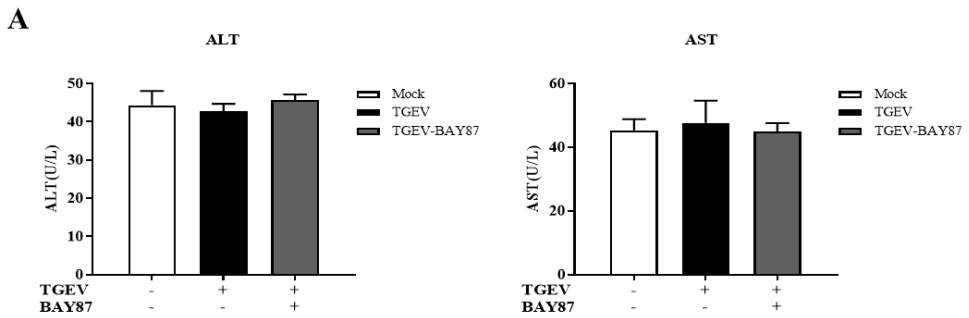

Supplementary Figure 16. BAY87 cannot change ALT and AST level in serum of pigs.

(A) ALT and AST were detected in serum from piglets sacrificed at 24 hpi. Results are presented as mean ± SD of data from three independent experiments ns, no significant.

Chapter 5

Hypoxia inducible factor-1α facilitates transmissible gastroenteritis virus replication by inhibiting type I and type III interferon production

Foreword

In Chapter 4, we uncovered the role of HIF-1α in TGEV-induced inflammation and found that it can also promote viral infection, though the underlying mechanism remains unclear.

To comprehensively explore the role of HIF-1α in TGEV infection, in our article published in May 2024, we confirmed its impact on TGEV infection in ST cells and intestinal organoid monolayers, and identified the specific stages of the viral life cycle affected by HIF-1α. Additionally, we elucidated the mechanism by which HIF-1α promotes TGEV infection. Finally, animal experiments corroborated these findings.

This chapter has been adapted from the article:

Zhang Y, Rui X, Li Y, Zhang Y, Cai Y, Tan C, Yang N, Liu Y, Fu Y, Liu G*. Hypoxia inducible factor-1α facilitates transmissible gastroenteritis virus replication by inhibiting type I and type III interferon production. **Veterinary Microbiology.** 2024 May;292:110055.

Summary

Transmissible gastroenteritis virus (TGEV) is characterized by watery diarrhea, vomiting, and dehydration and is associated with high mortality especially in newborn piglets, causing significant economic losses to the global pig industry. Hypoxia inducible factor-1α (HIF-1α) has been identified as a key regulator of TGEV-induced inflammation, but understanding of the effect of HIF-1α on TGEV infection remains limited. This study found that TGEV infection was associated with a marked increase in HIF-1α expression in ST cells and an intestinal organoid epithelial monolayer. Furthermore, HIF-1α was shown to facilitate TGEV infection by targeting viral replication, which was achieved by restraining type I and type III interferon (IFN) production. *In vivo* experiments in piglets demonstrated that the HIF-1α inhibitor BAY87-2243 significantly reduced HIF-1α expression and inhibited TGEV replication and pathogenesis by activating IFN expression. In summary, we unveiled that HIF-1α facilitates TGEV replication by restraining type I and type III IFN expression *in vitro*, *ex vivo*, and *in vivo*. The findings from this study suggest that HIF-1α could be a novel antiviral target and candidate drug against TGEV infection.

5.1 Introduction

Transmissible gastroenteritis virus (TGEV), a member of the genus *Alphacoronavirus* (family *Coronaviridae*, order *Nidovirales*), is a single-stranded, positive-sense RNA virus [53]. TGEV infection causes acute watery diarrhea, vomiting, dehydration, and anorexia and is associated with high morbidity and mortality, particularly in nursing piglets [9]. The innate immune response defends the host against invading pathogens. Upon TGEV infection, pattern recognition receptors (PRRs) such as toll-like receptors (TLRs) and retinoic acid inducible gene-I (RIG-I)-like receptors (RLRs) are activated through their recognition of pathogen-associated molecular patterns (PAMPs) released by TGEV. PRR activation induces downstream signaling cascades that recruit and activate TBK1/IKKε and cause the nuclear translocation of IRF3/7 and P65, resulting in the production of interferons (IFNs) and inflammatory cytokines [68]. Type I and type III IFNs interact with their receptors and induce the production of hundreds of IFN-stimulated genes (ISGs) through JAK/STAT signaling [72].

Type I and type III IFNs and ISGs play a critical role in the defense against virus infection [68, 153]. For example, IFN-β and IFN-λ1/3 have a strong antiviral effect on coronavirus infections, especially among pigs [69-70, 185]. Several ISGs are also reported to restrict infections with coronaviruses. For example, oligoadenylate synthetase-like (OASL) can significantly inhibit porcine epidemic diarrhea virus (PEDV) and TGEV infection [71]. In addition, IFN-stimulated gene 15 (ISG15) conjugation is essential for antiviral IFN responses against coronavirus infections [201]. Meanwhile, coronaviruses have evolved to subvert host immunity by targeting key proteins participating in the IFN response [202]. PEDV non-structure protein 1 (nsp1) inhibits type III IFN production by blocking the nuclear translocation of IRF1 and reducing the number of peroxisomes [70]. In addition, SARS-CoV-2 PLpro can cleave ISG15 from IRF3 and attenuate type I IFN responses [203]. Thus, positive regulation of type I and type III IFNs is one mechanism for improving the host antiviral response against invading viruses.

Hypoxia inducible factor-1α (HIF-1α) is a major transcriptional activator that allows cells to adapt to hypoxia and acts as a key regulator of the innate immune response [204]. Peng et al. reported that hypoxia-induced HIF-1α directly represses IRF5 and IRF3 transcription and negatively regulates type I IFN signaling, inducing inflammatory cytokine production by monocytes [205]. In addition, HIF-1α has been shown to regulate various viral infections, including SARS-CoV-2, vesicular stomatitis virus (VSV), herpes simplex virus type 1 (HSV-1), and H1N1 virus [200]. Furthermore, porcine reproductive and respiratory syndrome virus (PRRSV) nsp1β stabilizes HIF-1α to enhance viral replication[206]. However, the effect of HIF-1α on TGEV infection is unknown and warrants further investigation, with the aim of providing a reliable target against TGEV infection.

This study found that TGEV infection was associated with increased HIF-1α expression *in vitro* and *ex vivo*. HIF-1α promoted TGEV infection by targeting viral replication in ST cells and an intestinal organoid monolayer. The effect of HIF-1α on TGEV infection was primarily dependent on the downregulation of type I and type III IFN expression. *In vivo* experiments in pigs highlighted the same molecular mechanism by which HIF-1α promotes TGEV replication. In summary, HIF-1α was

shown to facilitate TGEV replication by restraining type I and type III IFN expression.

5.2 Materials and Methods

5.2.1. Cell culture, virus, and animals

ST cells and Vero-APN cells were maintained in Dulbecco's Modified Eagle's Medium (DMEM) (Sigma-Aldrich, USA, D6429) with 10% fetal bovine serum (Invigentech, Brazil, A6901). The cells were incubated at 37 °C in a humidified incubator with 5% CO_2. The TGEV Miller strain was maintained at a titer of $10^{7.25}$ $TCID_{50}$/mL, where $TCID_{50}$ is the 50% tissue culture infectious dose. Porcine intestines used for crypt isolation were obtained from the Luoniushan Co., Ltd slaughterhouse in Hainan Province, China.

5.2.2. Porcine intestinal 3D organoid culture

Porcine ileum crypts were isolated from pigs and cultured in Matrigel (Corning, USA, 356231) and Organoid Growth Medium (OGM) (Stem Cell, Canada, 06010) containing 10 μM of the ATP-competitive inhibitor of Rho-associated kinases (Y-27632; CST, USA, 72302) as previously described [147].

5.2.3. Establishment of the intestinal organoid monolayer

After 5 days of culture, 3D ileum organoids were collected using ice-cold DMEM and centrifuged at 250 *g* for 5 min. The organoid pellet without Matrigel was disassociated into single cells or small fragments at 37 ℃ using TrypLE Express (Gibco, USA, 12605-010) by repeated pipetting to release the organoids after two 5 min intervals. Signal cells or small fragments were resuspended in OGM containing 10 μM Y-27632 and seeded into a 48-well plate with 1.5% Matrigel. The monolayer reached confluency after 3 days of culture and was used for follow-up experiments [148].

5.2.4. Virus infection in the intestinal organoid monolayer

The organoid monolayer cultured for 3 days was inoculated with the TGEV Miller strain (multiplicity of infection [MOI] = 1) for 2 h at 37 °C. Residual viruses were removed by washing with phosphate-buffered saline (PBS). The organoid monolayer was then cultured with OGM (with 10 μM Y-27632) for the indicated times [148].

5.2.5. Histopathological and immunofluorescence analysis

The small intestine was collected, fixed for 24 h in 10% formalin, dehydrated according to the standard protocol, embedded in paraffin, and stained with hematoxylin and eosin using standard procedures [207]. For immunofluorescence analysis, ST cells or different segments of the small intestine were fixed with 4% paraformaldehyde for 20 min and permeabilized with 0.1% Triton X-100 (Beyotime, China, ST797) for 20 min at 37 °C. The samples were blocked with 5% bovine serum albumin (Biofroxx, Germany, 4240GR100) for 1 h and labeled with primary antibodies overnight at 4 °C. After rinsing, the samples were incubated with secondary antibodies for 1 h at room temperature. The nuclei were then stained with 4', 6'-diamidino-2-phenylindole (DAPI; Beyotime, China, C1006). After washing, the

samples were visualized using confocal laser-scanning microscopy (Zeiss LSM 900, Germany).

5.2.6. Western blotting

Proteins were separated by sodium dodecyl sulfate-polyacrylamide gel electrophoresis (SDS-PAGE) and transferred onto a polyvinylidene fluoride (PVDF) membrane (GE, USA, 10600023). The membranes were blocked in 5% nonfat milk at room temperature for 2 h and incubated overnight with the primary antibodies specified in **Table 5**. The membranes were then incubated with a secondary antibody for 1 h at room temperature. Finally, proteins were visualized using WesternBright ECL (Advansta, USA, K-12045-D50) [150].

Table 5. Antibodies used in this study

Antibody	Type	Supplier	Product Number
HIF-1α	Rabbit	Proteintech	20960-1-AP
GAPDH	Rabbit	Proteintech	10494-1-AP

5.2.7. RNA extraction, real-time quantitative PCR (RT-qPCR), and enzyme-linked immunosorbent assay (ELISA)

Total RNA was extracted using RNAiso reagent (TaKaRa, Japan, 9109) and reverse transcribed into cDNA using HiScript Q RT SuperMix for qPCR (Vazyme, China, R223-01), according to the manufacturer's instructions. The TGEV virus copy number was detected using a TaqMan probe-based RT-qPCR developed previously [149]. Relative qPCR was performed using the ChamQ SYBR qPCR master mix (Vazyme, China, Q311-02) and calculated with the $2^{-\Delta\Delta CT}$ method. The primers and probe used in this study are listed in **Table 6.** For the ELISA assay, IFN-β in the supernatant of TGEV-infected ST cells and the intestinal content of piglets sacrificed at 24 h post-infection (hpi) was detected using a commercial kit according to the manufacturer's instructions (NEWA, China, SY-P00306).

Table 6. Primers used for real-time qPCR

Names	Primer or probe	Sequence (5'-3')
TGEV N	Forward	TGCCATGAACAAACCAAC
	Reverse	GGCACTTTACCATCGAAT
	Probe	HEX-TAGCACCACGACTACCAAGC-BHQ1*a*
GRP78	Forward	TCTACTCGCATCCCAAAG
	Reverse	CTCCCACGGTTTCAATAC
ATF4	Forward	TGGAGCAGAACAAGACAGC
	Reverse	CTTTACATTCGCCAGTGAG
LC3B	Forward	CCGAACCTTCGAACAGAGAG
	Reverse	AGGCTTGGTTAGCATTGAGC

ATG7	Forward	AGATTGCCTGGTGGGTGGT
	Reverse	GGGTGATGCTGGAGGAGTTG
Caspase3	Forward	TGGGATTGAGACGGACAGTG
	Reverse	CGCTGCACAAAGTGACTGGA
FasL	Forward	GGGTTCTCCTGTCACTGGTA
	Reverse	TCAGCATGTTTCCGTTTGCC
IFN-β	Forward	CCACCACAGCTCTTTCCATGA
	Reverse	TGAGGAGTCCCAGGCAACT
IFN-λ1	Forward	CCACGTCGAACTTCAGGCTT
	Reverse	ATGTGCAAGTCTCCACTGGT
IFN-λ3	Forward	GCCAAGGATGCCTTTGAAGAG
	Reverse	CAGGACGCTGAGGGTCAGG
OASL	Forward	TCCCTGGGAAGAATGTGCAG
	Reverse	CCCTGGCAAGAGCATAGTGT
HIF-1α	Forward	GGCGCGAACGACAAGAAAAA
	Reverse	GTGGCAACTGATGAGCAAGC
ISG15	Forward	GGTGAGGAACGACAAGGGTC
	Reverse	GGCTTGAGGTCATACTCCCC
ISG56	Forward	AAATGAATGAAGCCCTGGAGTATT
	Reverse	AGGGATCAAGTCCCACAGATTTT

5.2.8. Animal experiments

Neonatal pigs spontaneously delivered from sows did not receive colostrum and were confirmed to be negative for TGEV by RT-qPCR and enzyme-linked immunosorbent assay. They were kept into animal house for one day and fed with milk replacer in Biosafety Level 3 Laboratory (BSL-3). The piglets were randomly separated into three groups: mock (3), TGEV (3), and TGEV-BAY87 (3). In the TGEV group, the piglets were orally infected with 1.245×10^8 plaque-forming units (PFU) of TGEV Miller strain. In the TGEV-BAY87 group, piglets were orally infected with 1.245×10^8 PFU of TGEV Miller stain and treated with BAY87 (10 mg/kg). All piglets were euthanized at 24 hpi, and the intestinal tissues were collected for RT-qPCR, western blotting, and pathological examination.

5.2.9. Ethics statement

All animals were handled in strict accordance with good animal practice according to the Animal Ethics Procedures and Guidelines of the People's Republic of China. The study was approved by The Animal Administration and Ethics Committee of Lanzhou Veterinary Research Institute, Chinese Academy of Agricultural Sciences (Permit No. LVRIAEC-2020-030).

5.2.10. Statistical analysis

All data were analyzed using GraphPad Prism 8.0 software (GraphPad, La Jolla, CA, USA) by one-/two-way analysis of variance. Results are presented as the mean ± standard deviation of data from three independent experiments. *, $P \leq 0.05$; **, $P \leq 0.01$; ***, $P \leq 0.001$; ns, not significant. Each experiment was performed with three biological replicates.

5.3 Results

5.3.1 TGEV infection promotes HIF-1α expression in vitro and ex vivo

TGEV infection can upregulate HIF-1α expression in apical-out intestinal organoids at 48 hpi (unpublished data). To examine the response of HIF-1α to TGEV infection in different cell models at various times, an intestinal organoid monolayer was established **(Fig. S17A and B)**. ST cells and the intestinal organoid monolayer were infected with TGEV and the kinetics of HIF-1α expression were assessed at different time points. TGEV infection was found to promote HIF-1α protein and mRNA expression in ST cells and the intestinal organoid monolayer **(Fig. 29A–D)**.

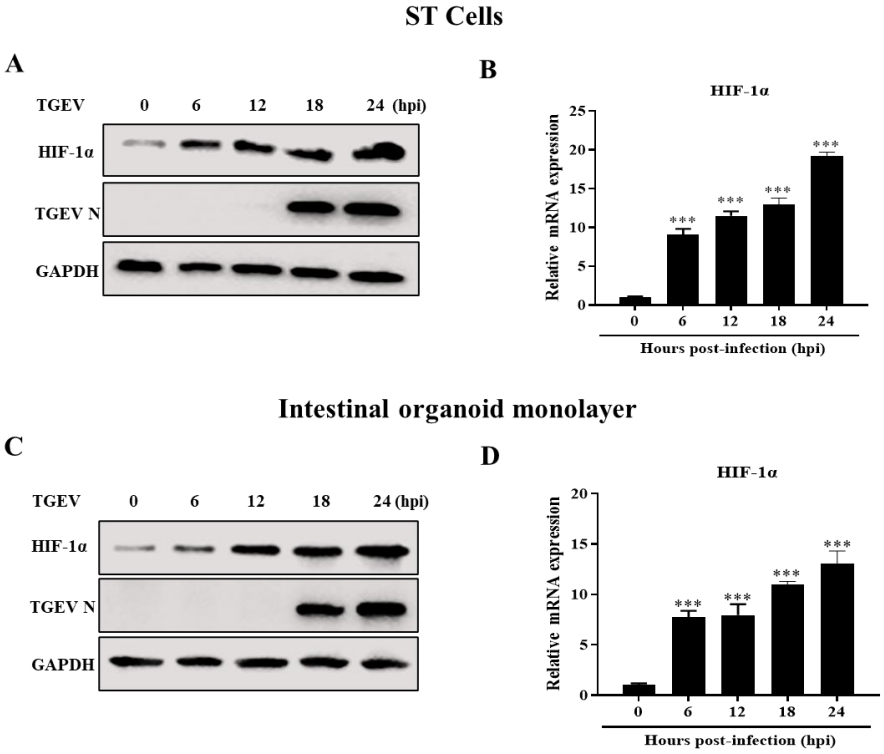

Figure 29. TGEV infection promotes HIF-1α expression *in vitro* and *ex vivo*.

(A, B) ST cells were infected with TGEV at a multiplicity of infection (MOI) of 1 for 0, 6, 12,

18, and 24 h, and HIF-1α expression was measured by western blotting (A) and RT-qPCR (B). (C, D) The intestinal organoid monolayer was infected with TGEV at an MOI of 1 for the indicated time points and HIF-1α expression was measured by western blotting (C) and RT-qPCR (D). Results are presented as the mean ± standard deviation of data from three independent experiments. ***, $P \leq 0.001$.

5.3.2 HIF-1α promotes TGEV infection in ST cells and the intestinal organoid monolayer

To further investigate the effect of HIF-1α on TGEV infection, the HIF-1α agonist $CoCl_2$ and HIF-1α inhibitor BAY87 were employed. A cytotoxicity assay demonstrated that $CoCl_2$ at a concentration less than 50 μM and BAY87 at a concentration less than 20 μM had no effect on ST cells and intestinal organoid monolayer **(Fig. S18A)**. Subsequently, ST cells and the intestinal organoid monolayer were treated with $CoCl_2$ for 1 h followed by infection with TGEV for 19 h. This $CoCl_2$ treatment induced HIF-1α expression and led to an increase in TGEV infection **(Fig. 30A and B)**. HIF-1α overexpression was also shown by RT-qPCR, $TCID_{50}$, and western blotting to enhance TGEV infection **(Fig. 30C)**. In contrast, BAY87 downregulated HIF-1α expression and inhibited TGEV infection in ST cells **(Fig. 30D)** and the intestinal organoid monolayer **(Fig. 30E)**. These results indicated that HIF-1α can promote TGEV infection in ST cells and the intestinal organoid monolayer.

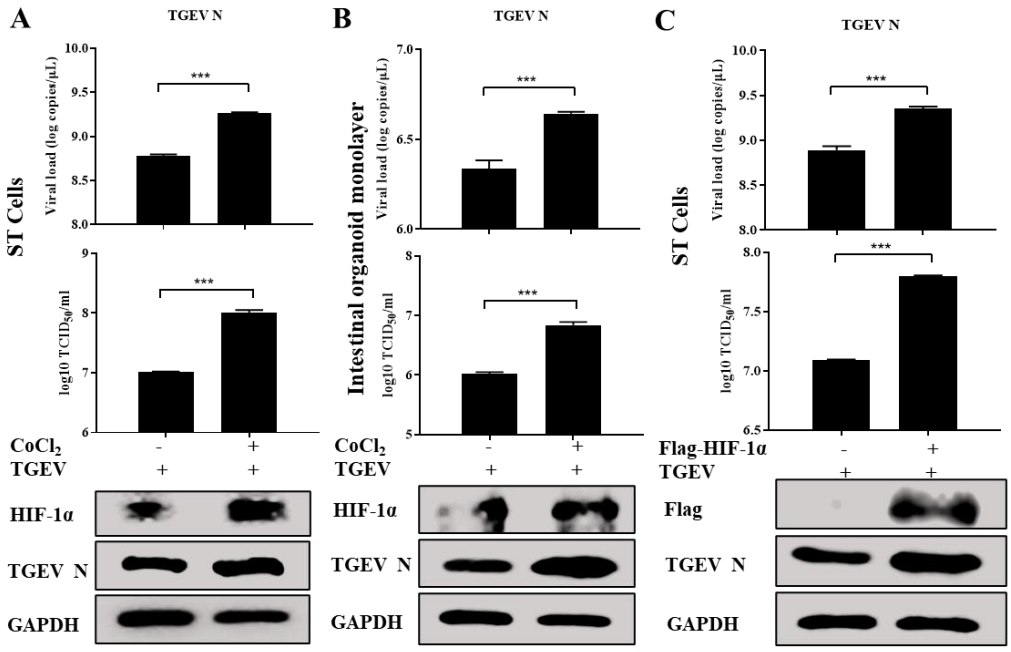

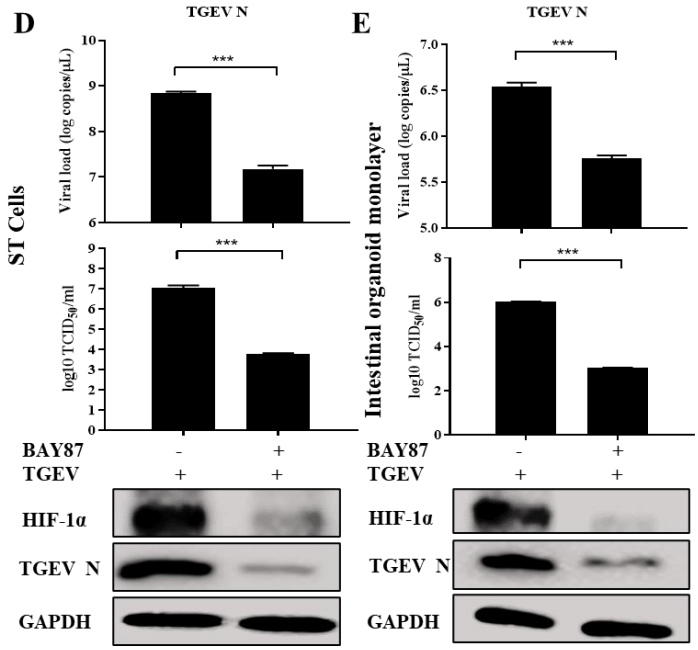

Figure 30. HIF-1α promotes TGEV infection in ST cells and the intestinal organoid monolayer.

(A, B) ST cells (A) or the intestinal organoid monolayer (B) were pretreated with $CoCl_2$ (25 μM) for 1 h, infected with TGEV (multiplicity of infection [MOI]=1) for 1 h, and treated again with $CoCl_2$ at 37 °C for 19 h. Cell samples were collected and examined by RT-qPCR, 50% tissue culture infectious dose ($TCID_{50}$) assay, and western blotting. (C) ST cells were transfected with Flag-HIF-1α for 24 h and infected with TGEV (MOI=1) for 20 h. HIF-1α was detected by RT-qPCR, $TCID_{50}$ assay, and western blotting. (D, E) ST cells (D) or the intestinal organoid monolayer (E) were pretreated with BAY87 (10 μM) for 1 h and then infected with TGEV (MOI=1) for 20 h. Cell samples were collected and examined by RT-qPCR, $TCID_{50}$ assay, and western blotting. Results are presented as the mean ± standard deviation of data from three independent experiments ***, $P \leq 0.001$.

5.3.3 HIF-1α enhances TGEV infection by targeting viral replication

A time-of-drug-addition assay was performed to determine which step of TGEV infection was affected by HIF-1α[152, 154]. The impact of HIF-1α on the adsorption, internalization, replication, and release of TGEV was evaluated in ST cells and the intestinal organoid monolayer. $CoCl_2$ and BAY87 treatment had no effect on virus adsorption, entry, or release **(Fig. 31A, B, and D and Fig. S19A)** but significantly affected TGEV replication **(Fig. 31C and S20A)**. These findings suggested that HIF-1α can upregulate TGEV infection by targeting viral replication.

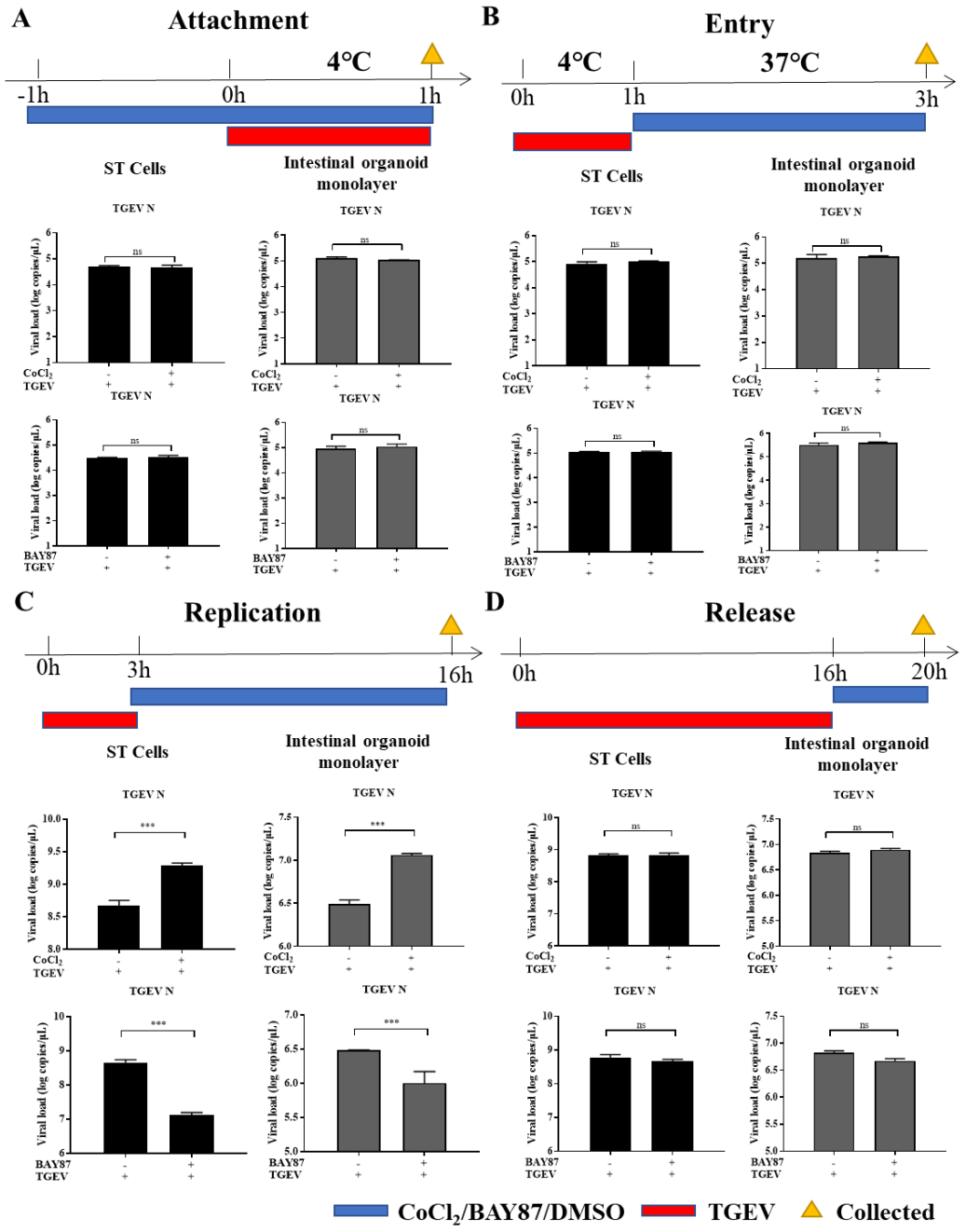

Figure 31. HIF-1α enhances TGEV infection by targeting viral replication.

(A) Adsorption assay. ST cells (left) or the intestinal organoid monolayer (right) were

pretreated with $CoCl_2$ (25 μM), BAY87 (10 μM), or DMSO for 1 h at 37 °C, and the media were replaced by a mixture of $CoCl_2$ (25 μM), BAY87 (10 μM), or DMSO and TGEV (multiplicity of infection [MOI]=1) for 1 h at 4 °C. After washing with PBS, TGEV N mRNA levels were measured by RT-qPCR. (B) Penetration assay. ST cells (left) or the intestinal organoid monolayer (right) were infected with TGEV (MOI=1) for 1 h at 4 °C and then treated with $CoCl_2$ (25 μM), BAY87 (10 μM), or DMSO for 2 h at 37 °C after washing with PBS. Cell samples were washed using sodium citrate buffer and examined using RT-qPCR. (C) Replication assay. ST cells (left) or the intestinal organoid monolayer (right) infected with TGEV (MOI=1) were incubated at 37 °C for 3 h and washed with sodium citrate buffer. The cells were then treated with $CoCl_2$ (25 μM), BAY87(10 μM), or DMSO for 13 h. The cells were harvested and examined by RT-qPCR. (D) Release assay. ST cells (left) or the intestinal organoid monolayer (right) were infected with TGEV (MOI=1) for 16 h, and then $CoCl_2$ (25 μM), BAY87 (10 μM), or DMSO was added to the cells for 4 h. RT-PCR was used to test the viral load in the supernatant. Results are presented as the mean ± standard deviation of data from three independent experiments ***, $P \leq 0.001$; ns, not significant.

5.3.4 HIF-1α facilitates TGEV replication by downregulating type I and type III IFN expression

The mechanism by which HIF-1α facilitates TGEV replication was explored by evaluating intrinsic antiviral defenses, including endoplasmic reticulum (ER) stress (glucose-regulated protein 78 [GRP78] and activating transcription factor 4 [ATF4]), autophagy (LC3B and autophagy-related 7 [ATG7]), apoptosis (caspase 3 and FasL), and IFN responses, after overexpressing HIF-1α in TGEV-infected cells. HIF-1α slightly regulated GRP78, ATF4, and caspase 3 expression, but significantly inhibited type I and type III IFN expression **(Fig. 32A and Fig. S21A)**. In addition, BAY87 treatment resulted in an obvious increase in TGEV-induced IFN and ISGs production, whereas $CoCl_2$ treatment significantly downregulated TGEV-induced IFN and ISGs production *in vitro* and *ex vivo* **(Fig. 32B and C)**. ELISA results indicated a similar trend **(Fig. 32D)**. To explore whether type I and type III IFN expression correlated with HIF-1α-induced TGEV infection, the cells were treated with ruxolitinib, which disrupts the IFN response by inhibiting Janus kinase 1 (JAK1) and Janus kinase 2 (JAK2). TGEV-induced IFN responses were significantly decreased by ruxolitinib treatment **(Fig. S22A)**. Furthermore, HIF-1α overexpression was unable to enhance TGEV infection after ruxolitinib treatment compared to DMSO treatment **(Fig. 32E and F)**. Vero-APN cells, characterized by their deficiency in IFN responses, were utilized to further investigate the correlation between IFN responses and the promotion of TGEV infection by HIF-1α. The results confirm that HIF-1α is unable to enhance TGEV replication under IFN-deficient conditions **(Fig. S23A)**. Collectively, these findings illustrated that HIF-1α enhanced TGEV replication by downregulating type I and type III IFN expression.

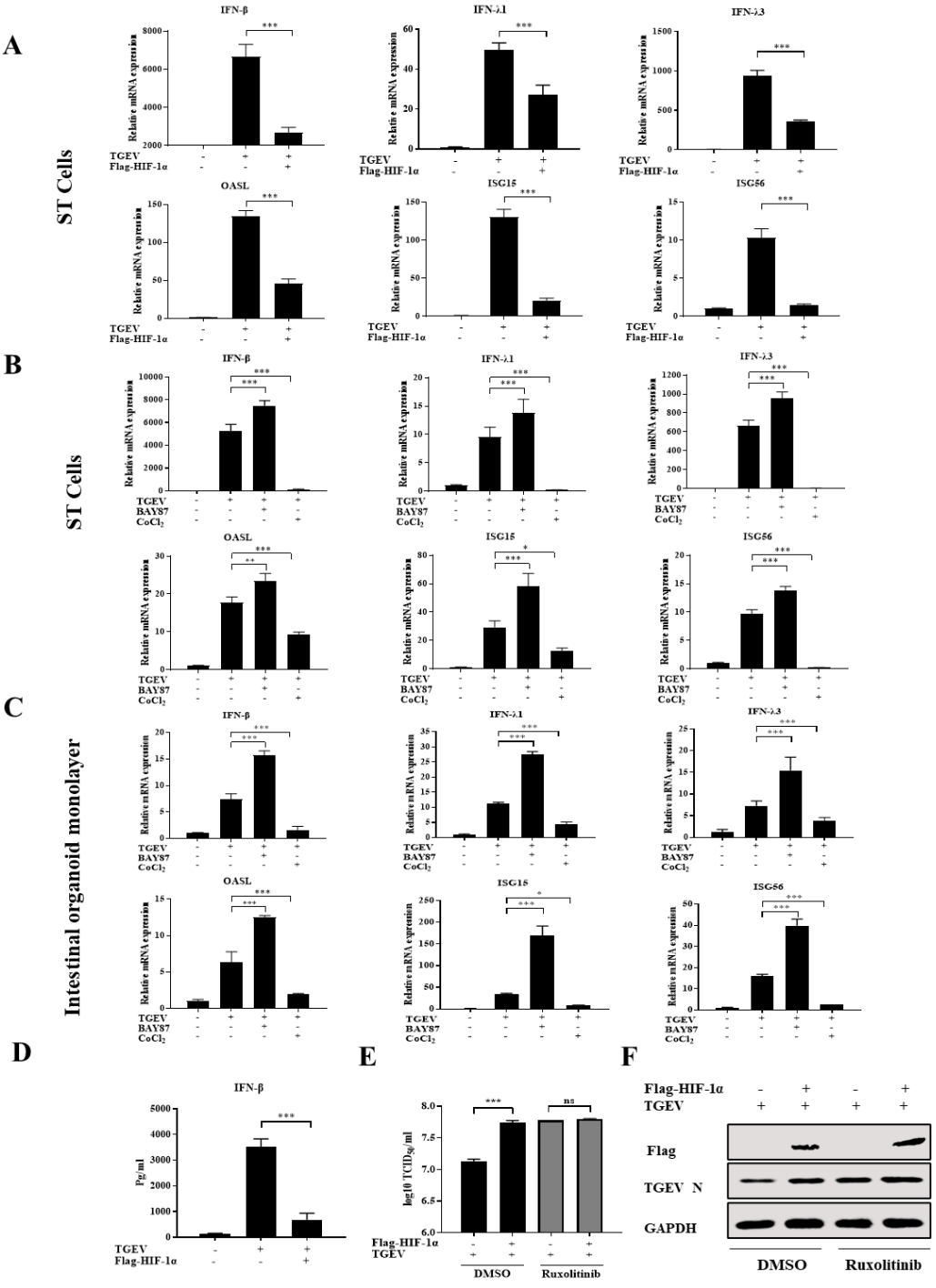
A
ST Cells
IFN-β
IFN-λ1
IFN-λ3
OASL
ISG15
ISG56
Relative mRNA expression
TGEV
Flag-HIF-1α
B
ST Cells
BAY87
CoCl2
C
Intestinal organoid monolayer
D
IFN-β
Pg/ml
TGEV
Flag-HIF-1α
E
log[10 TCID]g/ml
ns
DMSO
Ruxolitinib
F
Flag-HIF-1α
TGEV
Flag
TGEV N
GAPDH
DMSO
Ruxolitinib

Figure 32. HIF-1α facilitates TGEV replication by downregulating type I and type III IFN expression.

(A) ST cells transfected with Flag-HIF-1α for 24 h were infected with TGEV (multiplicity of infection [MOI]=1) for 20 h. Transcriptional levels of IFN-β, IFN-λ1, IFN-λ3, OASL, ISG15, and ISG56 were evaluated by RT-qPCR. (B, C) ST cells (B) or the intestinal organoid monolayer (C) were treated with BAY87(10 μM) or $CoCl_2$ (25 μM) and infected with TGEV (MOI=1) for 20 h. Transcriptional levels of IFN-β, IFN-λ1, IFN-λ3, OASL, ISG15, and ISG56 were detected by RT-qPCR. (D) ST cells transfected with Flag-HIF-1α for 24 h were infected with TGEV (MOI=1) for 20 h. IFN-β was measured in the supernatant by enzyme-linked immunosorbent assay. (E, F) ST cells were treated with ruxolitinib (4 μM) and transfected with Flag-HIF-1α for 24 h, and then infected with TGEV (MOI=1) for 20 h. HIF-1α in the supernatant and cell samples was detected by 50% tissue culture infectious dose ($TCID_{50}$) assay and western blotting. Results are presented as the mean ± standard deviation of data from three independent experiments *, $P \leq 0.05$; **, $P \leq 0.01$; ***, $P \leq 0.001$; ns, not significant.

5.3.5 Pharmaceutical inhibition of HIF-1α suppresses TGEV replication and pathogenesis in vivo

The *in vitro* and *ex vivo* results suggested that HIF-1α could be a potential target for controlling TGEV infection in piglets. To explore this theory, the effect of HIF-1α on TGEV infection was assessed in neonatal pigs *in vivo*. Piglets were treated with BAY87 or DMEM and individually inoculated with TGEV through oral administration **(Fig. 33A)**. Anal swabs were collected every 12 h. Animals in the TGEV group exhibited higher viral shedding than those receiving BAY87 **(Fig. 33B)**, and RT-qPCR and western blotting indicated that the TGEV burden and HIF-1α expression in the small intestine were substantially lower in the BAY87-TGEV group than in the TEGV group **(Fig. 33C)**. Immunofluorescence analysis showed that TGEV N protein production was almost entirely inhibited by BAY87 treatment **(Fig. 33D)**. To further examine the effect of BAY87 on TGEV-induced damage to the small intestine, segments of the small intestine were paraffin-embedded, sliced, and stained with hematoxylin and eosin. BAY87 almost reversed the villous atrophy of small intestinal segments **(Fig. 33E and F)**. Collectively, these data demonstrated that the inhibition of HIF-1α by BAY87 treatment restricted TGEV replication and pathogenesis *in vivo*.

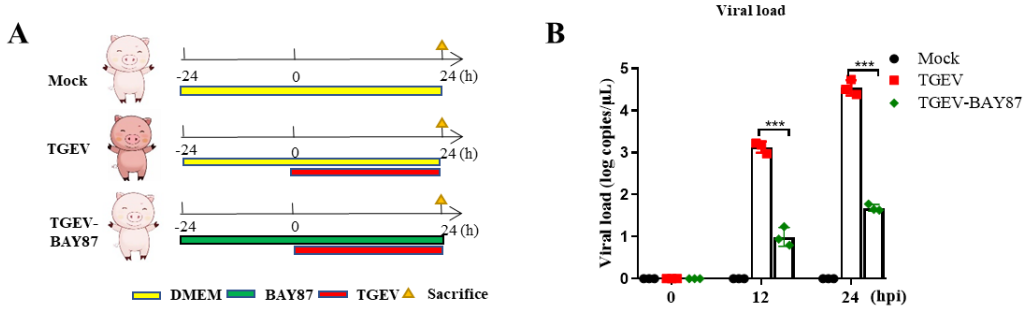

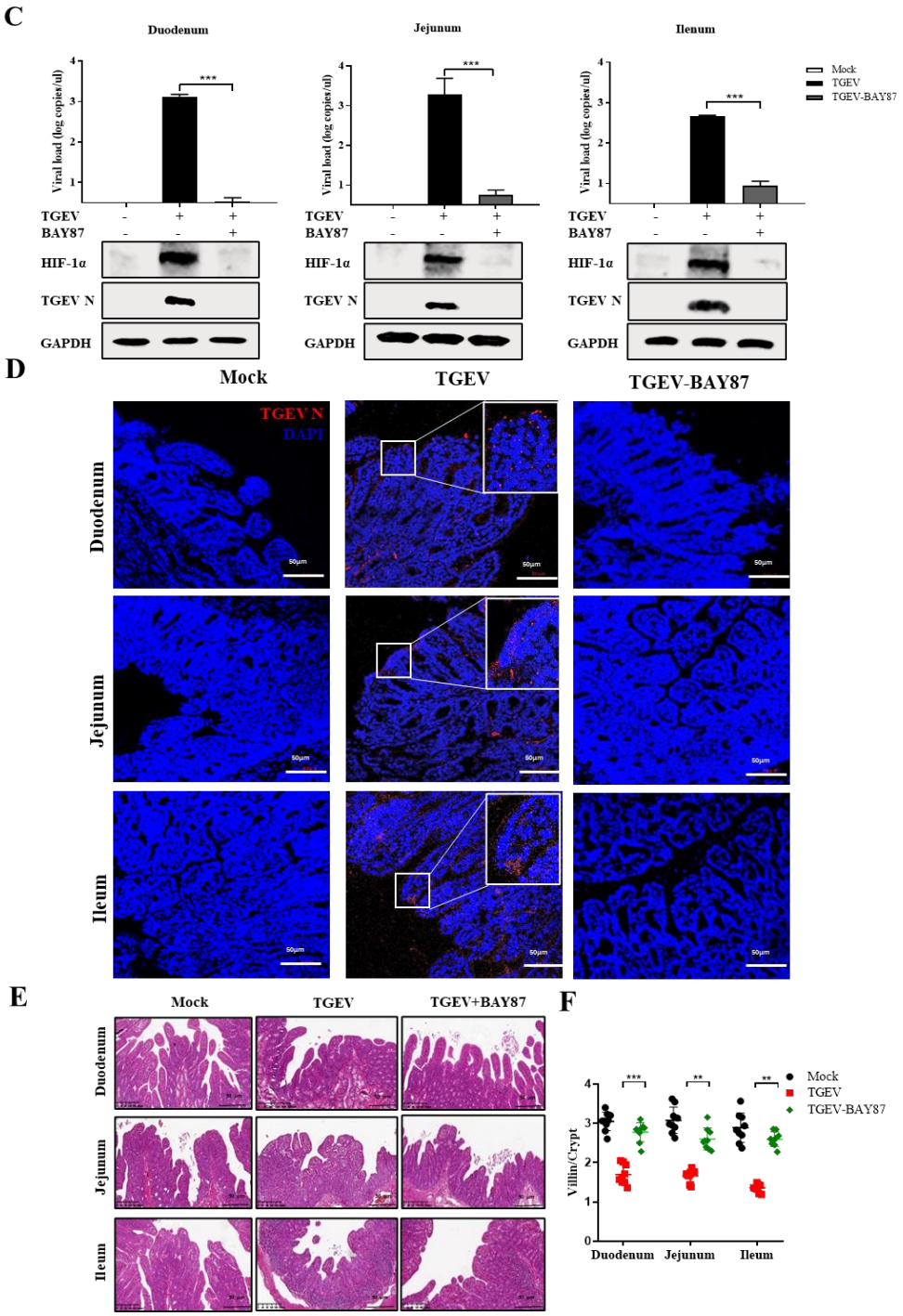

Figure 33. Pharmaceutical inhibition of HIF-1α suppresses TGEV replication and

pathogenesis *in vivo*.

(A) Experimental schemes for assessing the efficacy of BAY87 treatment against TGEV challenge in three groups of piglets. (B) Viral shedding was measured by RT-qPCR every 12 h post-infection (hpi). (C) TGEV genome copy numbers in the duodenum, jejunum, and ileum were detected by RT-qPCR, and HIF-1α and TGEV N levels in the small intestine were determined by western blotting of samples from piglets sacrificed at 24 hpi. (D) Immunofluorescence analysis of TGEV N was conducted on different segments of the small intestine from piglets sacrificed at 24 hpi. Scale bar: 50 μM. (E) Hematoxylin and eosin staining of three segments of the small intestine from piglets sacrificed at 24 hpi. Scale bar: 50 μm. (F) Villin/crypt was calculated by Image J. Results are presented as the mean ± standard deviation of data from three independent experiments **, $P \leq 0.01$; ***, $P \leq 0.001$.

5.3.6 Oral administration of the HIF-1α inhibitor BAY87 induces an antiviral state in the piglet intestine by upregulating type I and type III IFN expression

To confirm whether HIF-1α could serve as a target for controlling TGEV infection, the mRNA expression levels of type I IFN, type III IFN, and ISGs were assessed in different segments of the small intestine. Oral administration of BAY87 to piglets upregulated IFN-β, IFN-λ1, IFN-λ3, OASL, ISG15, and ISG56 in the duodenum (Fig. 34A), jejunum (Fig. 34B), and ileum (Fig. 34C). In addition, ELISA results demonstrated that pharmaceutical inhibition of HIF-1α upregulated IFN-β secretion in the intestinal digesta (Fig. 34D). These findings confirmed that the suppression of HIF-1α by BAY87 strengthened the ability of the intestine to prevent TGEV replication *in vivo*.

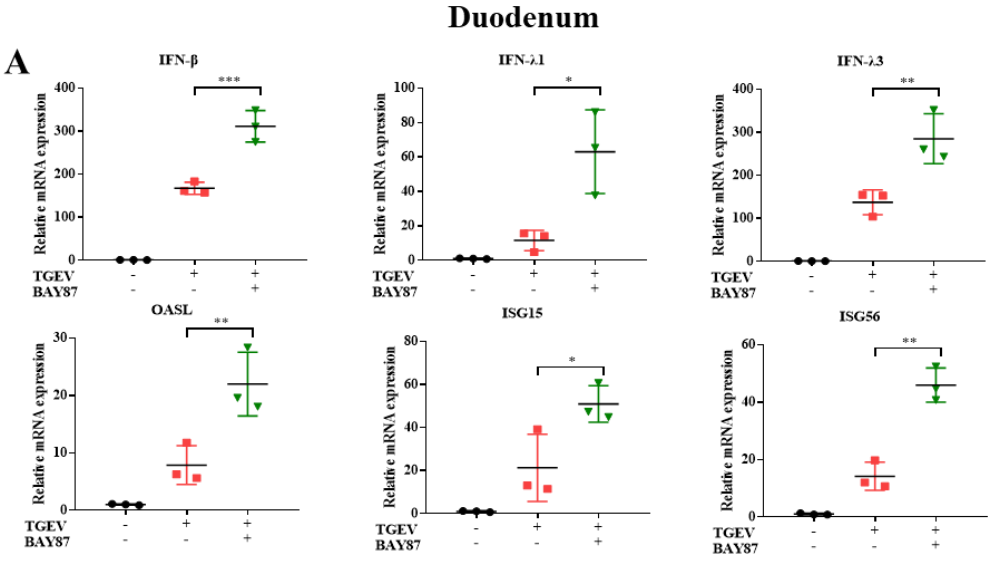

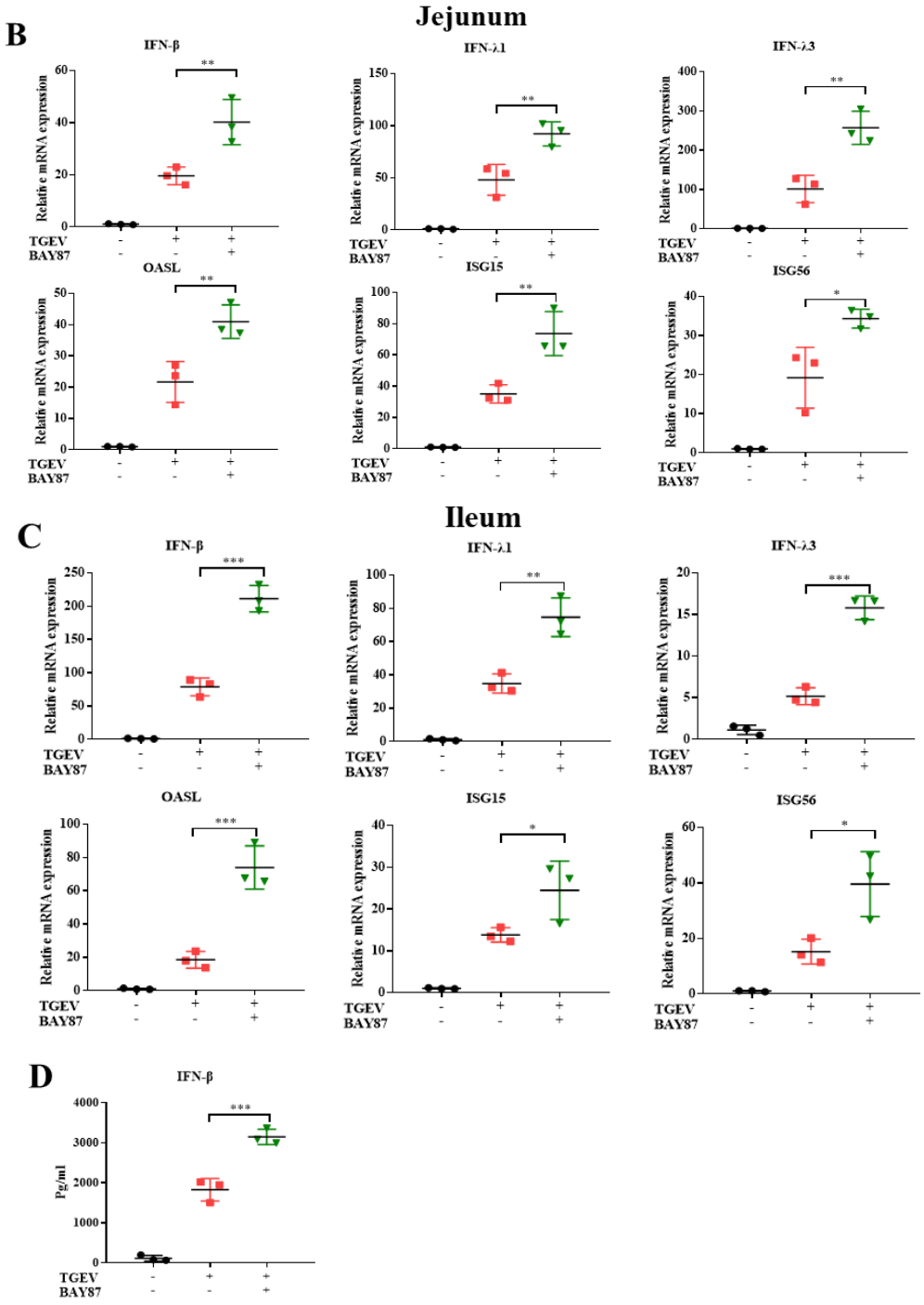

Figure 34. Oral administration of the HIF-1α inhibitor BAY87 induces an antiviral state

in the piglet intestine by upregulating type I and type III IFN expression.

(A–C) Transcriptional levels of IFN-β, IFN-λ1, IFN-λ3, OASL, ISG15, and ISG56 in the duodenum (A), jejunum (B), and ileum (C) of piglets sacrificed at 24 h post-infection (hpi) were detected by RT-qPCR. (D) IFN-β levels in the intestinal digesta of piglets sacrificed at 24 hpi were measured by enzyme-linked immunosorbent assay. Results are presented as the mean ± standard deviation of data from three independent experiments *, $P \leq 0.05$; **, $P \leq 0.01$; ***, $P \leq 0.001$.

5.4 Discussion

The ability of viruses to manipulate host factors is a vital immune evasion strategy that aids viral replication [202]. For example, many viruses hijack HIF-1α to promote infection. SARS-CoV-2 open reading frame 3a (ORF3a) induces HIF-1α expression [122], whereas PRRSV nsp1β stabilizes HIF-1α to enhance viral replication [206]. This study found that TGEV infection significantly promoted HIF-1α expression at different times in ST cells, the intestinal organoid monolayer, and *in vivo*, suggesting that this transcription factor participates in regulating TGEV infection.

HIF-1α expression can be induced by an optimal concentration of $CoCl_2$ and is repressed by the appropriate concentration of BAY87 [208-209]. Consequently, several researchers have used these two chemical compounds to regulate HIF-1α expression. This study found that $CoCl_2$ treatment of ST cells and the intestinal organoid monolayer induced HIF-1α and enhanced TGEV infection. In contrast, BAY87 treatment markedly reduced HIF-1α expression and TGEV infection *in vitro* and *ex vivo*. HIF-1α overexpression showed a similar trend. Although organoids are considered a physiological model for mimicking the intestinal microenvironment, animal experiments remain the most ideal model for exploiting the function of genes or drugs. In this study, experiments in piglets revealed that pharmaceutical inhibition of HIF-1α suppressed TGEV replication and pathogenesis, suggesting that HIF-1α could be a potential anti-TGEV target for the treatment of TGEV infection.

ER stress, autophagy, apoptosis, and IFN production are the primary intrinsic immune responses responsible for inhibiting virus replication [210]. In this study, HIF-1α facilitated TGEV infection by specifically targeting viral replication, not viral attachment, entry, or release. This finding suggests that HIF-1α may impact TGEV replication by regulating ER stress, autophagy, apoptosis, and IFN responses. Subsequent analyses demonstrated that pharmaceutical upregulation or eukaryotic overexpression of HIF-1α significantly restricted IFN-β, IFN-λ1, IFN-λ3, OASL, ISG15, and ISG56 production *in vitro* and *ex vivo*. In addition, pharmaceutical inhibition of HIF-1α upregulated the production of these cytokines *in vitro*, *ex vivo*, and *in vivo*. Several studies have shown that IFN-β, IFN-λ1, IFN-λ3, OASL, and ISG15 have obvious antiviral effects on coronavirus replication [69-71, 185], explaining how HIF-1α can negatively regulate IFN responses to promote TGEV infection. ST cells (an immortal cell line), the intestinal organoids, and piglet intestine samples all showed the same trend throughout this study. A possible explanation for the congruent results despite organoids being a more physiological model than cell lines is that HIF-1α is a high-expressed gene to promote TGEV replication by restraining IFN responses in different models or tissues. It is reported that HIF-1α is also a

transcriptional repressor of IRF5 and IRF3, which are transcription factors required for IFN responses in human monocytes [205]. This may be the molecular mechanism by which HIF-1α downregulates IFN responses in porcine cell models, although further research is required to confirm this mechanism.

In conclusion, this study is the first to illustrate that HIF-1α enhances TGEV infection by restraining type I and type III IFN responses in ST cells, the intestinal organoid monolayer, and in piglets **(Fig. 35)**. The findings provide novel insight into the use of HIF-1α as a potential therapeutic target for controlling TGEV infection.

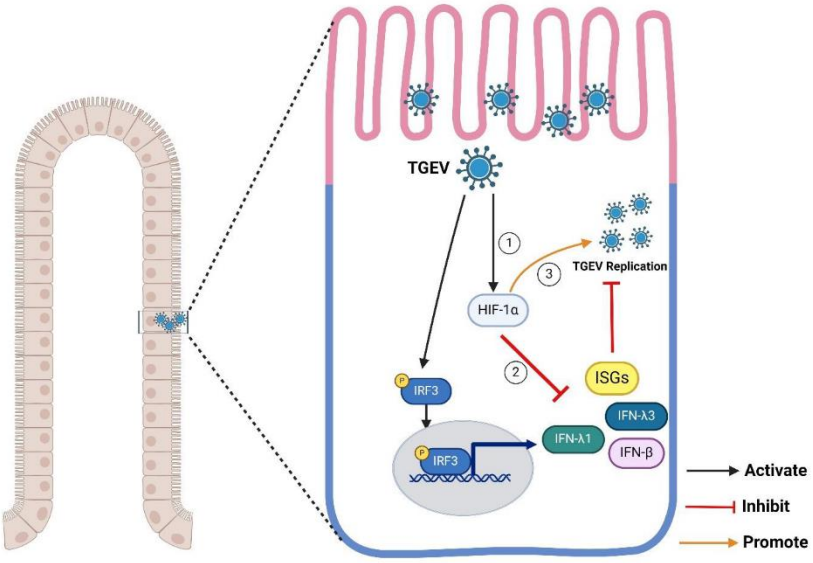

Figure 35. Proposed model of HIF-1α facilitating TGEV replication by restraining type I and type III IFN expression.

Step ①, TGEV infection upregulates HIF-1α expression. Step ②-③, HIF-1α inhibits type I and type III IFN expression to promote TGEV replication. The diagram was created in BioRender.com.

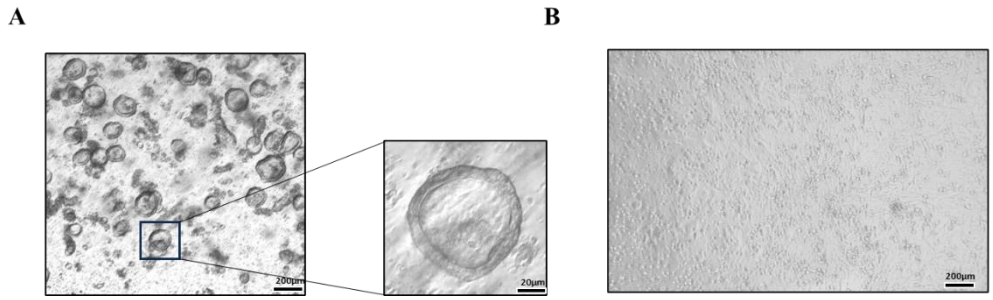

Supplementary Figure 17. Establishment of intestinal organoids monolayer.

(A) Intestinal organoids after culturing for 5 days. (B) Generation of intestinal organoids monolayer after 3 days of culture.

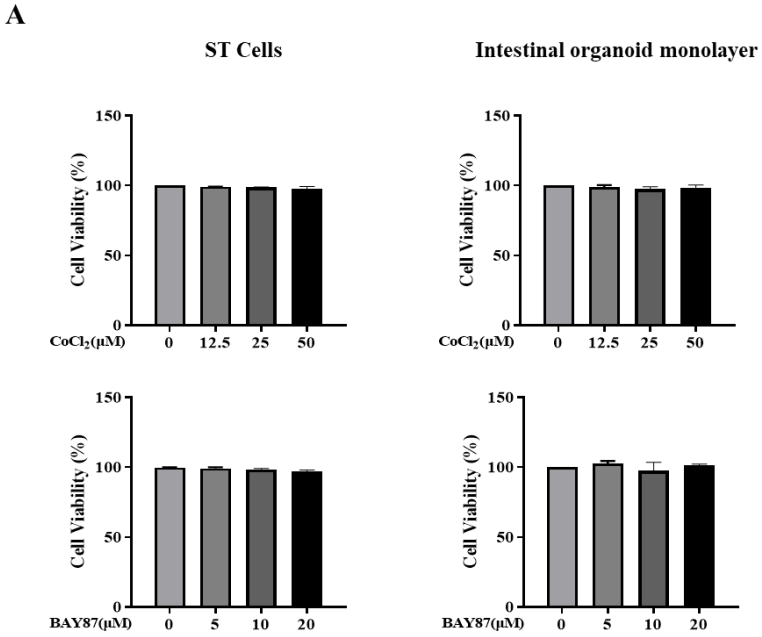

Supplementary Figure 18. $CoCl_2$ and BAY87 exhibited no cytotoxicity in ST cells and intestinal organoid monolayer.

(A) ST cells or the intestinal organoid monolayer were incubated with different concentrations of $CoCl_2$ or BAY87 for 24 h and assessed using the Cell Counting Kit 8. Results are presented as the mean ± standard deviation of data from three independent experiments ns, not significant.

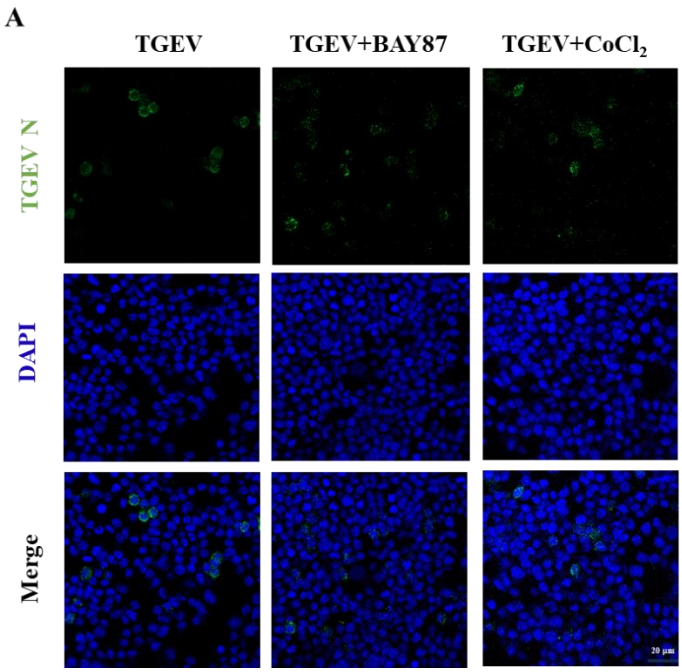

Supplementary Figure 19. HIF-1α cannot affect TGEV.

(A) Adsorption assay. ST cells were pretreated with $CoCl_2$ (25 μM), BAY87 (10 μM), or DMSO for 1 h at 37°C, and the media were replaced by a mixture of $CoCl_2$ (25 μM), BAY87 (10 μM), or DMSO and TGEV (multiplicity of infection=5) for 1 h at 4°C. After washing with PBS, TGEV N was measured by IFA. Scale bar: 20 μm.

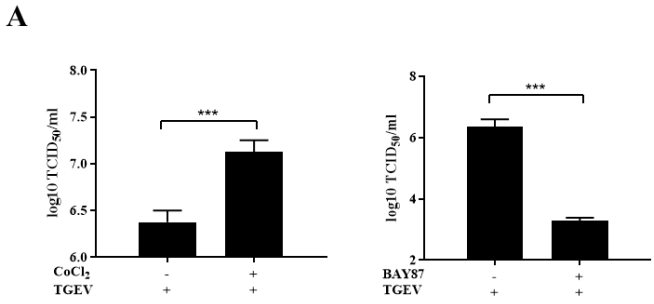

Supplementary Figure 20. HIF-1 α enhances TGEV infection by targeting viral replication.

(A) Replication assay. ST cells infected with TGEV (MOI=1) were incubated at 37 °C for 3 h and washed with sodium citrate buffer. The cells were then treated with $CoCl_2$ (25 μM), BAY87(10 μM), or DMSO for 13 h. The cells were subjected to three cycles of repeated

freeze-thawing, and the virus in the supernatant was quantified using the $TCID_{50}$ method. Results are presented as the mean ± standard deviation of data from three independent experiments ***, $P \leq 0.001$.

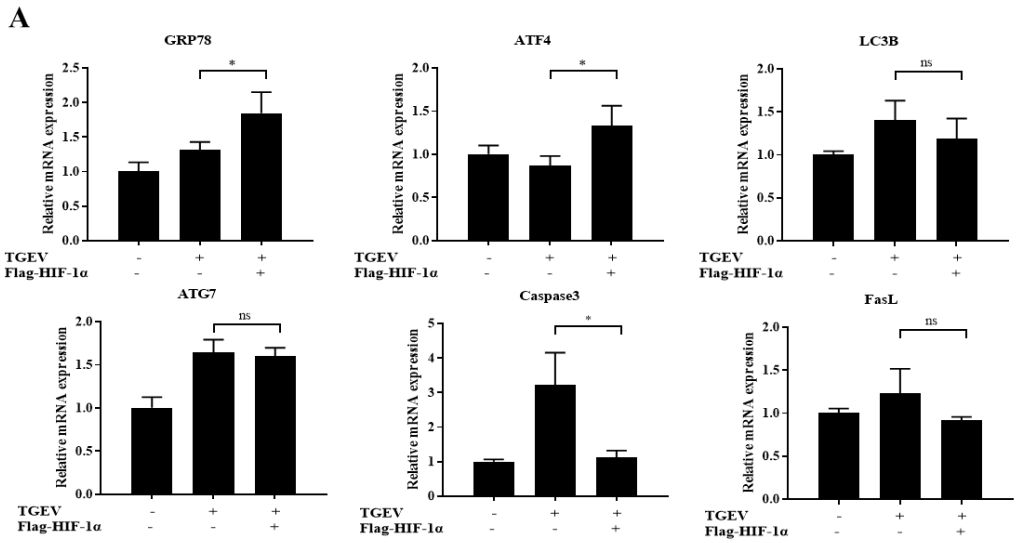

Supplementary Figure 21. HIF-1α slightly regulates GRP78, ATF4 and Caspase 3 expression.

(A) ST cells transfected with Flag-HIF-1α for 24 h were infected with TGEV (multiplicity of infection=1) for 20 h. The transcription levels of GRP78, ATF4, LC3B, ATG7, Caspase 3 and FasL were then evaluated by RT-qPCR. Results are presented as mean ± standard deviation of data from three independent experiments *, $P \leq 0.05$; ns, not significant.

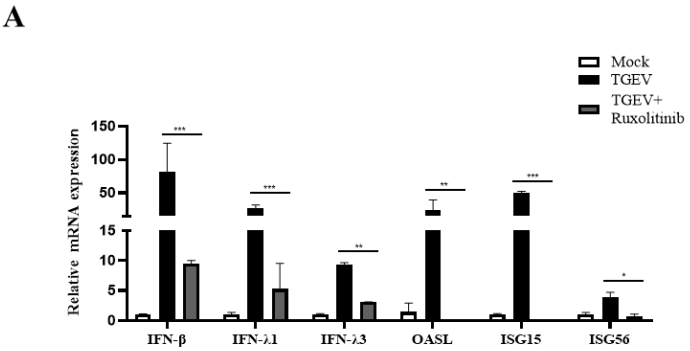

Supplementary Figure 22. Ruxolitinib significantly inhibits TGEV-induced type I and type III IFN expression.

(A) ST cells were treated with Ruxolitinib (4 μM) and infected with TGEV for 20 h. The transcriptional levels of IFN-β, IFN-λ1, IFN-λ3, OASL, ISG15 and ISG56 were detected by

RT-qPCR. Results are presented as the mean ± standard deviation of data from three independent experiments *, $P \leq 0.05$; **, $P \leq 0.01$; ***, $P \leq 0.001$; ns, no significance.

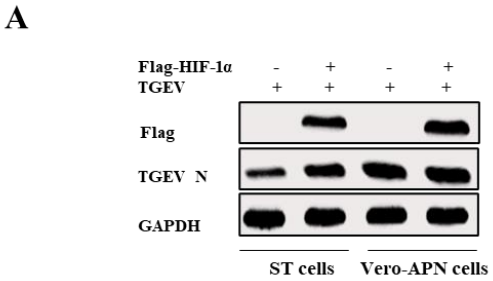

Supplementary Figure 23. HIF-1α cannot promote TGEV replication in Vero-APN cells.

(A) ST cells and Vero-APN cells were transfected with Flag-HIF-1α for 24 h, and then infected with TGEV (multiplicity of infection=1) for 20 h. The HIF-1α and TGEV N were detected by Western blot**.**

Chapter 6

Discussion and conclusion

Coronavirus infections have long posed significant risks to both human and animal health. Porcine coronaviruses have been particularly damaging, causing severe gastrointestinal, respiratory, and neurological diseases in pigs. These infections lead to considerable economic losses worldwide, affecting swine production and increasing veterinary expenses. Despite various control measures, these viruses continue to challenge the global swine industry. Therefore, identifying new, effective strategies to combat porcine coronaviruses and understanding their underlying mechanisms are urgently needed.

In my thesis, the first strategy demonstrated that PM can inhibit cell receptor APN expression to control APN-dependent coronaviruses infection. Subsequently, we investigated porcine coronavirus-induced inflammatory responses to discover a novel proinflammatory factor HIF-1α. Lastly, further study elucidated the role of HIF-1α on porcine coronaviruses infection. Collectively, our aim is to develop novel and potent strategies for preventing porcine coronaviruses infection.

6.1 The role of cell receptors in coronavirus infection

The infection of coronaviruses depends on whether the corresponding cell receptors are expressed on the surface of the host cells. The engagement of cell receptors is the initial step for coronavirus to initiate infection. It is reported that SARS-CoV-2 enters cells through various receptors and co-receptors. In specific, ACE2 was reported to be a major cell entry receptor for SARS-CoV-2[211]. Wang et al. found that diltiazem inhibits SARS-CoV-2 attachment and entry by reducing ACE2 expression in various cell lines and mouse lungs[156]. Ursodeoxycholic acid (UDCA)-mediated downregulation of ACE2 reduces susceptibility to SARS-CoV-2 infection *in vitro* and *in vivo*[212]. In addition, metabotropic glutamate receptor subtype 2 (mGluR2) is also found to cooperate with ACE2 to promote SARS-CoV-2 entry by via clathrin-mediated endocytosis (CME), and the knockout of mGluR2 eliminated SARS-CoV-2 infection in the nasal turbinates and greatly diminished viral presence in the lungs of mice[213]. Besides, DDP4 was a functional receptor for MERS-CoV, SARS-CoV-2 and PHEV internalization[160, 214-215]. Inhibitors of the cell receptor DPP4 could modulate the pathogenesis of MERS-CoV infection and serve as potential therapeutics[216]. For most of porcine coronaviruses, APN serves as a primary cell receptor for their penetration. Previous studies indicated that TGEV, PRCV and PDCoV infiltrate host cells through APN's binding to their spike proteins[54, 128, 217]. Chimeric APN gene-edited neonatal pigs were less susceptible to PDCoV infection[218]. Additionally, APN-KO piglets have been found to be resistant to TGEV but not PEDV infection[49, 159] It means that APN is the essential receptor for TGEV, PRCV and PDCoV entry. Due to the coronavirus' propensity for mutation, controlling the expression of viral receptors has been proposed as an ideal approach to shut the door on coronavirus entry, thus controlling coronavirus and its variants infection. In chapter 3, PM can negatively regulate the expression of APN in porcine, human, and mouse cells, suggesting that PM not only inhibits the entry of APN-dependent porcine coronaviruses but may also play a significant role in controlling APN-dependent human and mouse coronaviruses. Besides, PM does not exhibit a degradative effect on the coronavirus receptors ACE2 and CEACAM1. However, it does target DPP4, the cell receptor for MERS-CoV,

SARS-CoV-2 and PHEV, for degradation[56, 160]. These findings suggest that PM may have potential in impeding MERS-CoV, SARS-CoV-2 and PHEV infections by targeting DPP4 for degradation. Nonetheless, this possibility requires further exploration. Based on those results of chapter 3, PM can negatively regulate APN-dependent coronaviruses infection, but the prevention and control of PEDV and SADS-CoV remain challenging, necessitating further experiments to identify functional cellular receptors for these two viruses. Furthermore, novel strategies should be developed to block their cell receptors for controlling PEDV and SADS-CoV infection.

6.2 Autophagic degradation of cell receptors

Three primary pathways involved in protein degradation are the autophagy-lysosome pathway, the proteasome pathway, and the apoptotic pathway[168-169, 219-221]. Autophagy is a vital and conserved process that cells use to degrade intracellular components[222]. This includes soluble and aggregated proteins, organelles, macromolecular complexes, and foreign bodies. The process involves the formation of a double-membrane structure, called the autophagosome, which encloses the sequestered cytoplasmic material and eventually fuses with the lysosome for degradation[223]. In Chapter 3, it was shown that PM degrades APN expression, thereby obstructing APN-restricted coronavirus entry through the autophagy-lysosome pathway. This suggests that PM-mediated autophagy plays a regulatory role in coronavirus infection. Autophagy has been reported to negatively impact TGEV infection[102], though the precise mechanisms behind this effect remain unexplored. Here, the PM induced PIK3C3-mediated autophagy to degrade APN through, which may explain why autophagy inhibited TGEV infection. Moreover, while autophagic degradation typically occurs in the cytoplasm, the degradation mechanism of APN, a membrane protein, remains unclear. Studies have shown that autophagy cargo receptor TOLLIP can interact with membrane protein ACE2 for selective autophagic degradation, and endosomes, PAK1-mediated cytoskeleton rearrangement is involved in the autophagic degradation of membrane proteins[178-180]. We hypothesize that these mechanisms may facilitate the autophagic degradation of APN. Further research is needed to elucidate this process in detail.

6.3 Coronavirus-induced inflammation

6.3.1 The role of inflammation in coronavirus pathogenesis

Coronavirus infection triggers inflammatory responses, leading to a robust immune response in the host. The intricate network of inflammatory regulation is pivotal in the host antiviral defense[224]. However, an excessive inflammatory response can result in a "cytokine storm," causing pathological damage to the host's target organs and potentially leading to death[225]. This phenomenon plays a critical role in the pathogenesis of viral infections. In specific, SARS-CoV-2 and MERS-CoV infection can trigger a "cytokine storm," leading to damage in the lung parenchyma. This damage can subsequently result in acute respiratory distress syndrome (ARDS) and

possibly lead to death[226]. Additionally, swine enteric coronavirus induces inflammation in the small intestine, leading to severe diarrhea in piglets. The consequent nutrient loss significantly increases mortality rates[129]. Collectively, inflammation plays a crucial role in coronavirus pathogenesis.

6.3.2 The mechanism of coronavirus-induced inflammation

The activation of PRRs is a key strategy used by coronaviruses to manipulate inflammatory responses. It is reported that TLR2 and Myd88 were required for β-coronavirus-induced inflammatory responses[227]. Specifically, TLR2 plays a crucial role in inflammation induced by the SARS-CoV-2 spike protein by activating the NF-κB pathway[228]. For the porcine coronaviruses, PEDV infection activates NF-κB pathway through the TLR2, TLR3, and TLR9 in porcine intestinal epithelial cells[229]. And TGEV infection significantly upregulated mRNA expression of RIG-I and MDA5 to induce inflammation in ST cells[79]. In chapter 4, which PRRs mediate TGEV-induced inflammation in intestinal organoids and *in vivo* was explored. We observed that TGEV induces inflammation by upregulating RIG-I expression in apical-out organoids and pigs, rather than activating MDA5. The discrepancy in results may be due to the different infection models we used upon TGEV infection.

The production of inflammatory cytokines can be induced through various pathways, primarily the NF-κB and MAPK-AP-1 pathways[230-231]. The classical NF-κB activation cascade begins with stimulus-induced ubiquitinated degradation of IκBα, which releases NF-κB dimers, facilitating their nuclear translocation[188]. On the other hand, the AP-1 pathway consists of JUN, FOS, or ATF subunits, and its activation involves the phosphorylation of JUN. Some studies have reported that most of coronaviruses induces inflammatory responses through the NF-κB pathway in different cell and animal models[78-79, 228-229]. Our findings show a similar trend in apical-out organoids and pigs, suggesting that targeting the NF-κB pathway could be an effective strategy to control coronavirus-induced inflammation.

Furthermore, coronavirus-induced inflammation involves numerous proinflammatory factors. It has been reported that HIF-1α promotes SARS-CoV-2 infection and exacerbates inflammatory responses to COVID-19[122]. And mtROS/HIF-1α is necessary for CoV-2 replication and monocyte cytokine production[193]. However, the role of HIF-1α in porcine coronaviruses has not yet been studied. Here, our results showed that HIF-1α expression can be regulated by the RIG-I-NF-κB pathway during TGEV infection. Notably, HIF-1α showed higher expression in intestinal organoids and tissues compared to conventional cell lines, such as ST cells (data not shown). This suggests a potential involvement of HIF-1α in TGEV-induced inflammation. Subsequent findings revealed that HIF-1α serves as a crucial mediator of TGEV-induced inflammatory responses in intestinal organoids and the porcine ileum, underscoring the superior ability of intestinal organoids to mimic *in vivo* environments compared to conventional cell lines. However, the detailed molecular mechanism underlying the regulation of NF-κB and HIF-1α remains unclear. Some reports suggest that NF-κB1 p50 stabilizes HIF-1α protein by suppressing ATG7-dependent autophagy[199]. Therefore, we speculate that p50 may stabilize HIF-1α protein during TGEV infection by similar mechanism[199], but further research is needed to validate this hypothesis. Notably, we also found that HIF-1α can promote TGEV infection *ex*

vivo and *in vivo*. The mechanism was further explored in chapter 5, which demonstrated that HIF-1α facilitate TGEV infection by downregulating type I and type III IFN responses. Moreover, Codo et al. reported that SARS-CoV-2 stabilized HIF-1α expression, which induced monocyte-derived cytokines by activating glycolysis[193]. We also found that HIF-1α facilitates TGEV-induced inflammation by regulating glycolysis, providing novel mechanistic insights into this process. Additionally, similar to HIF-1α, the activation of glycolysis can also enhance TGEV infection. These findings provide a novel insight into potential therapeutic targets for TGEV-caused swine enteritis.

In chapter 4, we focused on the ileum as the primary site of analysis due to its previous use in organoid research and our intent to draw comparisons. However, it is important to acknowledge the limitations associated with this choice. The ileum presents challenges in maintaining normal morphology, as it is filled with lymphoid tissues that can obscure the typical villus structure. This can lead to difficulties in accurately assessing the extent of viral replication and its effects on the tissue. Given that our hypothesis centers around the cytokine burst and its implications for viral replication, the ileum may not be the optimal target for this investigation. In contrast, the jejunum represents a more relevant site for observing significant tissue destruction and exudate leakage, which are critical components of the immune response to viral infections. The jejunum structure is likely to provide a clearer understanding of the pathophysiological changes occurring during TGEV infection. Future research should prioritize including the jejunum in analyses to gain a comprehensive understanding of viral replication dynamics and inflammatory responses.

6.4 The effect of HIF-1α on virus infection and IFN responses

HIF-1α has been reported to be a host factor which evade immune system to support viral replication[232]. For instance, SARS-CoV-2 ORF3a triggers the expression of HIF-1α to support viral replication[122]; PRRSV nsp1β enhances viral replication by stabilizing HIF-1α[206]; Respiratory syncytial virus (RSV) infection increased HIF-1α-mediated glycolysis to favor the production of infectious virus[125]. In chapter 4 and 5, we found that TGEV infection can upregulate HIF-1α expression to facilitate viral replication in ST cells, organoids model and piglets.

For the mechanism, further investigation unveiled HIF-1α can inhibit type I and III IFN responses to promote viral replication. A great variety of studies reported that type I and III IFNs and ISGs are crucial for antiviral defense[233-234]. In specific, IFN-β and IFN-λ1/3 have strong antiviral effects against coronaviruses, especially in pigs. Additionally, some of ISGs can restrict coronavirus infections[71,201]. But the specific underlying mechanism of this phenomenon remains unclear. It has been reported that H1N1-induced HIF-1α can promote glycolysis, leading to lactate production. This, in turn, reduces the accumulation of the RIG-I–MAVS complex and IFN responses, thereby promoting viral infection[123]. Based on this finding, we guess that HIF-1α represent similar mechanism to negatively regulate IFN responses to promote TGEV replication in chapter 5. Moreover, HIF-1α has also been reported to act as a transcriptional repressor of IRF5 and IRF3, which are essential for IFN responses in

human monocytes[205]. This suppression may explain how HIF-1α diminishes IFN responses in porcine cell models. Further in-depth studies are needed to elucidate this aspect. We have also confirmed that HIF-1α enhances TGEV replication by inhibiting the production of type I and III IFNs. The role of HIF-1α in promoting infection by other porcine coronaviruses through similar mechanisms remains to be elucidated. Future research may establish HIF-1α as a critical broad-spectrum target for combating porcine coronavirus infections.

6.5 The potential for clinical application of antiviral strategies

6.5.1 The potential for clinical application of PM

APN, a member of the M1 zinc metallopeptidase family, is a versatile metalloenzyme expressed in various cell types. It is reported that APN knockout pigs not only resist infection by APN-dependent porcine coronaviruses but also exhibit no differences from wild-type pigs in terms of meat production or reproductive performance traits[46, 218]. This aligns with our observations that oral PM-induced APN inhibition does not exhibit cytotoxic effects on piglets. Beyond the effect of APN facilitating coronavirus entry, it has also been implicated in the progression of several cancers and is being considered a promising target for anti-cancer therapies[235], implying that PM may be used as an anti-cancer drug in pigs. In addition, some basic conditions that need to be considered and investigated for the clinical application of PM include the timing, frequency, and method of administration. Our results in Chapter 3 indicate that PM exhibits similar efficacy when used both therapeutically and prophylactically *in vivo*, suggesting its potential for both preventing and treating APN-dependent coronavirus-induced diseases. Regarding frequency, we found that oral administration of PM every 12 hours is optimal for maintaining its activation, ensuring effective APN inhibition in the small intestine of piglets. For the method of administration, drug delivery systems may be the better approaches, because they can enhance the effectiveness of drugs by allowing them to release in the target organs[236]. The optimal drug delivery system for PM still requires further investigation. Besides, PM can exert synergistic effects when co-administered with antiviral drugs targeting other coronavirus-specific pathways, like drugs targeting 3CL Protease[237] etc. This could potentially result in enhanced antiviral efficacy against coronaviruses. Given this, PM holds significant potential for clinical application in combating APN-dependent coronavirus entry.

6.5.2 The potential for clinical application of HIF-1α inhibitor

HIF-1α plays a crucial role in regulating oxygen homeostasis and acts as a key transcription factor in response to hypoxic conditions[238]. Many viruses can induce a hypoxic environment to stabilize HIF-1α expression, thereby enhancing their replication and inflammation[123, 125, 206]. In chapter 4 and 5, we have uncovered the essential role of HIF-1α in TGEV replication and the accompanying inflammatory response. HIF-1α inhibitor BAY87 was found to inhibit TGEV replication and alleviate TGEV-induced inflammation *in vitro, ex vivo* and *in vivo.* Our results

demonstrated that oral administration of BAY87 (10 mg/kg) is non-cytotoxic and plays a significant role in preventing TGEV infection in piglets. However, for clinical application, further investigation into the drug's half-life and an optimal dosing regimen is needed. Additionally, the mode of administration of BAY87 is also a critical factor that requires careful consideration. Based on the entire study, BAY87 may potentially exhibit synergistic antiviral effects against coronaviruses when co-administered with PM. This hypothesis requires further experimental validation. Lastly, we have not yet explored whether HIF-1α inhibition by BAY87 affects the replication of other porcine coronaviruses, such as PEDV, PRCV, PDCoV, SADS-CoV, and PHEV. Further research is required to elucidate the effect of BAY87 in managing these other coronaviruses.

6.6 Conclusion

In summary, this thesis introduces two innovative and effective antiviral strategies to combat porcine coronaviruses infections. Firstly, we identified that PM inhibits APN-dependent coronavirus entry by degrading receptors through PIK3C3-mediated autophagy. Furthermore, we elucidated the mechanism of TGEV-induced inflammation, revealing HIF-1α as a novel antiviral target. Our subsequent research demonstrated that inhibiting HIF-1α not only restricts TGEV replication but also alleviates virus-induced inflammation. These findings provide valuable insights and propose potential strategies for preventing porcine coronaviruses infection.

Chapter 7

Publications

7.1 Publications in scientific journals as first (co)-author:

Zhang Y[#], Zhang N[#], Zhang Y, Yang L, Yang N, Cai Y, Tan C, Zhao J, Li W, Liu Y, Rui X, Wu J, Fu Y, Liu G[*]. Potassium Molybdate blocks APN-dependent coronavirus entry by degrading receptor via PIK3C3-mediated autophagy. **Journal of Virology**. (Accepted).

Zhang Y, Yang N, Li Y, Tan C, Cai Y, Rui X, Liu Y, Fu Y[*]& Liu G[*]. Transmissible gastroenteritis virus induces inflammatory responses via RIG-I/NF-κB/HIF-1α/glycolysis axis in intestinal organoids and in *vivo*. **Journal of Virology.** 2024 May 23:e0046124.

Zhang Y, Rui X, Li Y, Zhang Y, Cai Y, Tan C, Yang N, Liu Y, Fu Y, Liu G[*]. Hypoxia inducible factor-1α facilitates transmissible gastroenteritis virus replication by inhibiting type I and type III interferon production. **Veterinary Microbiology.** 2024 May;292:110055.

Chapter 8

Bibliography

1. Fehr, A. R.; Perlman, S., Coronaviruses: an overview of their replication and pathogenesis. *Methods Mol Biol* **2015,** *1282*, 1-23.
2. Woo, P. C. Y.; Huang, Y.; Lau, S. K. P.; Yuen, K. Y., Coronavirus genomics and bioinformatics analysis. *Viruses* **2010,** *2* (8), 1804-1820.
3. Su, S.; Wong, G.; Shi, W.; Liu, J.; Lai, A. C. K.; Zhou, J.; Liu, W.; Bi, Y.; Gao, G. F., Epidemiology, Genetic Recombination, and Pathogenesis of Coronaviruses. *Trends Microbiol* **2016,** *24* (6), 490-502.
4. Turlewicz-Podbielska, H.; Pomorska-Mol, M., Porcine Coronaviruses: Overview of the State of the Art. *Virol Sin* **2021,** *36* (5), 833-851.
5. Yan, Q.; Liu, X.; Sun, Y.; Zeng, W.; Li, Y.; Zhao, F.; Wu, K.; Fan, S.; Zhao, M.; Chen, J.; Yi, L., Swine Enteric Coronavirus: Diverse Pathogen-Host Interactions. *Int J Mol Sci* **2022,** *23* (7).
6. Zhou, P.; Fan, H.; Lan, T.; Yang, X. L.; Shi, W. F.; Zhang, W.; Zhu, Y.; Zhang, Y. W.; Xie, Q. M.; Mani, S.; Zheng, X. S.; Li, B.; Li, J. M.; Guo, H.; Pei, G. Q.; An, X. P.; Chen, J. W.; Zhou, L.; Mai, K. J.; Wu, Z. X.; Li, D.; Anderson, D. E.; Zhang, L. B.; Li, S. Y.; Mi, Z. Q.; He, T. T.; Cong, F.; Guo, P. J.; Huang, R.; Luo, Y.; Liu, X. L.; Chen, J.; Huang, Y.; Sun, Q.; Zhang, X. L.; Wang, Y. Y.; Xing, S. Z.; Chen, Y. S.; Sun, Y.; Li, J.; Daszak, P.; Wang, L. F.; Shi, Z. L.; Tong, Y. G.; Ma, J. Y., Fatal swine acute diarrhoea syndrome caused by an HKU2-related coronavirus of bat origin. *Nature* **2018,** *556* (7700), 255-258.
7. Chen, F.; Knutson, T. P.; Rossow, S.; Saif, L. J.; Marthaler, D. G., Decline of transmissible gastroenteritis virus and its complex evolutionary relationship with porcine respiratory coronavirus in the United States. *Sci Rep* **2019,** *9* (1), 3953.
8. Sanchez, C. M.; Gebauer, F.; Sune, C.; Mendez, A.; Dopazo, J.; Enjuanes, L., Genetic evolution and tropism of transmissible gastroenteritis coronaviruses. *Virology* **1992,** *190* (1), 92-105.
9. Chen, Y.; Zhang, Y.; Wang, X.; Zhou, J.; Ma, L.; Li, J.; Yang, L.; Ouyang, H.; Yuan, H.; Pang, D., Transmissible Gastroenteritis Virus: An Update Review and Perspective. *Viruses* **2023,** *15* (2).
10. Pensaert, M.; Cox, E.; van Deun, K.; Callebaut, P., A sero-epizootiological study of porcine respiratory coronavirus in Belgian swine. *Vet Q* **1993,** *15* (1), 16-20.
11. Krempl, C.; Schultze, B.; Laude, H.; Herrler, G., Point mutations in the S protein connect the sialic acid binding activity with the enteropathogenicity of transmissible gastroenteritis coronavirus. *J Virol* **1997,** *71* (4), 3285-7.

12. Halbur, P. G.; Pallares, F. J.; Opriessnig, T.; Vaughn, E. M.; Paul, P. S., Pathogenicity of three isolates of porcine respiratory coronavirus in the USA. *Vet Rec* **2003,** *152* (12), 358-61.
13. Song, D.; Park, B., Porcine epidemic diarrhoea virus: a comprehensive review of molecular epidemiology, diagnosis, and vaccines. *Virus Genes* **2012,** *44* (2), 167-75.
14. Fan, H.; Zhang, J.; Ye, Y.; Tong, T.; Xie, K.; Liao, M., Complete genome sequence of a novel porcine epidemic diarrhea virus in south China. *J Virol* **2012,** *86* (18), 10248-9.
15. Cui, J.; Li, F.; Shi, Z. L., Origin and evolution of pathogenic coronaviruses. *Nat Rev Microbiol* **2019,** *17* (3), 181-192.
16. Pan, Y.; Tian, X.; Qin, P.; Wang, B.; Zhao, P.; Yang, Y. L.; Wang, L.; Wang, D.; Song, Y.; Zhang, X.; Huang, Y. W., Discovery of a novel swine enteric alphacoronavirus (SeACoV) in southern China. *Vet Microbiol* **2017,** *211*, 15-21.
17. Wang, Q.; Vlasova, A. N.; Kenney, S. P.; Saif, L. J., Emerging and re-emerging coronaviruses in pigs. *Curr Opin Virol* **2019,** *34*, 39-49.
18. Yang, Y. L.; Yu, J. Q.; Huang, Y. W., Swine enteric alphacoronavirus (swine acute diarrhea syndrome coronavirus): An update three years after its discovery. *Virus Res* **2020,** *285*, 198024.
19. Roe, C. K.; Alexander, T. J., A Disease of Nursing Pigs Previously Unreported in Ontario. *Can J Comp Med Vet Sci* **1958,** *22* (9), 305-7.
20. Greig, A. S.; Mitchell, D.; Corner, A. H.; Bannister, G. L.; Meads, E. B.; Julian, R. J., A Hemagglutinating Virus Producing Encephalomyelitis in Baby Pigs. *Can J Comp Med Vet Sci* **1962,** *26* (3), 49-56.
21. Mora-Diaz, J. C.; Pineyro, P. E.; Houston, E.; Zimmerman, J.; Gimenez-Lirola, L. G., Porcine Hemagglutinating Encephalomyelitis Virus: A Review. *Front Vet Sci* **2019,** *6*, 53.
22. Shi, J.; Li, Z.; Zhang, J.; Xu, R.; Lan, Y.; Guan, J.; Gao, R.; Wang, Z.; Lu, H.; Xu, B.; Zhao, K.; Gao, F.; He, W., PHEV infection: A promising model of betacoronavirus-associated neurological and olfactory dysfunction. *PLoS Pathog* **2022,** *18* (6), e1010667.
23. Woo, P. C.; Lau, S. K.; Lam, C. S.; Lau, C. C.; Tsang, A. K.; Lau, J. H.; Bai, R.; Teng, J. L.; Tsang, C. C.; Wang, M.; Zheng, B. J.; Chan, K. H.; Yuen, K. Y., Discovery of seven novel Mammalian and avian coronaviruses in the genus deltacoronavirus supports bat coronaviruses as the gene source of

alphacoronavirus and betacoronavirus and avian coronaviruses as the gene source of gammacoronavirus and deltacoronavirus. *J Virol* **2012,** *86* (7), 3995-4008.
24. He, W. T.; Ji, X.; He, W.; Dellicour, S.; Wang, S.; Li, G.; Zhang, L.; Gilbert, M.; Zhu, H.; Xing, G.; Veit, M.; Huang, Z.; Han, G. Z.; Huang, Y.; Suchard, M. A.; Baele, G.; Lemey, P.; Su, S., Genomic Epidemiology, Evolution, and Transmission Dynamics of Porcine Deltacoronavirus. *Mol Biol Evol* **2020,** *37* (9), 2641-2654.
25. Zhang, J., Porcine deltacoronavirus: Overview of infection dynamics, diagnostic methods, prevalence and genetic evolution. *Virus Res* **2016,** *226*, 71-84.
26. Duan, C.; Luo, Y.; Liang, X.; Wang, X., A Review of Bioactive Compounds against Porcine Enteric Coronaviruses. *Viruses* **2022,** *14* (10).
27. Neuman, B. W.; Buchmeier, M. J., Supramolecular Architecture of the Coronavirus Particle. *Adv Virus Res* **2016,** *96*, 1-27.
28. Masters, P. S., The molecular biology of coronaviruses. *Adv Virus Res* **2006,** *66*, 193-292.
29. Neuman, B. W.; Kiss, G.; Kunding, A. H.; Bhella, D.; Baksh, M. F.; Connelly, S.; Droese, B.; Klaus, J. P.; Makino, S.; Sawicki, S. G.; Siddell, S. G.; Stamou, D. G.; Wilson, I. A.; Kuhn, P.; Buchmeier, M. J., A structural analysis of M protein in coronavirus assembly and morphology. *J Struct Biol* **2011,** *174* (1), 11-22.
30. Hartenian, E.; Nandakumar, D.; Lari, A.; Ly, M.; Tucker, J. M.; Glaunsinger, B. A., The molecular virology of coronaviruses. *J Biol Chem* **2020,** *295* (37), 12910-12934.
31. Lee, C., Porcine epidemic diarrhea virus: An emerging and re-emerging epizootic swine virus. *Virol J* **2015,** *12*, 193.
32. Gui, M.; Song, W.; Zhou, H.; Xu, J.; Chen, S.; Xiang, Y.; Wang, X., Cryo-electron microscopy structures of the SARS-CoV spike glycoprotein reveal a prerequisite conformational state for receptor binding. *Cell Res* **2017,** *27* (1), 119-129.
33. Walls, A. C.; Tortorici, M. A.; Bosch, B. J.; Frenz, B.; Rottier, P. J. M.; DiMaio, F.; Rey, F. A.; Veesler, D., Cryo-electron microscopy structure of a coronavirus spike glycoprotein trimer. *Nature* **2016,** *531* (7592), 114-117.
34. Leutenegger, C. M.; Boretti, F. S.; Mislin, C. N.; Flynn, J. N.; Schroff, M.; Habel, A.; Junghans, C.; Koenig-Merediz, S. A.; Sigrist, B.; Aubert, A.;

Pedersen, N. C.; Wittig, B.; Lutz, H., Immunization of cats against feline immunodeficiency virus (FIV) infection by using minimalistic immunogenic defined gene expression vector vaccines expressing FIV gp140 alone or with feline interleukin-12 (IL-12), IL-16, or a CpG motif. *J Virol* **2000,** *74* (22), 10447-57.
35. Wang, X. W.; Wang, M.; Zhan, J.; Liu, Q. Y.; Fang, L. L.; Zhao, C. Y.; Jiang, P.; Li, Y. F.; Bai, J., Pathogenicity and immunogenicity of a new strain of porcine epidemic diarrhea virus containing a novel deletion in the N gene. *Vet Microbiol* **2020,** *240*, 108511.
36. Gong, L.; Li, J.; Zhou, Q.; Xu, Z.; Chen, L.; Zhang, Y.; Xue, C.; Wen, Z.; Cao, Y., A New Bat-HKU2-like Coronavirus in Swine, China, 2017. *Emerg Infect Dis* **2017,** *23* (9), 1607-9.
37. Kim, Y.; Lee, K. M.; Jang, G.; Lee, C., Complete genome sequence of a novel porcine hemagglutinating encephalomyelitis virus strain identified in South Korea. *Arch Virol* **2022,** *167* (5), 1381-1385.
38. Jung, K.; Hu, H.; Saif, L. J., Porcine deltacoronavirus infection: Etiology, cell culture for virus isolation and propagation, molecular epidemiology and pathogenesis. *Virus Res* **2016,** *226*, 50-59.
39. Belouzard, S.; Millet, J. K.; Licitra, B. N.; Whittaker, G. R., Mechanisms of coronavirus cell entry mediated by the viral spike protein. *Viruses* **2012,** *4* (6), 1011-33.
40. Kirchdoerfer, R. N.; Cottrell, C. A.; Wang, N.; Pallesen, J.; Yassine, H. M.; Turner, H. L.; Corbett, K. S.; Graham, B. S.; McLellan, J. S.; Ward, A. B., Pre-fusion structure of a human coronavirus spike protein. *Nature* **2016,** *531* (7592), 118-21.
41. Hulswit, R. J.; de Haan, C. A.; Bosch, B. J., Coronavirus Spike Protein and Tropism Changes. *Adv Virus Res* **2016,** *96*, 29-57.
42. Millet, J. K.; Jaimes, J. A.; Whittaker, G. R., Molecular diversity of coronavirus host cell entry receptors. *FEMS Microbiol Rev* **2021,** *45* (3).
43. Walls, A. C.; Park, Y. J.; Tortorici, M. A.; Wall, A.; McGuire, A. T.; Veesler, D., Structure, Function, and Antigenicity of the SARS-CoV-2 Spike Glycoprotein. *Cell* **2020,** *181* (2), 281-292 e6.
44. Saleem, W.; Ren, X.; Van Den Broeck, W.; Nauwynck, H., Changes in intestinal morphology, number of mucus-producing cells and expression of coronavirus receptors APN, DPP4, ACE2 and TMPRSS2 in pigs with aging. *Vet Res* **2023,** *54* (1), 34.

45. Cui, T.; Theuns, S.; Xie, J.; Van den Broeck, W.; Nauwynck, H. J., Role of Porcine Aminopeptidase N and Sialic Acids in Porcine Coronavirus Infections in Primary Porcine Enterocytes. *Viruses* **2020,** *12* (4).
46. Xu, K.; Zhou, Y.; Mu, Y.; Liu, Z.; Hou, S.; Xiong, Y.; Fang, L.; Ge, C.; Wei, Y.; Zhang, X.; Xu, C.; Che, J.; Fan, Z.; Xiang, G.; Guo, J.; Shang, H.; Li, H.; Xiao, S.; Li, J.; Li, K., CD163 and pAPN double-knockout pigs are resistant to PRRSV and TGEV and exhibit decreased susceptibility to PDCoV while maintaining normal production performance. *Elife* **2020,** *9*.
47. Hu, W.; Zhang, S.; Shen, Y.; Yang, Q., Epidermal growth factor receptor is a co-factor for transmissible gastroenteritis virus entry. *Virology* **2018,** *521*, 33-43.
48. Schwegmann-Wessels, C.; Zimmer, G.; Laude, H.; Enjuanes, L.; Herrler, G., Binding of transmissible gastroenteritis coronavirus to cell surface sialoglycoproteins. *J Virol* **2002,** *76* (12), 6037-43.
49. Luo, L.; Wang, S.; Zhu, L.; Fan, B.; Liu, T.; Wang, L.; Zhao, P.; Dang, Y.; Sun, P.; Chen, J.; Zhang, Y.; Chang, X.; Yu, Z.; Wang, H.; Guo, R.; Li, B.; Zhang, K., Aminopeptidase N-null neonatal piglets are protected from transmissible gastroenteritis virus but not porcine epidemic diarrhea virus. *Sci Rep* **2019,** *9* (1), 13186.
50. Li, W.; van Kuppeveld, F. J. M.; He, Q.; Rottier, P. J. M.; Bosch, B. J., Cellular entry of the porcine epidemic diarrhea virus. *Virus Res* **2016,** *226*, 117-127.
51. Zhang, S.; Cao, Y.; Yang, Q., Transferrin receptor 1 levels at the cell surface influence the susceptibility of newborn piglets to PEDV infection. *PLoS Pathog* **2020,** *16* (7), e1008682.
52. Chen, X.; Liang, Y.; Weng, Z.; Hu, C.; Peng, Y.; Sun, Y.; Gao, Q.; Huang, Z.; Tang, S.; Gong, L.; Zhang, G., ALIX and TSG101 are essential for cellular entry and replication of two porcine alphacoronaviruses. *PLoS Pathog* **2024,** *20* (3), e1012103.
53. Liu, Q.; Wang, H. Y., Porcine enteric coronaviruses: an updated overview of the pathogenesis, prevalence, and diagnosis. *Vet Res Commun* **2021,** *45* (2-3), 75-86.
54. Ji, W.; Peng, Q.; Fang, X.; Li, Z.; Li, Y.; Xu, C.; Zhao, S.; Li, J.; Chen, R.; Mo, G.; Wei, Z.; Xu, Y.; Li, B.; Zhang, S., Structures of a deltacoronavirus spike protein bound to porcine and human receptors. *Nat Commun* **2022,** *13* (1), 1467.

55. Hu, Y.; Meng, X.; Zhang, F.; Xiang, Y.; Wang, J., The in vitro antiviral activity of lactoferrin against common human coronaviruses and SARS-CoV-2 is mediated by targeting the heparan sulfate co-receptor. *Emerg Microbes Infect* **2021,** *10* (1), 317-330.
56. Shi, J.; Hu, S.; Wei, H.; Zhang, L.; Lan, Y.; Guan, J.; Zhao, K.; Gao, F.; He, W.; Li, Z., Dipeptidyl peptidase 4 interacts with porcine coronavirus PHEV spikes and mediates host range expansion. *J Virol* **2024**, e0075324.
57. Gao, Y.; Yan, L.; Huang, Y.; Liu, F.; Zhao, Y.; Cao, L.; Wang, T.; Sun, Q.; Ming, Z.; Zhang, L.; Ge, J.; Zheng, L.; Zhang, Y.; Wang, H.; Zhu, Y.; Zhu, C.; Hu, T.; Hua, T.; Zhang, B.; Yang, X.; Li, J.; Yang, H.; Liu, Z.; Xu, W.; Guddat, L. W.; Wang, Q.; Lou, Z.; Rao, Z., Structure of the RNA-dependent RNA polymerase from COVID-19 virus. *Science* **2020,** *368* (6492), 779-782.
58. Liao, S.; Chen, Y.; Yang, Y.; Wang, G.; Wang, Q.; Liu, J.; Wu, H.; Luo, Q.; Chen, Y., Detection of RNA-dependent RNA polymerase of porcine epidemic diarrhea virus. *J Immunol Methods* **2023,** *515*, 113442.
59. Bai, C.; Zhong, Q.; Gao, G. F., Overview of SARS-CoV-2 genome-encoded proteins. *Sci China Life Sci* **2022,** *65* (2), 280-294.
60. Cheng, Y. R.; Li, X.; Zhao, X.; Lin, H., Cell Entry of Animal Coronaviruses. *Viruses* **2021,** *13* (10).
61. Akira, S.; Uematsu, S.; Takeuchi, O., Pathogen recognition and innate immunity. *Cell* **2006,** *124* (4), 783-801.
62. Thompson, M. R.; Kaminski, J. J.; Kurt-Jones, E. A.; Fitzgerald, K. A., Pattern recognition receptors and the innate immune response to viral infection. *Viruses* **2011,** *3* (6), 920-40.
63. Fitzgerald, K. A.; McWhirter, S. M.; Faia, K. L.; Rowe, D. C.; Latz, E.; Golenbock, D. T.; Coyle, A. J.; Liao, S. M.; Maniatis, T., IKKepsilon and TBK1 are essential components of the IRF3 signaling pathway. *Nat Immunol* **2003,** *4* (5), 491-6.
64. Zhang, S. Y.; Boisson-Dupuis, S.; Chapgier, A.; Yang, K.; Bustamante, J.; Puel, A.; Picard, C.; Abel, L.; Jouanguy, E.; Casanova, J. L., Inborn errors of interferon (IFN)-mediated immunity in humans: insights into the respective roles of IFN-alpha/beta, IFN-gamma, and IFN-lambda in host defense. *Immunol Rev* **2008,** *226*, 29-40.
65. Ivashkiv, L. B.; Donlin, L. T., Regulation of type I interferon responses. *Nat Rev Immunol* **2014,** *14* (1), 36-49.
66. Liu, W.; Zhang, S.; Wang, J., IFN-gamma, should not be ignored in SLE.

Front Immunol **2022,** *13*, 954706.
67. Mesev, E. V.; LeDesma, R. A.; Ploss, A., Decoding type I and III interferon signalling during viral infection. *Nat Microbiol* **2019,** *4* (6), 914-924.
68. Zhang, K.; Lin, S.; Li, J.; Deng, S.; Zhang, J.; Wang, S., Modulation of Innate Antiviral Immune Response by Porcine Enteric Coronavirus. *Front Microbiol* **2022,** *13*, 845137.
69. Ding, L.; Li, J.; Li, W.; Fang, Z.; Li, N.; Guo, Q.; Qu, H.; Feng, D.; Li, J.; Hong, M., p53 mediated IFN-beta signaling to affect viral replication upon TGEV infection. *Vet Microbiol* **2018,** *227*, 61-68.
70. Zhang, Q.; Ke, H.; Blikslager, A.; Fujita, T.; Yoo, D., Type III Interferon Restriction by Porcine Epidemic Diarrhea Virus and the Role of Viral Protein nsp1 in IRF1 Signaling. *J Virol* **2018,** *92* (4).
71. Song, L.; Chen, J.; Hao, P.; Jiang, Y.; Xu, W.; Li, L.; Chen, S.; Gao, Z.; Jin, N.; Ren, L.; Li, C., Differential Transcriptomics Analysis of IPEC-J2 Cells Single or Coinfected With Porcine Epidemic Diarrhea Virus and Transmissible Gastroenteritis Virus. *Front Immunol* **2022,** *13*, 844657.
72. Schneider, W. M.; Chevillotte, M. D.; Rice, C. M., Interferon-stimulated genes: a complex web of host defenses. *Annu Rev Immunol* **2014,** *32*, 513-45.
73. George, J. A.; Mayne, E. S., The Novel Coronavirus and Inflammation. *Adv Exp Med Biol* **2021,** *1321*, 127-138.
74. Li, G.; Fan, Y.; Lai, Y.; Han, T.; Li, Z.; Zhou, P.; Pan, P.; Wang, W.; Hu, D.; Liu, X.; Zhang, Q.; Wu, J., Coronavirus infections and immune responses. *J Med Virol* **2020,** *92* (4), 424-432.
75. Gholami, M.; Adibipour, F.; Valipour, S. M.; Ulloa, L.; Motaghinejad, M., Potential Regulation of NF-kappaB by Curcumin in Coronavirus-Induced Cytokine Storm and Lung Injury. *Int J Prev Med* **2022,** *13*, 156.
76. Song, K.; Li, S., The Role of Ubiquitination in NF-kappaB Signaling during Virus Infection. *Viruses* **2021,** *13* (2).
77. Leonardi, A.; Chariot, A.; Claudio, E.; Cunningham, K.; Siebenlist, U., CIKS, a connection to Ikappa B kinase and stress-activated protein kinase. *Proc Natl Acad Sci U S A* **2000,** *97* (19), 10494-9.
78. Wang, L.; Qiao, X.; Zhang, S.; Qin, Y.; Guo, T.; Hao, Z.; Sun, L.; Wang, X.; Wang, Y.; Jiang, Y.; Tang, L.; Xu, Y.; Li, Y., Porcine transmissible gastroenteritis virus nonstructural protein 2 contributes to inflammation via NF-kappaB activation. *Virulence* **2018,** *9* (1), 1685-1698.
79. Ding, Z.; An, K.; Xie, L.; Wu, W.; Zhang, R.; Wang, D.; Fang, Y.; Chen,

H.; Xiao, S.; Fang, L., Transmissible gastroenteritis virus infection induces NF-kappaB activation through RLR-mediated signaling. *Virology* **2017,** *507*, 170-178.
80. Sun, Y.; Liu, W. Z.; Liu, T.; Feng, X.; Yang, N.; Zhou, H. F., Signaling pathway of MAPK/ERK in cell proliferation, differentiation, migration, senescence and apoptosis. *J Recept Signal Transduct Res* **2015,** *35* (6), 600-4.
81. Schonthaler, H. B.; Guinea-Viniegra, J.; Wagner, E. F., Targeting inflammation by modulating the Jun/AP-1 pathway. *Ann Rheum Dis* **2011,** *70 Suppl 1*, i109-12.
82. Yu, J.; Liu, Y.; Zhang, Y.; Zhu, X.; Ren, S.; Guo, L.; Liu, X.; Sun, W.; Chen, Z.; Cong, X.; Chen, L.; Shi, J.; Du, Y.; Li, J.; Wu, J.; Wang, J., The integrity of PRRSV nucleocapsid protein is necessary for up-regulation of optimal interleukin-10 through NF-kappaB and p38 MAPK pathways in porcine alveolar macrophages. *Microb Pathog* **2017,** *109*, 319-324.
83. Tung, W. H.; Lee, I. T.; Hsieh, H. L.; Yang, C. M., EV71 induces COX-2 expression via c-Src/PDGFR/PI3K/Akt/p42/p44 MAPK/AP-1 and NF-kappaB in rat brain astrocytes. *J Cell Physiol* **2010,** *224* (2), 376-86.
84. Gao, R.; Zhang, Y.; Kang, Y.; Xu, W.; Jiang, L.; Guo, T.; Huan, C., Glycyrrhizin Inhibits PEDV Infection and Proinflammatory Cytokine Secretion via the HMGB1/TLR4-MAPK p38 Pathway. *Int J Mol Sci* **2020,** *21* (8).
85. Mizushima, N.; Levine, B.; Cuervo, A. M.; Klionsky, D. J., Autophagy fights disease through cellular self-digestion. *Nature* **2008,** *451* (7182), 1069-75.
86. Levine, B.; Kroemer, G., Autophagy in the pathogenesis of disease. *Cell* **2008,** *132* (1), 27-42.
87. Parzych, K. R.; Klionsky, D. J., An overview of autophagy: morphology, mechanism, and regulation. *Antioxid Redox Signal* **2014,** *20* (3), 460-73.
88. Pohl, C.; Dikic, I., Cellular quality control by the ubiquitin-proteasome system and autophagy. *Science* **2019,** *366* (6467), 818-822.
89. Mizushima, N.; Komatsu, M., Autophagy: renovation of cells and tissues. *Cell* **2011,** *147* (4), 728-41.
90. Mizushima, N.; Yoshimori, T.; Ohsumi, Y., The role of Atg proteins in autophagosome formation. *Annu Rev Cell Dev Biol* **2011,** *27*, 107-32.
91. Liu, D.; Liu, Y.; Chen, G.; He, L.; Tang, C.; Wang, C.; Yang, D.; Li, H.; Dong, Z.; Liu, H., Rapamycin Enhances Repressed Autophagy and Attenuates

Aggressive Progression in a Rat Model of IgA Nephropathy. *Am J Nephrol* **2017,** *45* (4), 293-300.
92. Laplante, M.; Sabatini, D. M., mTOR signaling in growth control and disease. *Cell* **2012,** *149* (2), 274-93.
93. Suzuki, K.; Kubota, Y.; Sekito, T.; Ohsumi, Y., Hierarchy of Atg proteins in pre-autophagosomal structure organization. *Genes Cells* **2007,** *12* (2), 209-18.
94. Kang, R.; Zeh, H. J.; Lotze, M. T.; Tang, D., The Beclin 1 network regulates autophagy and apoptosis. *Cell Death Differ* **2011,** *18* (4), 571-80.
95. Kihara, A.; Noda, T.; Ishihara, N.; Ohsumi, Y., Two distinct Vps34 phosphatidylinositol 3-kinase complexes function in autophagy and carboxypeptidase Y sorting in Saccharomyces cerevisiae. *J Cell Biol* **2001,** *152* (3), 519-30.
96. Fimia, G. M.; Stoykova, A.; Romagnoli, A.; Giunta, L.; Di Bartolomeo, S.; Nardacci, R.; Corazzari, M.; Fuoco, C.; Ucar, A.; Schwartz, P.; Gruss, P.; Piacentini, M.; Chowdhury, K.; Cecconi, F., Ambra1 regulates autophagy and development of the nervous system. *Nature* **2007,** *447* (7148), 1121-5.
97. Mizushima, N.; Noda, T.; Yoshimori, T.; Tanaka, Y.; Ishii, T.; George, M. D.; Klionsky, D. J.; Ohsumi, M.; Ohsumi, Y., A protein conjugation system essential for autophagy. *Nature* **1998,** *395* (6700), 395-8.
98. Galluzzi, L.; Green, D. R., Autophagy-Independent Functions of the Autophagy Machinery. *Cell* **2019,** *177* (7), 1682-1699.
99. Liu, S.; Yao, S.; Yang, H.; Liu, S.; Wang, Y., Autophagy: Regulator of cell death. *Cell Death Dis* **2023,** *14* (10), 648.
100. Xie, Z.; Klionsky, D. J., Autophagosome formation: core machinery and adaptations. *Nat Cell Biol* **2007,** *9* (10), 1102-9.
101. Lin, L. T.; Dawson, P. W.; Richardson, C. D., Viral interactions with macroautophagy: a double-edged sword. *Virology* **2010,** *402* (1), 1-10.
102. Guo, L.; Yu, H.; Gu, W.; Luo, X.; Li, R.; Zhang, J.; Xu, Y.; Yang, L.; Shen, N.; Feng, L.; Wang, Y., Autophagy Negatively Regulates Transmissible Gastroenteritis Virus Replication. *Sci Rep* **2016,** *6*, 23864.
103. Yang, X.; Kong, N.; Qin, W.; Zhai, X.; Song, Y.; Tong, W.; Li, L.; Liu, C.; Zheng, H.; Yu, H.; Zhang, W.; Tong, G.; Shan, T., PGAM5 degrades PDCoV N protein and activates type I interferon to antagonize viral replication. *J Virol* **2023,** *97* (11), e0147023.
104. Kong, N.; Shan, T.; Wang, H.; Jiao, Y.; Zuo, Y.; Li, L.; Tong, W.; Yu, L.;

Jiang, Y.; Zhou, Y.; Li, G.; Gao, F.; Yu, H.; Zheng, H.; Tong, G., BST2 suppresses porcine epidemic diarrhea virus replication by targeting and degrading virus nucleocapsid protein with selective autophagy. *Autophagy* **2020,** *16* (10), 1737-1752.
105. Wang, J.; Kan, X.; Li, X.; Sun, J.; Xu, X., Porcine epidemic diarrhoea virus (PEDV) infection activates AMPK and JNK through TAK1 to induce autophagy and enhance virus replication. *Virulence* **2022,** *13* (1), 1697-1712.
106. Su, J.; Shen, S.; Hu, Y.; Chen, S.; Cheng, L.; Cai, Y.; Wei, W.; Wang, Y.; Rui, Y.; Yu, X. F., SARS-CoV-2 ORF3a inhibits cGAS-STING-mediated autophagy flux and antiviral function. *J Med Virol* **2023,** *95* (1), e28175.
107. Jiao, Y.; Zhao, P.; Xu, L. D.; Yu, J. Q.; Cai, H. L.; Zhang, C.; Tong, C.; Yang, Y. L.; Xu, P.; Sun, Q.; Chen, N.; Wang, B.; Huang, Y. W., Enteric coronavirus nsp2 is a virulence determinant that recruits NBR1 for autophagic targeting of TBK1 to diminish the innate immune response. *Autophagy* **2024**, 1-18.
108. Vassilaki, N.; Frakolaki, E., Virus-host interactions under hypoxia. *Microbes Infect* **2017,** *19* (3), 193-203.
109. Yang, C.; Zhong, Z. F.; Wang, S. P.; Vong, C. T.; Yu, B.; Wang, Y. T., HIF-1: structure, biology and natural modulators. *Chin J Nat Med* **2021,** *19* (7), 521-527.
110. Thompson, C. B., Into Thin Air: How We Sense and Respond to Hypoxia. *Cell* **2016,** *167* (1), 9-11.
111. Youssef, S.; Ren, W.; Ai, H. W., A Genetically Encoded FRET Sensor for Hypoxia and Prolyl Hydroxylases. *ACS Chem Biol* **2016,** *11* (9), 2492-8.
112. Huang, R.; Huestis, M.; Gan, E. S.; Ooi, E. E.; Ohh, M., Hypoxia and viral infectious diseases. *JCI Insight* **2021,** *6* (7).
113. Schodel, J.; Ratcliffe, P. J., Mechanisms of hypoxia signalling: new implications for nephrology. *Nat Rev Nephrol* **2019,** *15* (10), 641-659.
114. Zheng, J.; Chen, P.; Zhong, J.; Cheng, Y.; Chen, H.; He, Y.; Chen, C., HIF-1alpha in myocardial ischemia-reperfusion injury (Review). *Mol Med Rep* **2021,** *23* (5).
115. Semenza, G. L., Hypoxia-inducible factors in physiology and medicine. *Cell* **2012,** *148* (3), 399-408.
116. Tirpe, A. A.; Gulei, D.; Ciortea, S. M.; Crivii, C.; Berindan-Neagoe, I., Hypoxia: Overview on Hypoxia-Mediated Mechanisms with a Focus on the Role of HIF Genes. *Int J Mol Sci* **2019,** *20* (24).

117.Semenza, G. L., HIF-1 and mechanisms of hypoxia sensing. *Curr Opin Cell Biol* **2001,** *13* (2), 167-71.
118.Semenza, G. L.; Jiang, B. H.; Leung, S. W.; Passantino, R.; Concordet, J. P.; Maire, P.; Giallongo, A., Hypoxia response elements in the aldolase A, enolase 1, and lactate dehydrogenase A gene promoters contain essential binding sites for hypoxia-inducible factor 1. *J Biol Chem* **1996,** *271* (51), 32529-37.
119.Kierans, S. J.; Taylor, C. T., Regulation of glycolysis by the hypoxia-inducible factor (HIF): implications for cellular physiology. *J Physiol* **2021,** *599* (1), 23-37.
120. Kelly, B.; O'Neill, L. A., Metabolic reprogramming in macrophages and dendritic cells in innate immunity. *Cell Res* **2015,** *25* (7), 771-84.
121. Behrooz, A.; Ismail-Beigi, F., Stimulation of Glucose Transport by Hypoxia: Signals and Mechanisms. *News Physiol Sci* **1999,** *14*, 105-110.
122. Tian, M.; Liu, W.; Li, X.; Zhao, P.; Shereen, M. A.; Zhu, C.; Huang, S.; Liu, S.; Yu, X.; Yue, M.; Pan, P.; Wang, W.; Li, Y.; Chen, X.; Wu, K.; Luo, Z.; Zhang, Q.; Wu, J., HIF-1alpha promotes SARS-CoV-2 infection and aggravates inflammatory responses to COVID-19. *Signal Transduct Target Ther* **2021,** *6* (1), 308.
123. Meng, X.; Zhu, Y.; Yang, W.; Zhang, J.; Jin, W.; Tian, R.; Yang, Z.; Wang, R., HIF-1alpha promotes virus replication and cytokine storm in H1N1 virus-induced severe pneumonia through cellular metabolic reprogramming. *Virol Sin* **2024,** *39* (1), 81-96.
124. Duette, G.; Pereyra Gerber, P.; Rubione, J.; Perez, P. S.; Landay, A. L.; Crowe, S. M.; Liao, Z.; Witwer, K. W.; Holgado, M. P.; Salido, J.; Geffner, J.; Sued, O.; Palmer, C. S.; Ostrowski, M., Induction of HIF-1alpha by HIV-1 Infection in CD4(+) T Cells Promotes Viral Replication and Drives Extracellular Vesicle-Mediated Inflammation. *mBio* **2018,** *9* (5).
125. Chen, L. F.; Cai, J. X.; Zhang, J. J.; Tang, Y. J.; Chen, J. Y.; Xiong, S.; Li, Y. L.; Zhang, H.; Liu, Z.; Li, M. M., Respiratory syncytial virus co-opts hypoxia-inducible factor-1alpha-mediated glycolysis to favor the production of infectious virus. *mBio* **2023,** *14* (5), e0211023.
126. de Wit, E.; van Doremalen, N.; Falzarano, D.; Munster, V. J., SARS and MERS: recent insights into emerging coronaviruses. *Nat Rev Microbiol* **2016,** *14* (8), 523-34.
127. Li, W.; Luo, R.; He, Q.; van Kuppeveld, F. J. M.; Rottier, P. J. M.; Bosch,

B. J., Aminopeptidase N is not required for porcine epidemic diarrhea virus cell entry. *Virus Res* **2017,** *235*, 6-13.
128. Delmas, B.; Gelfi, J.; Sjostrom, H.; Noren, O.; Laude, H., Further characterization of aminopeptidase-N as a receptor for coronaviruses. *Adv Exp Med Biol* **1993,** *342*, 293-8.
129. Xia, L.; Yang, Y.; Wang, J.; Jing, Y.; Yang, Q., Impact of TGEV infection on the pig small intestine. *Virol J* **2018,** *15* (1), 102.
130. Costantini, V.; Lewis, P.; Alsop, J.; Templeton, C.; Saif, L. J., Respiratory and fecal shedding of porcine respiratory coronavirus (PRCV) in sentinel weaned pigs and sequence of the partial S-gene of the PRCV isolates. *Arch Virol* **2004,** *149* (5), 957-74.
131. Wang, P.; Bai, J.; Liu, X.; Wang, M.; Wang, X.; Jiang, P., Tomatidine inhibits porcine epidemic diarrhea virus replication by targeting 3CL protease. *Vet Res* **2020,** *51* (1), 136.
132. Zhang, Y.; Chen, H.; Zou, M.; Oerlemans, R.; Shao, C.; Ren, Y.; Zhang, R.; Huang, X.; Li, G.; Cong, Y., Hypericin Inhibit Alpha-Coronavirus Replication by Targeting 3CL Protease. *Viruses* **2021,** *13* (9).
133. Li, L.; Yu, X.; Zhang, H.; Cheng, H.; Hou, L.; Zheng, Q.; Hou, J., In vitro antiviral activity of Griffithsin against porcine epidemic diarrhea virus. *Virus Genes* **2019,** *55* (2), 174-181.
134. Tang, R.; Guo, L.; Fan, Q.; Zhang, L.; Wang, Y.; Zhang, X.; Shi, D.; Wu, Y.; Shi, H.; Liu, J.; Chen, J.; Feng, L., Porcine deltacoronavirus infection is inhibited by Griffithsin in cell culture. *Vet Microbiol* **2022,** *264*, 109299.
135. V'Kovski, P.; Kratzel, A.; Steiner, S.; Stalder, H.; Thiel, V., Coronavirus biology and replication: implications for SARS-CoV-2. *Nat Rev Microbiol* **2021,** *19* (3), 155-170.
136. Palmer, B. F.; Clegg, D. J., Physiology and pathophysiology of potassium homeostasis. *Adv Physiol Educ* **2016,** *40* (4), 480-490.
137. Brunle, S.; Eisinger, M. L.; Poppe, J.; Mills, D. J.; Langer, J. D.; Vonck, J.; Ermler, U., Molybdate pumping into the molybdenum storage protein via an ATP-powered piercing mechanism. *Proc Natl Acad Sci U S A* **2019,** *116* (52), 26497-504.
138. Yang, Z.; Klionsky, D. J., Eaten alive: a history of macroautophagy. *Nat Cell Biol* **2010,** *12* (9), 814-22.
139. Klionsky, D. J.; Codogno, P., The mechanism and physiological function of macroautophagy. *J Innate Immun* **2013,** *5* (5), 427-33.

140. Codogno, P.; Mehrpour, M.; Proikas-Cezanne, T., Canonical and non-canonical autophagy: variations on a common theme of self-eating? *Nat Rev Mol Cell Biol* **2011,** *13* (1), 7-12.
141. Alers, S.; Loffler, A. S.; Wesselborg, S.; Stork, B., Role of AMPK-mTOR-Ulk1/2 in the regulation of autophagy: cross talk, shortcuts, and feedbacks. *Mol Cell Biol* **2012,** *32* (1), 2-11.
142. Galluzzi, L.; Pietrocola, F.; Levine, B.; Kroemer, G., Metabolic control of autophagy. *Cell* **2014,** *159* (6), 1263-76.
143. Munson, M. J.; Ganley, I. G., MTOR, PIK3C3, and autophagy: Signaling the beginning from the end. *Autophagy* **2015,** *11* (12), 2375-6.
144. Ma, B.; Cao, W.; Li, W.; Gao, C.; Qi, Z.; Zhao, Y.; Du, J.; Xue, H.; Peng, J.; Wen, J.; Chen, H.; Ning, Y.; Huang, L.; Zhang, H.; Gao, X.; Yu, L.; Chen, Y. G., Dapper1 promotes autophagy by enhancing the Beclin1-Vps34-Atg14L complex formation. *Cell Res* **2014,** *24* (8), 912-24.
145. Lamb, C. A.; Yoshimori, T.; Tooze, S. A., The autophagosome: origins unknown, biogenesis complex. *Nat Rev Mol Cell Biol* **2013,** *14* (12), 759-74.
146. Ko, S.; Gu, M. J.; Kim, C. G.; Kye, Y. C.; Lim, Y.; Lee, J. E.; Park, B. C.; Chu, H.; Han, S. H.; Yun, C. H., Rapamycin-induced autophagy restricts porcine epidemic diarrhea virus infectivity in porcine intestinal epithelial cells. *Antiviral Res* **2017,** *146*, 86-95.
147. Li, Y.; Yang, N.; Chen, J.; Huang, X.; Zhang, N.; Yang, S.; Liu, G.; Liu, G., Next-Generation Porcine Intestinal Organoids: an Apical-Out Organoid Model for Swine Enteric Virus Infection and Immune Response Investigations. *J Virol* **2020,** *94* (21).
148. Yang, N.; Zhang, Y.; Fu, Y.; Li, Y.; Yang, S.; Chen, J.; Liu, G., Transmissible Gastroenteritis Virus Infection Promotes the Self-Renewal of Porcine Intestinal Stem Cells via Wnt/beta-Catenin Pathway. *J Virol* **2022,** *96* (18), e0096222.
149. Huang, X.; Chen, J.; Yao, G.; Guo, Q.; Wang, J.; Liu, G., A TaqMan-probe-based multiplex real-time RT-qPCR for simultaneous detection of porcine enteric coronaviruses. *Appl Microbiol Biotechnol* **2019,** *103* (12), 4943-4952.
150. Zhang, N.; Shi, H.; Yan, M.; Liu, G., IFIT5 Negatively Regulates the Type I IFN Pathway by Disrupting TBK1-IKKepsilon-IRF3 Signalosome and Degrading IRF3 and IKKepsilon. *J Immunol* **2021,** *206* (9), 2184-2197.
151. Yang, S.; Huang, X.; Li, S.; Wang, C.; Jansen, C. A.; Savelkoul, H. F. J.;

Liu, G., Linoleic acid: a natural feed compound against porcine epidemic diarrhea disease. *J Virol* **2023,** *97* (12), e0170023.
152. Zhai, X.; Wang, N.; Jiao, H.; Zhang, J.; Li, C.; Ren, W.; Reiter, R. J.; Su, S., Melatonin and other indoles show antiviral activities against swine coronaviruses in vitro at pharmacological concentrations. *J Pineal Res* **2021,** *71* (2), e12754.
153. Zhang, Y.; Song, Z.; Wang, M.; Lan, M.; Zhang, K.; Jiang, P.; Li, Y.; Bai, J.; Wang, X., Cholesterol 25-hydroxylase negatively regulates porcine intestinal coronavirus replication by the production of 25-hydroxycholesterol. *Vet Microbiol* **2019,** *231*, 129-138.
154. Li, Y.; Wang, X.; Zhang, E.; Liu, R.; Yang, C.; Duan, Y.; Jiang, Y.; Yang, Q., Calpain-1: a Novel Antiviral Host Factor Identified in Porcine Small Intestinal Mucus. *mBio* **2022,** *13* (5), e0035822.
155. Siva Sankar, D.; Dengjel, J., Protein complexes and neighborhoods driving autophagy. *Autophagy* **2021,** *17* (10), 2689-2705.
156. Wang, X.; Luo, J.; Wen, Z.; Shuai, L.; Wang, C.; Zhong, G.; He, X.; Cao, H.; Liu, R.; Ge, J.; Hua, R.; Sun, Z.; Wang, X.; Wang, J.; Bu, Z., Diltiazem inhibits SARS-CoV-2 cell attachment and internalization and decreases the viral infection in mouse lung. *PLoS Pathog* **2022,** *18* (2), e1010343.
157. Reinhold, D.; Brocke, S., DPP4-directed therapeutic strategies for MERS-CoV. *Lancet Infect Dis* **2014,** *14* (2), 100-1.
158. Lu, C.; Amin, M. A.; Fox, D. A., CD13/Aminopeptidase N Is a Potential Therapeutic Target for Inflammatory Disorders. *J Immunol* **2020,** *204* (1), 3-11.
159. Ji, C. M.; Wang, B.; Zhou, J.; Huang, Y. W., Aminopeptidase-N-independent entry of porcine epidemic diarrhea virus into Vero or porcine small intestine epithelial cells. *Virology* **2018,** *517*, 16-23.
160. Li, Y.; Zhang, Z.; Yang, L.; Lian, X.; Xie, Y.; Li, S.; Xin, S.; Cao, P.; Lu, J., The MERS-CoV Receptor DPP4 as a Candidate Binding Target of the SARS-CoV-2 Spike. *iScience* **2020,** *23* (6), 101160.
161. Hood, M. I.; Skaar, E. P., Nutritional immunity: transition metals at the pathogen-host interface. *Nat Rev Microbiol* **2012,** *10* (8), 525-37.
162. Wang, C.; Guan, Y.; Lv, M.; Zhang, R.; Guo, Z.; Wei, X.; Du, X.; Yang, J.; Li, T.; Wan, Y.; Su, X.; Huang, X.; Jiang, Z., Manganese Increases the Sensitivity of the cGAS-STING Pathway for Double-Stranded DNA and Is Required for the Host Defense against DNA Viruses. *Immunity* **2018,** *48* (4),

675-687 e7.
163. te Velthuis, A. J.; van den Worm, S. H.; Sims, A. C.; Baric, R. S.; Snijder, E. J.; van Hemert, M. J., Zn(2+) inhibits coronavirus and arterivirus RNA polymerase activity in vitro and zinc ionophores block the replication of these viruses in cell culture. *PLoS Pathog* **2010,** *6* (11), e1001176.
164. Nimitvilai, S.; Suputtamongkol, Y.; Poolvivatchaikarn, U.; Rassamekulthana, D.; Rongkiettechakorn, N.; Mungaomklang, A.; Assanasaen, S.; Wongsawat, E.; Boonarkart, C.; Sawaengdee, W., A Randomized Controlled Trial of Combined Ivermectin and Zinc Sulfate versus Combined Hydroxychloroquine, Darunavir/Ritonavir, and Zinc Sulfate among Adult Patients with Asymptomatic or Mild Coronavirus-19 Infection. *J Glob Infect Dis* **2022,** *14* (2), 69-74.
165. Chen, Y. N.; Hsueh, Y. H.; Hsieh, C. T.; Tzou, D. Y.; Chang, P. L., Antiviral Activity of Graphene-Silver Nanocomposites against Non-Enveloped and Enveloped Viruses. *Int J Environ Res Public Health* **2016,** *13* (4), 430.
166. Yao, S.; Kang, J.; Guo, G.; Yang, Z.; Huang, Y.; Lan, Y.; Zhou, T.; Wang, L.; Wei, C.; Xu, Z.; Li, Y., The key micronutrient copper orchestrates broad-spectrum virus resistance in rice. *Sci Adv* **2022,** *8* (26), eabm0660.
167. Ito, T.; Sunada, K.; Nagai, T.; Ishiguro, H.; Nakano, R.; Suzuki, Y.; Nakano, A.; Yano, H.; Isobe, T.; Matsushita, S.; Nakajima, A., Preparation of cerium molybdates and their antiviral activity against bacteriophage Phi6 and SARS-CoV-2. *Mater Lett* **2021,** *290*, 129510.
168. Korolchuk, V. I.; Menzies, F. M.; Rubinsztein, D. C., Mechanisms of cross-talk between the ubiquitin-proteasome and autophagy-lysosome systems. *FEBS Lett* **2010,** *584* (7), 1393-8.
169. Stucki, J. W.; Simon, H. U., Mathematical modeling of the regulation of caspase-3 activation and degradation. *J Theor Biol* **2005,** *234* (1), 123-31.
170. Miller, K.; McGrath, M. E.; Hu, Z.; Ariannejad, S.; Weston, S.; Frieman, M.; Jackson, W. T., Coronavirus interactions with the cellular autophagy machinery. *Autophagy* **2020,** *16* (12), 2131-2139.
171. Zhou, C.; Qian, X.; Hu, M.; Zhang, R.; Liu, N.; Huang, Y.; Yang, J.; Zhang, J.; Bai, H.; Yang, Y.; Wang, Y.; Ali, D.; Michalak, M.; Chen, X. Z.; Tang, J., STYK1 promotes autophagy through enhancing the assembly of autophagy-specific class III phosphatidylinositol 3-kinase complex I. *Autophagy* **2020,** *16* (10), 1786-1806.

172. Jelikic-Stankov, M.; Uskokovic-Markovic, S.; Holclajtner-Antunovic, I.; Todorovic, M.; Djurdjevic, P., Compounds of Mo, V and W in biochemistry and their biomedical activity. *J Trace Elem Med Biol* **2007,** *21* (1), 8-16.
173. Huang, X. Y.; Hu, D. W.; Zhao, F. J., Molybdenum: More than an essential element. *J Exp Bot* **2022,** *73* (6), 1766-1774.
174. Llamas, A.; Tejada-Jimenez, M.; Fernandez, E.; Galvan, A., Molybdenum metabolism in the alga Chlamydomonas stands at the crossroad of those in Arabidopsis and humans. *Metallomics* **2011,** *3* (6), 578-90.
175. Corradi, G. R.; Mazzitelli, L. R.; Petrovich, G. D.; Grenon, P.; Sorensen, D. M.; Palmgren, M.; de Tezanos Pinto, F.; Adamo, H. P., Reduction of the P5A-ATPase Spf1p phosphoenzyme by a Ca2+-dependent phosphatase. *PLoS One* **2020,** *15* (4), e0232476.
176. Matsumoto, T.; Sunada, K.; Nagai, T.; Isobe, T.; Matsushita, S.; Ishiguro, H.; Nakajima, A., Effects of cerium and tungsten substitution on antiviral and antibacterial properties of lanthanum molybdate. *Mater Sci Eng C Mater Biol Appl* **2020,** *117*, 111323.
177. Lang, Y.; Li, F.; Liu, Q.; Xia, Z.; Ji, Z.; Hu, J.; Cheng, Y.; Gao, M.; Sun, F.; Shen, B.; Xie, C.; Yi, W.; Wu, Y.; Yao, J.; Cao, Z., The Kv1.3 ion channel acts as a host factor restricting viral entry. *FASEB J* **2021,** *35* (2), e20995.
178. Paudel, R. R.; Lu, D.; Roy Chowdhury, S.; Monroy, E. Y.; Wang, J., Targeted Protein Degradation via Lysosomes. *Biochemistry* **2023,** *62* (3), 564-579.
179. Liu, M.; Lu, B.; Li, Y.; Yuan, S.; Zhuang, Z.; Li, G.; Wang, D.; Ma, L.; Zhu, J.; Zhao, J.; Chan, C. C.; Poon, V. K.; Chik, K. K.; Zhao, Z.; Xian, H.; Zhao, J.; Zhao, J.; Chan, J. F.; Zhang, Y., P21-activated kinase 1 (PAK1)-mediated cytoskeleton rearrangement promotes SARS-CoV-2 entry and ACE2 autophagic degradation. *Signal Transduct Target Ther* **2023,** *8* (1), 385.
180. Jin, S.; He, X.; Ma, L.; Zhuang, Z.; Wang, Y.; Lin, M.; Cai, S.; Wei, L.; Wang, Z.; Zhao, Z.; Wu, Y.; Sun, L.; Li, C.; Xie, W.; Zhao, Y.; Songyang, Z.; Peng, K.; Zhao, J.; Cui, J., Suppression of ACE2 SUMOylation protects against SARS-CoV-2 infection through TOLLIP-mediated selective autophagy. *Nat Commun* **2022,** *13* (1), 5204.
181. Sato, T.; Vries, R. G.; Snippert, H. J.; van de Wetering, M.; Barker, N.; Stange, D. E.; van Es, J. H.; Abo, A.; Kujala, P.; Peters, P. J.; Clevers, H., Single Lgr5 stem cells build crypt-villus structures in vitro without a mesenchymal niche. *Nature* **2009,** *459* (7244), 262-5.

182. Salminen, A., Increased immunosuppression impairs tissue homeostasis with aging and age-related diseases. *J Mol Med (Berl)* **2021,** *99* (1), 1-20.
183. Tay, M. Z.; Poh, C. M.; Renia, L.; MacAry, P. A.; Ng, L. F. P., The trinity of COVID-19: immunity, inflammation and intervention. *Nat Rev Immunol* **2020,** *20* (6), 363-374.
184. Poeck, H.; Ruland, J., From virus to inflammation: mechanisms of RIG-I-induced IL-1beta production. *Eur J Cell Biol* **2012,** *91* (1), 59-64.
185. Park, A.; Iwasaki, A., Type I and Type III Interferons - Induction, Signaling, Evasion, and Application to Combat COVID-19. *Cell Host Microbe* **2020,** *27* (6), 870-878.
186. Fukata, M.; Arditi, M., The role of pattern recognition receptors in intestinal inflammation. *Mucosal Immunol* **2013,** *6* (3), 451-63.
187. Latz, E.; Xiao, T. S.; Stutz, A., Activation and regulation of the inflammasomes. *Nat Rev Immunol* **2013,** *13* (6), 397-411.
188. Lawrence, T., The nuclear factor NF-kappaB pathway in inflammation. *Cold Spring Harb Perspect Biol* **2009,** *1* (6), a001651.
189. Karin, M.; Liu, Z.; Zandi, E., AP-1 function and regulation. *Curr Opin Cell Biol* **1997,** *9* (2), 240-6.
190. Lee, W.; Lee, S. H.; Kim, M.; Moon, J. S.; Kim, G. W.; Jung, H. G.; Kim, I. H.; Oh, J. E.; Jung, H. E.; Lee, H. K.; Ku, K. B.; Ahn, D. G.; Kim, S. J.; Kim, K. S.; Oh, J. W., Vibrio vulnificus quorum-sensing molecule cyclo(Phe-Pro) inhibits RIG-I-mediated antiviral innate immunity. *Nat Commun* **2018,** *9* (1), 1606.
191. Cherry, A. D.; Piantadosi, C. A., Regulation of mitochondrial biogenesis and its intersection with inflammatory responses. *Antioxid Redox Signal* **2015,** *22* (12), 965-76.
192. Usta Sofu, G.; Erzurumlu, Y.; Karaca, U.; Candan, I. A.; Savran, M.; Asci, H.; Hasseyid, N., Melatonin receptor agonist ramelteon alleviates experimental acute ocular inflammation via HIF-1Alpha/VEGF/E-NOS signaling. *Eur J Ophthalmol* **2022**, 11206721221123878.
193. Codo, A. C.; Davanzo, G. G.; Monteiro, L. B.; de Souza, G. F.; Muraro, S. P.; Virgilio-da-Silva, J. V.; Prodonoff, J. S.; Carregari, V. C.; de Biagi Junior, C. A. O.; Crunfli, F.; Jimenez Restrepo, J. L.; Vendramini, P. H.; Reis-de-Oliveira, G.; Bispo Dos Santos, K.; Toledo-Teixeira, D. A.; Parise, P. L.; Martini, M. C.; Marques, R. E.; Carmo, H. R.; Borin, A.; Coimbra, L. D.; Boldrini, V. O.; Brunetti, N. S.; Vieira, A. S.; Mansour, E.; Ulaf, R. G.;

Bernardes, A. F.; Nunes, T. A.; Ribeiro, L. C.; Palma, A. C.; Agrela, M. V.; Moretti, M. L.; Sposito, A. C.; Pereira, F. B.; Velloso, L. A.; Vinolo, M. A. R.; Damasio, A.; Proenca-Modena, J. L.; Carvalho, R. F.; Mori, M. A.; Martins-de-Souza, D.; Nakaya, H. I.; Farias, A. S.; Moraes-Vieira, P. M., Elevated Glucose Levels Favor SARS-CoV-2 Infection and Monocyte Response through a HIF-1alpha/Glycolysis-Dependent Axis. *Cell Metab* **2020,** *32* (3), 437-446 e5.

194. Nolan, L. S.; Baldridge, M. T., Advances in understanding interferon-mediated immune responses to enteric viruses in intestinal organoids. *Front Immunol* **2022,** *13*, 943334.

195. Xue, M.; Wang, W.; He, H.; Li, L.; Zhang, X.; Shi, H.; Liu, P.; Feng, L., Different Mechanisms Are Utilized by Coronavirus Transmissible Gastroenteritis Virus To Regulate Interferon Lambda 1 and Interferon Lambda 3 Production. *J Virol* **2022,** *96* (24), e0138822.

196. Li, R.; Zhu, S., NLRP6 inflammasome. *Mol Aspects Med* **2020,** *76*, 100859.

197. Sharif, H.; Wang, L.; Wang, W. L.; Magupalli, V. G.; Andreeva, L.; Qiao, Q.; Hauenstein, A. V.; Wu, Z.; Nunez, G.; Mao, Y.; Wu, H., Structural mechanism for NEK7-licensed activation of NLRP3 inflammasome. *Nature* **2019,** *570* (7761), 338-343.

198. He, Y.; Zeng, M. Y.; Yang, D.; Motro, B.; Nunez, G., NEK7 is an essential mediator of NLRP3 activation downstream of potassium efflux. *Nature* **2016,** *530* (7590), 354-7.

199. Zhu, J.; Huang, S.; Li, Y.; Xu, J.; Chen, R.; Guo, M.; Qian, X.; Li, T.; Tian, Z.; Jin, H.; Huang, C., NF-kappaB1 p50 stabilizes HIF-1alpha protein through suppression of ATG7-dependent autophagy. *Cell Death Dis* **2022,** *13* (12), 1076.

200. Meng, X.; Zhu, Y.; Yang, W.; Zhang, J.; Jin, W.; Tian, R.; Yang, Z.; Wang, R., HIF-1alpha promotes virus replication and cytokine storm in H1N1 virus-induced severe pneumonia through cellular metabolic reprogramming. *Virol Sin* **2023**.

201. Liu, G.; Lee, J. H.; Parker, Z. M.; Acharya, D.; Chiang, J. J.; van Gent, M.; Riedl, W.; Davis-Gardner, M. E.; Wies, E.; Chiang, C.; Gack, M. U., ISG15-dependent activation of the sensor MDA5 is antagonized by the SARS-CoV-2 papain-like protease to evade host innate immunity. *Nat Microbiol* **2021,** *6* (4), 467-478.

202. Bouhaddou, M.; Reuschl, A. K.; Polacco, B. J.; Thorne, L. G.; Ummadi, M. R.; Ye, C.; Rosales, R.; Pelin, A.; Batra, J.; Jang, G. M.; Xu, J.; Moen, J. M.; Richards, A. L.; Zhou, Y.; Harjai, B.; Stevenson, E.; Rojc, A.; Ragazzini, R.; Whelan, M. V. X.; Furnon, W.; De Lorenzo, G.; Cowton, V.; Syed, A. M.; Ciling, A.; Deutsch, N.; Pirak, D.; Dowgier, G.; Mesner, D.; Turner, J. L.; McGovern, B. L.; Rodriguez, M. L.; Leiva-Rebollo, R.; Dunham, A. S.; Zhong, X.; Eckhardt, M.; Fossati, A.; Liotta, N. F.; Kehrer, T.; Cupic, A.; Rutkowska, M.; Mena, I.; Aslam, S.; Hoffert, A.; Foussard, H.; Olwal, C. O.; Huang, W.; Zwaka, T.; Pham, J.; Lyons, M.; Donohue, L.; Griffin, A.; Nugent, R.; Holden, K.; Deans, R.; Aviles, P.; Lopez-Martin, J. A.; Jimeno, J. M.; Obernier, K.; Fabius, J. M.; Soucheray, M.; Huttenhain, R.; Jungreis, I.; Kellis, M.; Echeverria, I.; Verba, K.; Bonfanti, P.; Beltrao, P.; Sharan, R.; Doudna, J. A.; Martinez-Sobrido, L.; Patel, A. H.; Palmarini, M.; Miorin, L.; White, K.; Swaney, D. L.; Garcia-Sastre, A.; Jolly, C.; Zuliani-Alvarez, L.; Towers, G. J.; Krogan, N. J., SARS-CoV-2 variants evolve convergent strategies to remodel the host response. *Cell* **2023,** *186* (21), 4597-4614 e26.

203. Shin, D.; Mukherjee, R.; Grewe, D.; Bojkova, D.; Baek, K.; Bhattacharya, A.; Schulz, L.; Widera, M.; Mehdipour, A. R.; Tascher, G.; Geurink, P. P.; Wilhelm, A.; van der Heden van Noort, G. J.; Ovaa, H.; Muller, S.; Knobeloch, K. P.; Rajalingam, K.; Schulman, B. A.; Cinatl, J.; Hummer, G.; Ciesek, S.; Dikic, I., Papain-like protease regulates SARS-CoV-2 viral spread and innate immunity. *Nature* **2020,** *587* (7835), 657-662.

204. Koyasu, S.; Kobayashi, M.; Goto, Y.; Hiraoka, M.; Harada, H., Regulatory mechanisms of hypoxia-inducible factor 1 activity: Two decades of knowledge. *Cancer Sci* **2018,** *109* (3), 560-571.

205. Peng, T.; Du, S. Y.; Son, M.; Diamond, B., HIF-1alpha is a negative regulator of interferon regulatory factors: Implications for interferon production by hypoxic monocytes. *Proc Natl Acad Sci U S A* **2021,** *118* (26).

206. Pang, Y.; Zhou, Y.; Wang, Y.; Sun, Z.; Liu, J.; Li, C.; Xiao, S.; Fang, L., Porcine Reproductive and Respiratory Syndrome Virus nsp1beta Stabilizes HIF-1alpha to Enhance Viral Replication. *Microbiol Spectr* **2022,** *10* (6), e0317322.

207. Yang, S.; Yang, N.; Huang, X.; Li, Y.; Liu, G.; Jansen, C. A.; Savelkoul, H. F. J.; Liu, G., Pigs' intestinal barrier function is more refined with aging. *Dev Comp Immunol* **2022,** *136*, 104512.

208. Yue, Y.; Tang, Y.; Huang, H.; Zheng, D.; Liu, C.; Zhang, H.; Liu, Y.; Li,

Y.; Sun, X.; Lu, L., VBP1 negatively regulates CHIP and selectively inhibits the activity of hypoxia-inducible factor (HIF)-1alpha but not HIF-2alpha. *J Biol Chem* **2023,** *299* (6), 104829.
209. Chang, H. A.; Ou Yang, R. Z.; Su, J. M.; Nguyen, T. M. H.; Sung, J. M.; Tang, M. J.; Chiu, W. T., YAP nuclear translocation induced by HIF-1alpha prevents DNA damage under hypoxic conditions. *Cell Death Discov* **2023,** *9* (1), 385.
210. Majdoul, S.; Compton, A. A., Lessons in self-defence: inhibition of virus entry by intrinsic immunity. *Nat Rev Immunol* **2022,** *22* (6), 339-352.
211.Scialo, F.; Daniele, A.; Amato, F.; Pastore, L.; Matera, M. G.; Cazzola, M.; Castaldo, G.; Bianco, A., ACE2: The Major Cell Entry Receptor for SARS-CoV-2. *Lung* **2020,** *198* (6), 867-877.
212. Brevini, T.; Maes, M.; Webb, G. J.; John, B. V.; Fuchs, C. D.; Buescher, G.; Wang, L.; Griffiths, C.; Brown, M. L.; Scott, W. E., 3rd; Pereyra-Gerber, P.; Gelson, W. T. H.; Brown, S.; Dillon, S.; Muraro, D.; Sharp, J.; Neary, M.; Box, H.; Tatham, L.; Stewart, J.; Curley, P.; Pertinez, H.; Forrest, S.; Mlcochova, P.; Varankar, S. S.; Darvish-Damavandi, M.; Mulcahy, V. L.; Kuc, R. E.; Williams, T. L.; Heslop, J. A.; Rossetti, D.; Tysoe, O. C.; Galanakis, V.; Vila-Gonzalez, M.; Crozier, T. W. M.; Bargehr, J.; Sinha, S.; Upponi, S. S.; Fear, C.; Swift, L.; Saeb-Parsy, K.; Davies, S. E.; Wester, A.; Hagstrom, H.; Melum, E.; Clements, D.; Humphreys, P.; Herriott, J.; Kijak, E.; Cox, H.; Bramwell, C.; Valentijn, A.; Illingworth, C. J. R.; Consortium, U.-P.; Dahman, B.; Bastaich, D. R.; Ferreira, R. D.; Marjot, T.; Barnes, E.; Moon, A. M.; Barritt, A. S. t.; Gupta, R. K.; Baker, S.; Davenport, A. P.; Corbett, G.; Gorgoulis, V. G.; Buczacki, S. J. A.; Lee, J. H.; Matheson, N. J.; Trauner, M.; Fisher, A. J.; Gibbs, P.; Butler, A. J.; Watson, C. J. E.; Mells, G. F.; Dougan, G.; Owen, A.; Lohse, A. W.; Vallier, L.; Sampaziotis, F., FXR inhibition may protect from SARS-CoV-2 infection by reducing ACE2. *Nature* **2023,** *615* (7950), 134-142.
213. Wang, J.; Yang, G.; Wang, X.; Wen, Z.; Shuai, L.; Luo, J.; Wang, C.; Sun, Z.; Liu, R.; Ge, J.; He, X.; Hua, R.; Wang, X.; Yang, X.; Chen, W.; Zhong, G.; Bu, Z., SARS-CoV-2 uses metabotropic glutamate receptor subtype 2 as an internalization factor to infect cells. *Cell Discov* **2021,** *7* (1), 119.
214. Chen, J.; Yang, X.; Si, H.; Gong, Q.; Que, T.; Li, J.; Li, Y.; Wu, C.; Zhang, W.; Chen, Y.; Luo, Y.; Zhu, Y.; Li, B.; Luo, D.; Hu, B.; Lin, H.; Jiang, R.; Jiang, T.; Li, Q.; Liu, M.; Xie, S.; Su, J.; Zheng, X.; Li, A.; Yao, Y.; Yang, Y.; Chen, P.; Wu, A.; He, M.; Lin, X.; Tong, Y.; Hu, Y.; Shi, Z. L.; Zhou, P., A bat MERS-

like coronavirus circulates in pangolins and utilizes human DPP4 and host proteases for cell entry. *Cell* **2023,** *186* (4), 850-863 e16.
215. Shi, J.; Hu, S.; Wei, H.; Zhang, L.; Lan, Y.; Guan, J.; Zhao, K.; Gao, F.; He, W.; Li, Z., Dipeptidyl peptidase 4 interacts with porcine coronavirus PHEV spikes and mediates host range expansion. *J Virol* **2024,** *98* (7), e0075324.
216. Yamamoto, M.; Matsuyama, S.; Li, X.; Takeda, M.; Kawaguchi, Y.; Inoue, J. I.; Matsuda, Z., Identification of Nafamostat as a Potent Inhibitor of Middle East Respiratory Syndrome Coronavirus S Protein-Mediated Membrane Fusion Using the Split-Protein-Based Cell-Cell Fusion Assay. *Antimicrob Agents Chemother* **2016,** *60* (11), 6532-6539.
217. Liang, Q. Z.; Wang, B.; Ji, C. M.; Hu, F.; Qin, P.; Feng, Y.; Tang, Y. D.; Huang, Y. W., Chicken or Porcine Aminopeptidase N Mediates Cellular Entry of Pseudoviruses Carrying Spike Glycoprotein from the Avian Deltacoronaviruses HKU11, HKU13, and HKU17. *J Virol* **2023,** *97* (2), e0194722.
218. Li, J.; Zhou, J.; Zhang, T.; Wu, H.; Li, F.; Qi, C.; Fan, L.; Yuan, X.; Wang, W.; Guo, R.; Fan, B.; Tang, X.; Pang, D.; Ouyang, H.; Xie, Z.; Li, B., Effective inhibition of PDCoV infection in chimeric APN gene-edited neonatal pigs. *J Virol* **2024**, e0061124.
219. Ciechanover, A., Proteolysis: from the lysosome to ubiquitin and the proteasome. *Nat Rev Mol Cell Biol* **2005,** *6* (1), 79-87.
220. Ohsumi, Y., Historical landmarks of autophagy research. *Cell Res* **2014,** *24* (1), 9-23.
221. Gu, X.; Nardone, C.; Kamitaki, N.; Mao, A.; Elledge, S. J.; Greenberg, M. E., The midnolin-proteasome pathway catches proteins for ubiquitination-independent degradation. *Science* **2023,** *381* (6660), eadh5021.
222. Yu, L.; Chen, Y.; Tooze, S. A., Autophagy pathway: Cellular and molecular mechanisms. *Autophagy* **2018,** *14* (2), 207-215.
223. Glick, D.; Barth, S.; Macleod, K. F., Autophagy: cellular and molecular mechanisms. *J Pathol* **2010,** *221* (1), 3-12.
224. Ye, D.; Wang, P.; Chen, L. L.; Guan, K. L.; Xiong, Y., Itaconate in host inflammation and defense. *Trends Endocrinol Metab* **2024,** *35* (7), 586-606.
225. Zhao, Z.; Wei, Y.; Tao, C., An enlightening role for cytokine storm in coronavirus infection. *Clin Immunol* **2021,** *222*, 108615.
226. Liu, T.; Feng, M.; Wen, Z.; He, Y.; Lin, W.; Zhang, M., Comparison of the Characteristics of Cytokine Storm and Immune Response Induced by

SARS-CoV, MERS-CoV, and SARS-CoV-2 Infections. *J Inflamm Res* **2021,** *14*, 5475-5487.
227. Zheng, M.; Karki, R.; Williams, E. P.; Yang, D.; Fitzpatrick, E.; Vogel, P.; Jonsson, C. B.; Kanneganti, T. D., TLR2 senses the SARS-CoV-2 envelope protein to produce inflammatory cytokines. *Nat Immunol* **2021,** *22* (7), 829-838.
228. Khan, S.; Shafiei, M. S.; Longoria, C.; Schoggins, J. W.; Savani, R. C.; Zaki, H., SARS-CoV-2 spike protein induces inflammation via TLR2-dependent activation of the NF-kappaB pathway. *Elife* **2021,** *10*.
229. Cao, L.; Ge, X.; Gao, Y.; Ren, Y.; Ren, X.; Li, G., Porcine epidemic diarrhea virus infection induces NF-kappaB activation through the TLR2, TLR3 and TLR9 pathways in porcine intestinal epithelial cells. *J Gen Virol* **2015,** *96* (Pt 7), 1757-67.
230. Ghosh, S.; Hayden, M. S., New regulators of NF-kappaB in inflammation. *Nat Rev Immunol* **2008,** *8* (11), 837-48.
231. Shaulian, E.; Karin, M., AP-1 as a regulator of cell life and death. *Nat Cell Biol* **2002,** *4* (5), E131-6.
232. Smolarczyk, R.; Cichon, T.; Pilny, E.; Jarosz-Biej, M.; Poczkaj, A.; Kulach, N.; Szala, S., Combination of anti-vascular agent - DMXAA and HIF-1alpha inhibitor - digoxin inhibits the growth of melanoma tumors. *Sci Rep* **2018,** *8* (1), 7355.
233. Lazear, H. M.; Schoggins, J. W.; Diamond, M. S., Shared and Distinct Functions of Type I and Type III Interferons. *Immunity* **2019,** *50* (4), 907-923.
234. Kotenko, S. V.; Durbin, J. E., Contribution of type III interferons to antiviral immunity: location, location, location. *J Biol Chem* **2017,** *292* (18), 7295-7303.
235. Wickstrom, M.; Larsson, R.; Nygren, P.; Gullbo, J., Aminopeptidase N (CD13) as a target for cancer chemotherapy. *Cancer Sci* **2011,** *102* (3), 501-8.
236. Li, Y.; Lee, J. S.; Kirtane, A. R.; Li, M.; Coffey, C. W., 3rd; Hess, K.; Lopes, A.; Collins, J.; Tamang, S.; Ishida, K.; Hayward, A.; Wainer, J.; Wentworth, A. J.; Traverso, G., Enzyme-Triggered Intestine-Specific Targeting Adhesive Platform for Universal Oral Drug Delivery. *Adv Healthc Mater* **2023,** *12* (27), e2301033.
237. Konno, S.; Kobayashi, K.; Senda, M.; Funai, Y.; Seki, Y.; Tamai, I.; Schakel, L.; Sakata, K.; Pillaiyar, T.; Taguchi, A.; Taniguchi, A.; Gutschow, M.; Muller, C. E.; Takeuchi, K.; Hirohama, M.; Kawaguchi, A.; Kojima, M.; Senda,

T.; Shirasaka, Y.; Kamitani, W.; Hayashi, Y., 3CL Protease Inhibitors with an Electrophilic Arylketone Moiety as Anti-SARS-CoV-2 Agents. *J Med Chem* **2022,** *65* (4), 2926-2939.
238. Korbecki, J.; Siminska, D.; Gassowska-Dobrowolska, M.; Listos, J.; Gutowska, I.; Chlubek, D.; Baranowska-Bosiacka, I., Chronic and Cycling Hypoxia: Drivers of Cancer Chronic Inflammation through HIF-1 and NF-kappaB Activation: A Review of the Molecular Mechanisms. *Int J Mol Sci* **2021,** *22* (19).